October 2007

Omnidirectional Horizontally Polarized UHF Antenna Design

Eugeny Sosnovsky
Worcester Polytechnic Institute

Jesse Oliver Sawyer
Worcester Polytechnic Institute

Project Number: <PH-GSI-0701>

OMNIDIRECTIONAL HORIZONTALLY POLARIZED UHF ANTENNA DESIGN

A Major Qualifying Project

submitted to the Faculty

of the

WORCESTER POLYTECHNIC INSTITUTE

in partial fulfillment of the requirements for the

Degree of Bachelor of Science

by

_____

Jesse Sawyer

_____

Eugeny Sosnovsky

Date: October 14, 2007

Approved:

_____

Professor Germano S. Iannacchione, Major Advisor

_____

Dr. Herbert M. Aumann, MIT Lincoln Laboratory Advisor

Keywords:
1. antenna
2. electromagnetism
3. applied physics

This work is sponsored by the Office of Naval Research under Air Force Contract FA8721-05-C-0002. Opinions, interpretations, conclusions, and recommendations are those of the authors and are not necessarily endorsed by the United States Air Force.

Abstract

For calibration of circular phased arrays, a highly omnidirectional horizontally polarized UHF antenna was required. Commercially available antennas are not omnidirectional enough for this application. In this project we compared several potential designs including an electrically small loop, curved crossed dipoles and n-petal wheel. 5-petal wheels had the best simulated performance so we then optimized it and built a prototype. The prototype was measured to be omnidirectional within +/- 0.4 dB. Detailed suggestions were made for further improving the design.

Acknowledgements

We would like to acknowledge the contributions of the following MIT Lincoln Laboratory staff and Worcester Polytechnic Institute faculty, without whom this project could never have been a success.

Our advisors, Dr. Herbert Aumann, Lincoln Laboratory, and Dr. Germano Iannacchione, WPI, for their advice and guidance. Emily Anesta, Lincoln Laboratory, for her invaluable assistance not only in coordinating the MIT Lincoln Laboratory MQP program, but with every conceivable aspect of our project as well. Eric Salvo, Lincoln Laboratory, for his patience and dedication in dealing with all of our manufacturing needs. David Bruno and Eric Carrera, both of Lincoln Laboratory, for their assistance in conducting measurements. Dr. David Mooradd, Anu Myne, Kristan Tuttle, Frank Willwerth, all of Lincoln Laboratory, as well as Dr. Sergey Makarov of WPI for answering our many antenna theory questions and always being on hand to offer advice and assistance.

Table of Contents

Table of Figures

List of Tables

1 Introduction

An *antenna*[1] is "that part of a transmitting or receiving system that is designed to radiate or to receive electromagnetic waves." [1] Antennas have become ubiquitous through their role in wireless transmission and reception of signals. With applications ranging from telecommunications to radar and long range tracking, antennas have proven themselves as a versatile and essential component of modern civilization.

The physics underlying antenna functionality are generally based on classical electromagnetic theory. Constructive and destructive interference of electromagnetic waves, principles of self-inductance, parallel and series oscillating RLC circuits and AC current theory in general all play a role in antenna design and analysis. Antenna design is further complicated by the difficulties in setting up accurate experiments, as all physical objects conductive and non-conductive, affect antenna performance without being part of the antenna. Therefore, constant consideration of unpredicted and not simulated difficulties is necessary in antenna design.

Group 39 at MIT Lincoln Laboratory specializes in Air Defense Techniques, working extensively with antenna hardware and signal processing for advanced radar and phased array antenna technologies. Antenna systems vary in several performance parameters, such as the direction in which they radiate most of the signal, the relative strength of that signal, or the *input impedance* of the antenna. These parameters are influenced primarily by the geometry of the antenna; thus, antenna design generally involves modeling antenna performance as a function of antennas geometry and optimizing it. Prototype measurement is a major step in antenna design as

[1] The *italicized* terms constitute just a few of the terms that are necessary in this report but may be unfamiliar to a typical applied physicist. Therefore, a Glossary section (see p. 99) has been constructed. The Glossary section defines the engineering terminology common in antenna and RF-circuit design.

well due to inability of most antenna modeling software and techniques to perfectly model antenna performance, particularly input impedance.

For the design of the largest and most complicated antenna structures – those made up of an array of smaller antenna elements – calibration of the individual elements is an important consideration. A secondary calibration antenna is commonly used for this purpose. The calibration antenna must have a significantly more precise *radiation pattern* than that of the individual elements. If the individual elements are equally sensitive, the intensity of the calibration antenna's signal must also be equal at all individual elements, to avoid their uneven calibration. Therefore, for calibration of a UHF circular array, an antenna was needed that displayed a consistent, *omnidirectional* radiation pattern in the azimuthal plane, while also operating in the *ultra-high frequency* band and having *horizontal wave polarization*.

To implement such an antenna, a variety of designs were considered, including simple and traditional antenna shapes, existing forms and prototypes noted for exhibiting the desired directionality, as well as less conventional structures. These configurations were then modeled and analyzed with numerical computer software to approximate their performance. The most promising design – a 5-petal wheel antenna – was then chosen based upon conformance to desired specifications and ease of implementation. A prototype was then manufactured, measured and recommendations made for optimization of the design.

The prototype fulfilled most ideal technical specifications given at the beginning of the project (see Table 1 below), although none of them perfectly. Particular emphasis was placed on omnidirectionality of the prototype antenna. Potential improvements over this final design include further prototyping to attempt to match antenna natively, without a *tuning stub*, and prototyping and physical measurement of potential design # 2 – curved crossed dipoles.

Table 1 Technical Specifications

Functional Requirement	Ideal Required Value	Final Prototype Value[2]
Frequency	420-450 MHz	≈ 465-480 MHz
VSWR	< 2:1 within band	2:1 within band
Polarization	Horizontal > Vertical by at least 20 dB in azimuthal plane	Horizontal > Vertical by more than 20dB
Pattern	Omnidirectional ± 0.25 dB	Omnidirectional ± 0.4 dB
Input power	2 kW peak (ideally)	Untested
Azimuthal power gain	≈ 2dBi	≈ -0.5dBi

1.1 Problem Statement

Commercially available horizontally polarized UHF antennas lack sufficient omnidirectionality to calibrate a circular phased array antenna.

1.2 Goal Statement

The goal of our project is to design, manufacture and measure an omnidirectional horizontally polarized transmitting UHF antenna fit for calibration.

[2] These are the measured specifications for our final prototype. With further refinement, the design could perform much better. See section 7 (p. 98) for our recommendations on how to refine this design.

2 Background

This project's primary purpose, as stated in section 1.2 above, was to design an *omnidirectional horizontally polarized UHF antenna*. The necessary researched background was subdivided into four parts: antenna engineering theory, antenna physics theory, antenna design and analysis methods, and existing designs.

2.1 Antenna Engineering Theory

This section describes the fundamental quantities and concepts associated with an antenna's functionality. These are the antenna's *radiation pattern*, *matching*, *bandwidth*, and *gain* in the position of interest.

2.1.1 Radiation Pattern

All antennas are designed to transmit or receive electromagnetic waves, usually with certain directions being optimized for stronger signal. The spatial distribution of signal strengths emitted or received by an antenna is referred to as the antenna's *radiation pattern*. Details of an antenna's geometry affect the way current flows (or stands) upon its elements' surfaces, which defines the shape of the electromagnetic field surrounding the antenna. This field, in turn, defines the radiation pattern for the given antenna. This pattern is then "a mathematical function or a graphical representation of the radiation properties of the antenna as a function of space coordinates." [2] These radiation properties may be either the magnitude of the electromagnetic field at a given radius, or (usually) the power density of radiation. Power patterns in particular may be plotted on either a linear or logarithmic (decibel) scale, with the latter being more common. [2]

Certain conventions are universally used when discussing radiation patterns and antenna geometry. A radiation pattern is gain (sometimes referred to as "power gain") as a function of

two angles, zenith/elevation angle and azimuthal angle. See section 2.1.4 below for the discussion of gain. Table 2 below and Fig. 1 below summarize the angle conventions used in this report.

Table 2 Angle Convention Definitions

Angle	Symbol	Description
Zenith angle	θ	Angle between the direction of interest and the +z axis
Elevation angle	ψ	Angle between the direction of interest and the x-y plane
Azimuthal angle	ϕ	Angle between the x-y projection of the direction of interest and the +x axis

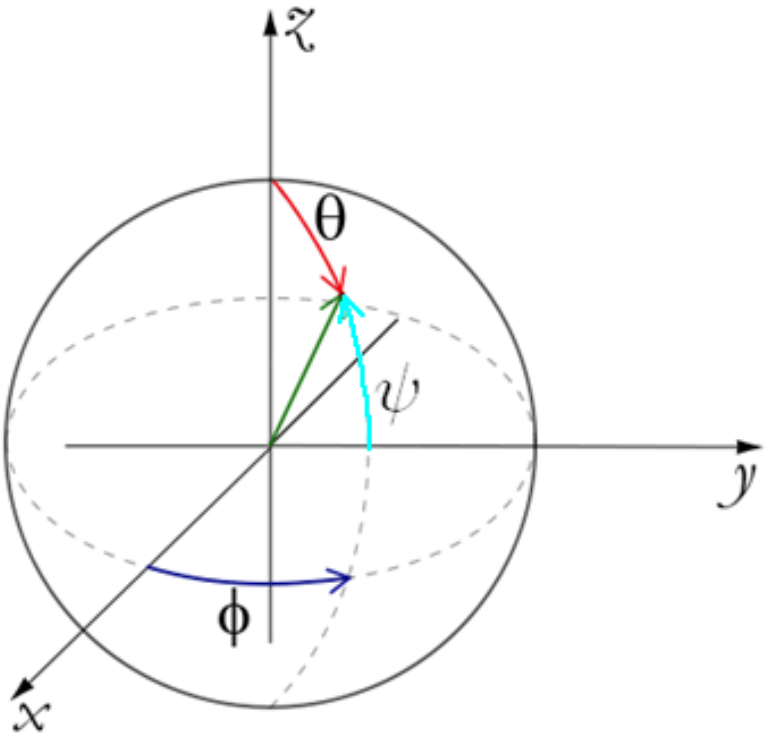

Fig. 1 Angle Convention Illustration
(adapted from [3])

Directions with $\boldsymbol{\theta \approx 90^{\circ}}$ are sometimes referred to as "azimuthal directions", and with $\boldsymbol{\theta \approx 0^{\circ}}$ - as "elevation directions". Thus, an antenna which radiates mostly perpendicular to the ground plane can be said to "radiate into elevation".

When 3D radiation patterns are plotted, they are typically plotted as surfaces defined in spherical coordinates, with the angles described according to Table 2 above and the radius being the power gain in the direction defined by those angles. Figure 2 below shows an example of such a plot, of an antenna designed for azimuthal omnidirectionality. In practice, 3D radiation pattern plots are rarely used; see section 2.3.1 below for the discussion of charts commonly used to describe antenna radiation patterns.

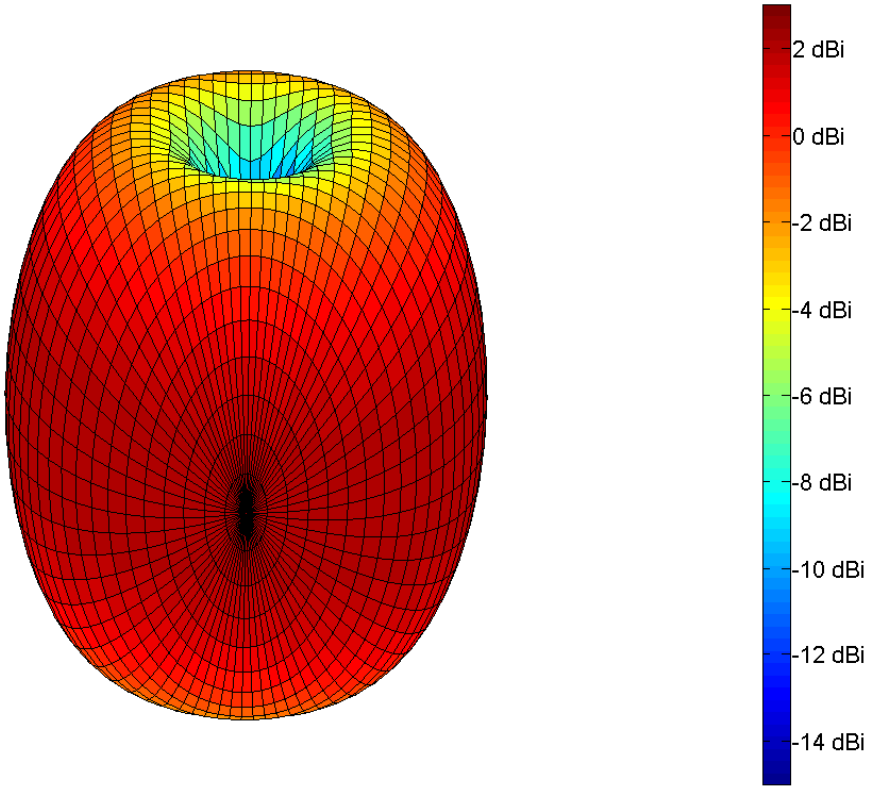

Fig. 2 Vertically Oriented Half-Wave Dipole 3D Radiation Pattern
(see section 2.1.5.2 below)

For an antenna made out of and functioning in a linear medium (such as conductive metal and vacuum or air), the radiation patterns in transmitting mode are always the same as the radiation pattern in receiving mode, as a consequence of Lorentz reciprocity theorem for linear media [2]. This principle is referred to as the radiation pattern *reciprocity* principle, and is used commonly to measure a transmitting antenna's pattern. To do so, a point directional transmitter with known characteristics can be used (in an *anechoic chamber*, to not introduce systematic error due to external sources), with the subject antenna used in receiving mode.

An important form of radiation pattern is that of the *omnidirectional antenna*. Such an antenna displays a uniform, directionally independent radiation pattern within a given plane, while having a non-uniform, directional pattern in an orthogonal plane. [2] The variation in omnidirectionality of an antenna is sometimes referred to as "*ripple*". When referring to such an antenna, its *omnidirectivity* defines the degree to which the antenna's pattern is uniform in the desired plane. Omnidirectional antennas are a subset of the directional antennas, which have "the property of radiating or receiving electromagnetic waves more effectively in some directions than in others." [2] Directional antennas are contrasted by the *isotropic radiator* which is a theoretical idealized antenna having a uniform pattern in all directions. [1, 2]

2.1.2 Matching

Any antenna acts as an element in an *RF*-circuit with some load *impedance* in the rest of the circuit. When a signal (an oscillating voltage) is transmitted or received by the antenna, the amount of power that will be transmitted or received by the antenna is a function of the difference between antenna's *input impedance* and the load impedance of the rest of the circuit. A significant difference in these impedances, also referred to as mismatch, will force most of the power to be reflected. Another (completely equivalent) way to define mismatch is as difference

between impedance toward the source and toward the load at the interface between the antenna and the transmission line.

Impedance is resistance generalized for oscillating (non-DC) currents, and is characterized not only by resistive but also by inductive and capacitive behavior of the load. It is a complex phasor, with the real part being the resistance $\boldsymbol{R}$ and the complex part being *reactance* $\boldsymbol{X}$, given by Eq. (2.1) [4]:

$$\begin{aligned} \boldsymbol{X} &= \boldsymbol{X_L} + \boldsymbol{X_C} = \boldsymbol{\omega L} - \frac{\boldsymbol{1}}{\boldsymbol{\omega C}} \\ \boldsymbol{X_L} &= \boldsymbol{\omega L} \\ \boldsymbol{X_C} &= -\frac{\boldsymbol{1}}{\boldsymbol{\omega C}} \end{aligned} \tag{2.1}$$

Where $\boldsymbol{X_C}$ is capacitive reactance, $\boldsymbol{X_L}$ is inductive reactance, $\boldsymbol{L}$ is inductance, $\boldsymbol{C}$ is capacitance and $\boldsymbol{\omega}$ is signal's angular frequency.

Impedance $\boldsymbol{Z}$ is thus given by Eq. (2.2) [4]:

$$\boldsymbol{Z} = \boldsymbol{R} + \boldsymbol{jX} \tag{2.2}$$

Where $\boldsymbol{X}$ is reactance and $\boldsymbol{R}$ is resistance.

At the interface between source and load, if impedance toward the source and impedance toward the load are unequal, the voltage wave will get reflected back, resulting in power being reflected back. *Reflection coefficient* $\boldsymbol{\Gamma}$ is used to describe this reflection; it is defined as "the amplitude of the reflected voltage wave normalized to the amplitude of the incident voltage wave". It is given by Eq. (2.3) [5]:

$$\boldsymbol{\Gamma} = \frac{\boldsymbol{Z_L} - \boldsymbol{Z_S}}{\boldsymbol{Z_L} + \boldsymbol{Z_S}} \tag{2.3}$$

In Eq. (2.3) Z_L is the impedance toward the load at the interface, and Z_S is the impedance toward the source at the interface. As seen from Eq. (2.3), Γ is a complex phasor. To convert from Γ into Z_L given Z_S Eq. (2.4) is used:

$$Z_L = Z_S \frac{1+\Gamma}{1-\Gamma} \tag{2.4}$$

One way to describe power transfer properties of an analog network is using the so called Scattering Matrix, S-matrix, or S-parameters. S-matrix is a square *n* by *n* matrix where *n* is the number of ports in the matrix. One basic parameter used to describe the degree of mismatch is S_{11}, defined as "the reflection coefficient seen looking into port 1 when all other ports are terminated in matched loads". [5] S_{11} refers to reflected power, while Γ refers to reflected voltage wave. S_{11} is typically measured in decibels (dB), and is given by Eq. (2.5) [5]:

$$S_{11} = 20 \log_{10} |\Gamma| \, dB \tag{2.5}$$

See section 2.1.4 below for a more detailed discussion of the decibel unit.

Another parameter that uniquely describes the mismatch of a load is *VSWR*, *Voltage Standing Wave Ratio*, which is the ratio of maximum to minimum peak voltage in the standing wave of a transmission line caused by reflections from impedance mismatch at a terminal. [6] *VSWR* is expressed by Eq. (2.6) [5]:

$$VSWR = \frac{1+|\Gamma|}{1-|\Gamma|} \tag{2.6}$$

Therefore, to convert from S_{11} in dB into VSWR and vice versa Eq. (2.7) is used:

$$VSWR = \frac{1 + 10^{S_{11}/20}}{1 - 10^{S_{11}/20}}$$
$$S_{11} = 20\log\left(\frac{VSWR - 1}{VSWR + 1}\right) \tag{2.7}$$

Typically, a well-matched antenna has $VSWR \leq 2:1$ within band. Impedance of the antenna is matched with transmission line supplying power to the antenna, which is normally $Z_{Line} = 50\Omega$ and is independent of frequency. Antenna impedance however is always highly frequency dependent because antenna reactance is frequency dependent (see Eq. (2.1)). Therefore, matching is often the limiting factor for antenna's operational band. Figure 3 below shows a sample VSWR vs Frequency plot of a well-matched antenna.

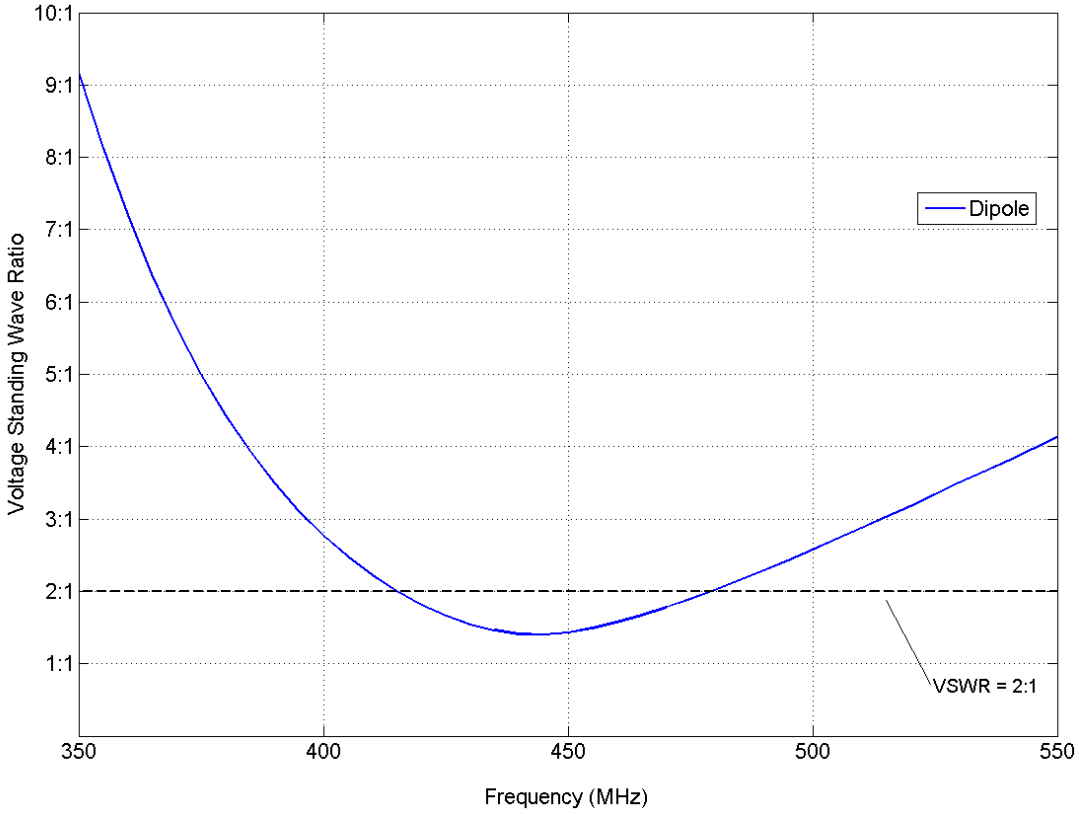

Fig. 3 Half-Wave Dipole VSWR vs Frequency Plot
(designed for $f = 435MHz$)

A useful graphical tool for displaying match as a function of frequency is the Smith chart; section 2.3.1 below discusses how to plot and use the Smith chart.

If an antenna is not natively matched, it is possible to use a matching circuit to match the antenna. Section 2.3.1 below describes several techniques for designing matching circuits. It is always possible to match any load at any specific frequency, however, the more influence the matching circuit has, the more narrow the matched bandwidth becomes. Therefore, if possible, matching circuits should be avoided, because it narrows the operational bandwidth. Also matching circuits significantly restrict the power that can be safely transferred through the antenna, because they require external circuit elements that are typically rated for much lower power than the large metallic elements of the antenna itself.

2.1.3 Bandwidth

Bandwidth is the antenna's effective operational frequency range, or band. Bandwidth is a general term, as it may be defined with respect to any of an antenna's parameters that have some dependence on frequency, and its specific form must be specified. Bandwidth is most often characterized either by a percentile deviation from a median frequency, or by a ratio of upper-to-lower frequencies, with the later being used for large bands and the former for small bands. Two bandwidth classes are generally defined to emphasize the distinction – pattern bandwidth and impedance bandwidth. [2] "Associated with pattern bandwidth are gain, side lobe level, beamwidth, polarization, and beam direction while input impedance and radiation efficiency are related to impedance bandwidth." [2] For the case of the omnidirectional horizontally polarized UHF antenna, only gain, input impedance, and polarization are of critical concern.

Often, particularly for UHF antennas, the limiting factor for input impedance bandwidth is the Voltage Standing Wave Ratio (VSWR), which is a measure of the match between the

antenna impedance and the transmission line impedance. See section 2.1.2 above for details on what VSWR is and what factors affect it. Generally, an antenna with VSWR-restricted bandwidth has nearly perfect match ($\boldsymbol{VSWR \approx 1}$) at some frequency within band, and increases as frequency gets away from the matched frequency until VSWR gets over a certain target value. That value is usually 2:1, at which about 89% of power is radiated and the rest reflected to the source.

Figure 4 below shows a typical VSWR vs frequency plot of a matched antenna, as well as the bandwidth region.

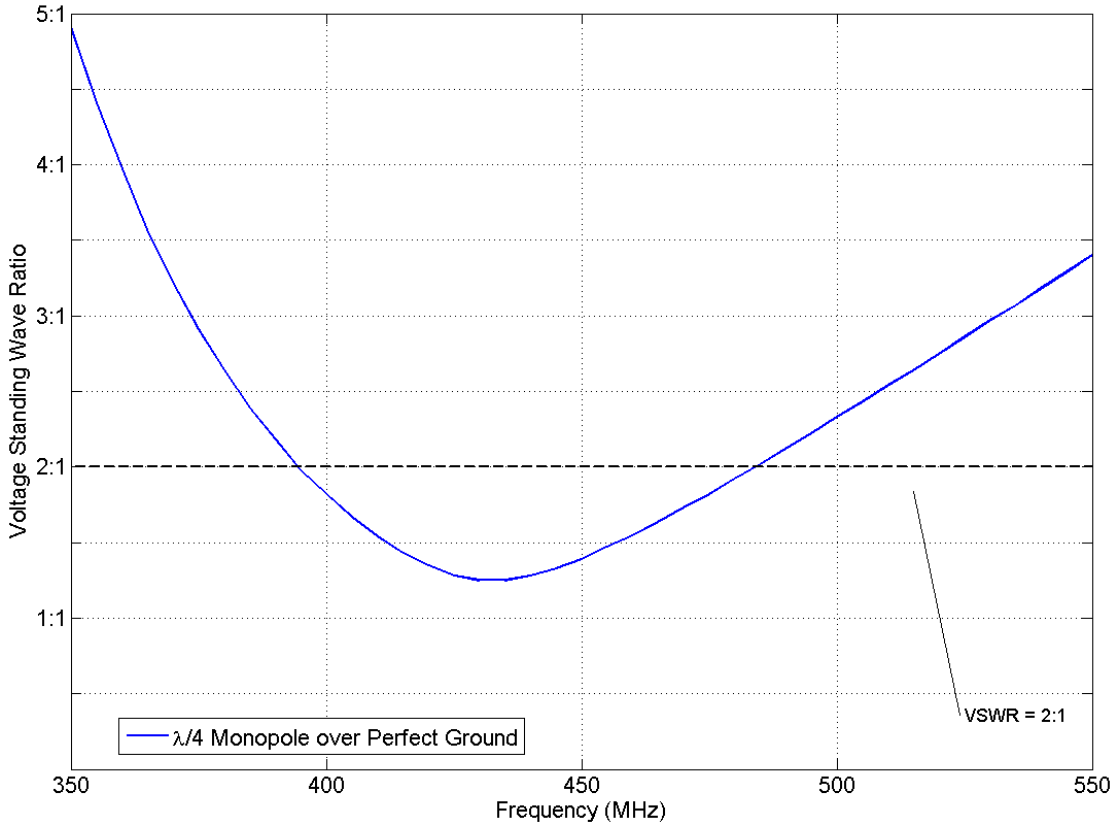

Fig. 4 Quarter-Wave Monopole VSWR vs Frequency
(match bandwidth from 395 to 480 MHz)

2.1.4 Gain

The gain of an antenna is a measure of its radiation intensity in a given direction with respect to a given input power, and without consideration for losses incurred due to power dissipation, impedance and polarization mismatches. Gain is calculated as Eq. (2.8):

$$G(\theta,\phi) = 4\pi\frac{U(\theta,\phi)}{P_{in}}, \tag{2.8}$$

where $U(\theta,\phi)$ is radiation intensity and P_{in} is total input power. In contrast, *absolute gain* takes these losses into consideration, but is otherwise equivalent. Gain relates closely to *directivity*, which is purely a measure of an antenna's directive properties, whereas gain additionally measures its radiation efficiency. [2] Gain is a dimensionless quantity normally measured in decibels (dB), which is a relative scale, so in practice it must be given with respect to some reference. Gain in decibels is given by Eq. (2.9):

$$G_{dB} = 10\log_{10}\left(\frac{G}{G_0}\right) \tag{2.9}$$

Where G_{dB} is the gain in decibels, G is the gain and G_0 is the reference gain. The most common reference is that of an isotropic radiator, a theoretical antenna assumed to radiate equally in all directions (see section 2.1.1 above). The units for gain with this reference are decibels over isotropic radiator, dBi. Specifically, a gain of n dBi in a given direction means that the antenna radiates $10^{\frac{n}{10}}$ times more power in that direction than an isotropic radiator would.

Although the isotropic radiator provides a simple and ideal reference, it is not physically possible to build such an antenna. Thus, a variety of more practical antennas are often used as a gain reference. In particular, the half-wave dipole is often used; the units for gain with this

reference are decibels over dipole (dBd). See section 2.1.5.2 below for information about half-wave dipoles.

In practice, an antenna's absolute gain is the same as antenna radiation pattern, calibrated to a gain standard (normally a half-wave dipole antenna, because its radiation properties are well known). It corresponds to the S_{21} scattering matrix parameter, and is measured by connecting the transmitter and receiver to a network analyzer, orienting the antenna in desired position and sending a signal. See section 2.1.2 above for information on the scattering matrix parameters. It is important to note that S_{21} corresponds to the absolute gain, and thus takes into account antenna imperfections, such as impedance and polarization mismatches and power dissipation.

For the omnidirectional UHF calibration antenna which was the goal of this project, gain is not a critical parameter. However, it is important that antenna's highest gain is in the direction of interest (azimuthal), otherwise a lot of power is wasted and, more importantly, pattern becomes significantly less reliable.

2.1.5 Fundamental Antennas

Certain fundamental antenna geometries exist. In this section, some of the simplest and most common antenna structures are examined, and their characteristic radiation patterns considered.

2.1.5.1 Monopole Antenna

The monopole is a simple antenna generally consisting of a single terminated wire constructed above an electromagnetically reflective imaging plane. Regardless of the physical geometry of the antenna, the desired effect is to "produce a radiation pattern approximating that of an electric dipole in the half-space above the imaging plane." [1] In practice, that imaging plane is usually the conductive ground, serving as the other half of the half-wave dipole (see

section 2.1.5.2 below for information on dipoles). Radio tower transmitters and hand-held radio antennas are common examples of monopole antennas. Figure 5 below shows an example of a monopole antenna.

Fig. 5 DVB – T Monopole Antenna Photograph
(from [7])

Monopole antennas have an omnidirectional pattern in the azimuthal plane. However, assuming horizontal azimuthal plane, their signal is vertically polarized, thus making this antenna completely unfit for this project's purposes. Since the monopole is intended to act as half of a half-wave dipole, typical monopole is a quarter wavelength of its intended frequency. Figure 6 below shows a simulated radiation pattern of a quarter-wavelength monopole antenna.

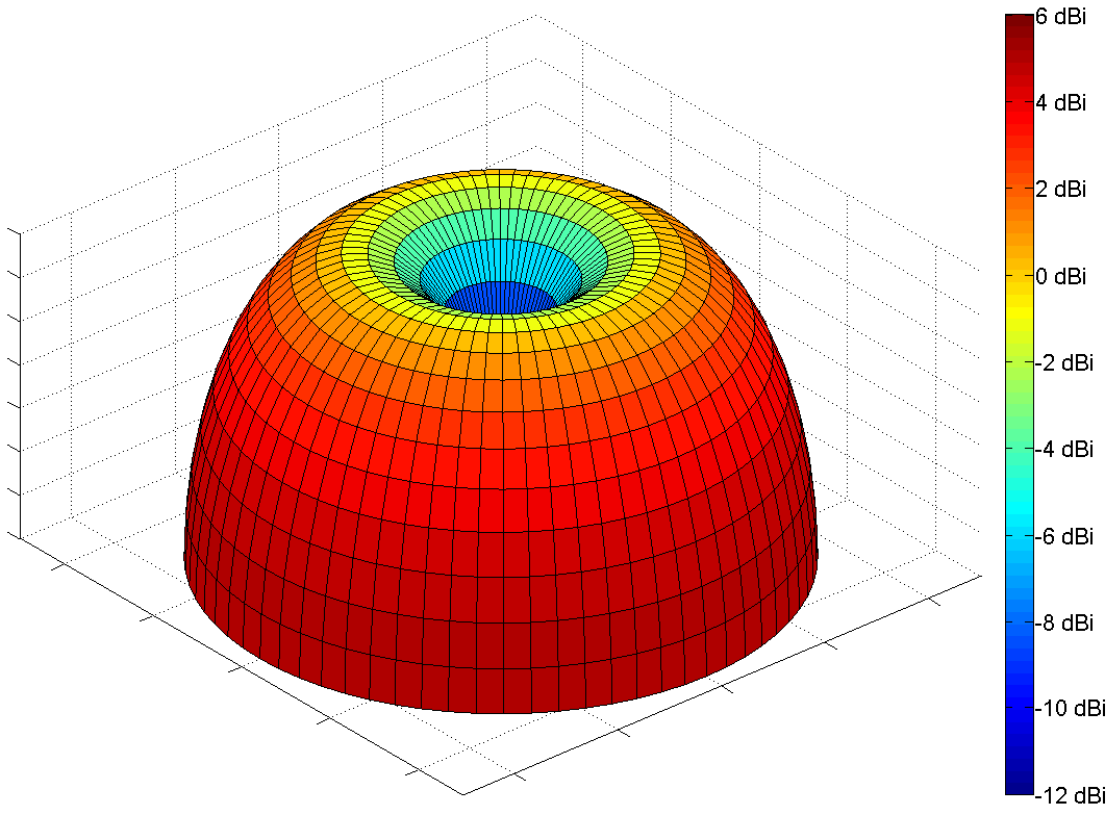

Fig. 6 Quarter-Wave Monopole Simulated 3D Radiation Pattern
(perfectly conductive infinite ground)

2.1.5.2 Dipole Antenna

Another simple, but commonly used antenna is the dipole antenna. Specifically, the dipole antenna is "any one of a class of antennas producing a radiation pattern approximating that of an elementary electric dipole." [1] The general form for such an antenna is "a metal radiating structure that supports a line current distribution similar to that of a thin straight wire so energized that the current has a node only at each end." [1] Figure 7 below shows an example of a UHF dipole antenna in the azimuthal plane.

Fig. 7 UHF Half-Wave Dipole Photograph
(from [8])

Dipoles are generally characterized by the length of the flared elements in terms of fractions of wavelengths for the given operational frequency. As mentioned in Section 2.1.4 above, the dipole antenna's ubiquity, simplicity, and consistency of radiation pattern has resulted in it being used as a common reference point against which other antennas may be compared. Figure 8 below shows a half-wave dipole's simulated three-dimensional radiation pattern.

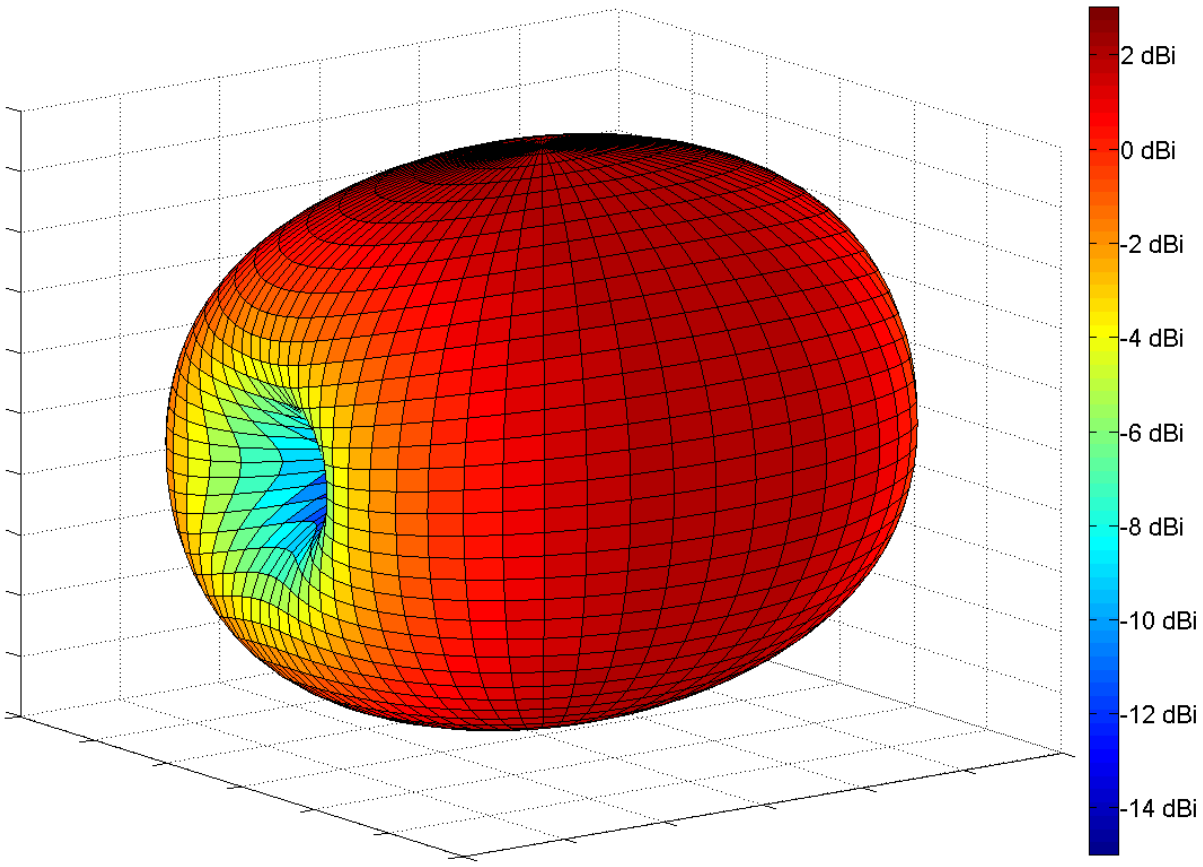

Fig. 8 Horizontally Oriented Half-Wave Dipole Simulated 3D Radiation Pattern

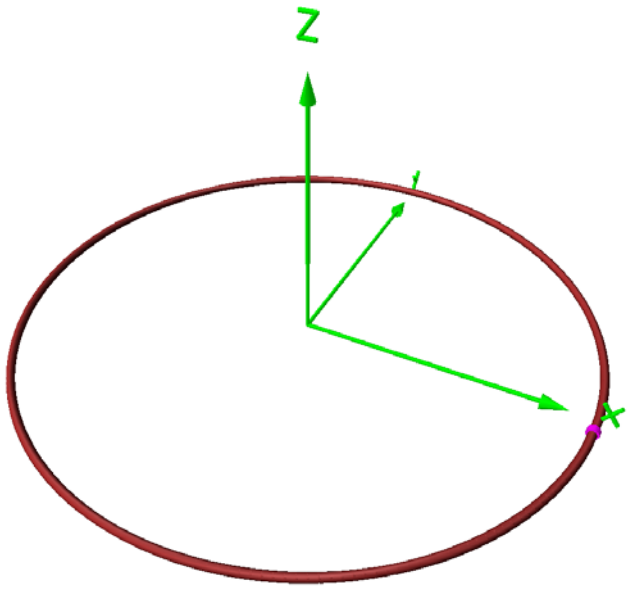

Fig. 9 Resonant Circular Loop 3D Rendering
(designed for $f = 435MHz$)

2.1.5.3 Loop Antenna

A loop antenna is simply any "antenna whose configuration is that of a loop." [1] The geometry of that loop may "take many different forms such as rectangle, square, triangle, ellipse, circle, and many other configurations." [2] Loops are generally characterized by their circumference, and categorized as either being electrically small or near-resonant. Small loops have relatively high azimuthal gain and produce near-omnidirectional toroidal radiation patterns much like those of small dipoles. In contrast, near-resonant loops tend to have the maximum of their radiation pattern along an axis normal to the plane of the loop, and not in the azimuthal plane. [2]

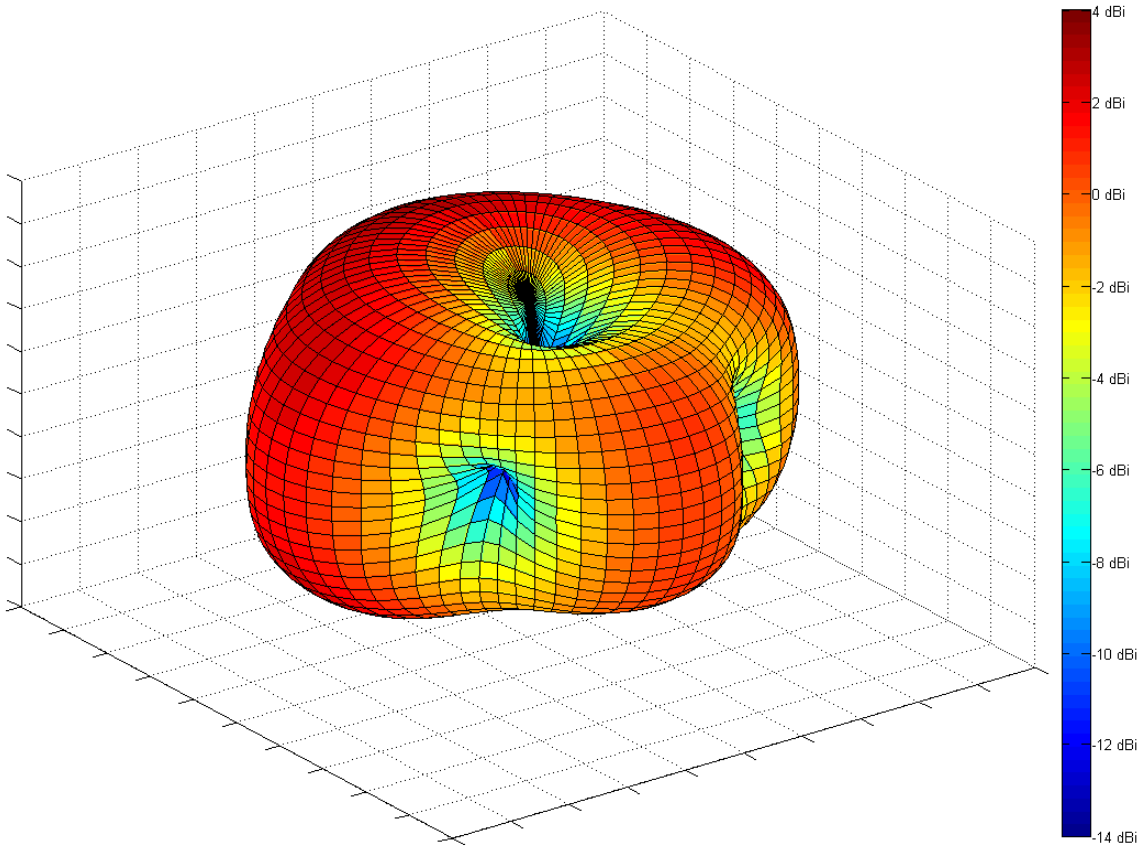

Fig. 10 Resonant Loop Antenna Simulated 3D Radiation Pattern
(circular loop, $f = 435MHz$)

Figure 9 above shows the geometry of a resonant loop antenna. Figure 10 above shows the 3D radiation pattern of a resonant circular loop. Resonant loop antennas are not omnidirectional. The problem with electrically small loops is that they approximate a zero-resistance $N = 1$ inductor, and thus require a highly capacitive matching network.

2.1.5.4 Electrically Small, Electrically Large and Resonant Antennas

Electrically small antennas are those with an overall circumference or radiator length of approximately $\frac{1}{10}\lambda$ or less. Electrically large antennas have a circumference or radiator length of approximately one wavelength. Resonant antennas are those antennas constructed such that the electric current in the antenna structure will resonate, thus existing in a standing wave on the radiator's surface.

Electrically small antennas' patterns approach omnidirectionality. However, they typically require a matching circuit, as natively their input impedance is very low and inductive in nature. Resonant antennas tend to have much better matching but are usually not omnidirectional.

2.2 Antenna Physics Theory

This section describes the physics involved in the function of transmitting and receiving antennas, including the theory of electromagnetic waves, oscillating current and RLC circuits.

2.2.1 Electromagnetic Wave Theory

Electromagnetic wave theory is the core principle underlying the operation of all antennas. In applications involving antennas electromagnetic waves are produced by alternating ("signal") currents flowing through conducting elements. Currents produce electromagnetic fields about them, and these fields change in magnitude and direction as the current changes.

Thus, when a sinusoidal alternating current is applied to an antenna element, the associated current within the conducting element creates an electromagnetic field that also oscillates sinusoidally, and at the same frequency as the current. However, as the changes in this field may not occur instantaneously, the changing field propagates away from the element at the speed of light as an electromagnetic wave. [9] The electric and magnetic fields of this wave are dependent on each other as the wave propagates. As the magnetic field "varies sinusoidally, it induces (via Faraday's law of induction) a perpendicular electric field that also varies sinusoidally." [9] Likewise, as the electric field oscillates, "it induces (via Maxwell's law of induction) a perpendicular magnetic field that also varies sinusoidally." [9]

An important characteristic of electromagnetic waves that has a large impact on antenna and radar design is the *polarization of the wave*. The polarization of a given wave is defined by the orientation of the oscillations of its electric field component. [9] Specifically, polarization is characterized by "the curve traced by the end point of the vector representing the instantaneous electric field." [2] Polarization is given as the shape of this trace, being elliptical, circular, or linear. The polarization of an antenna is directly equivalent to the polarization of the electromagnetic wave it transmits, or that of the incident radiation it is capable of receiving. [2] Figure 11 below illustrates a horizontally polarized electromagnetic wave.

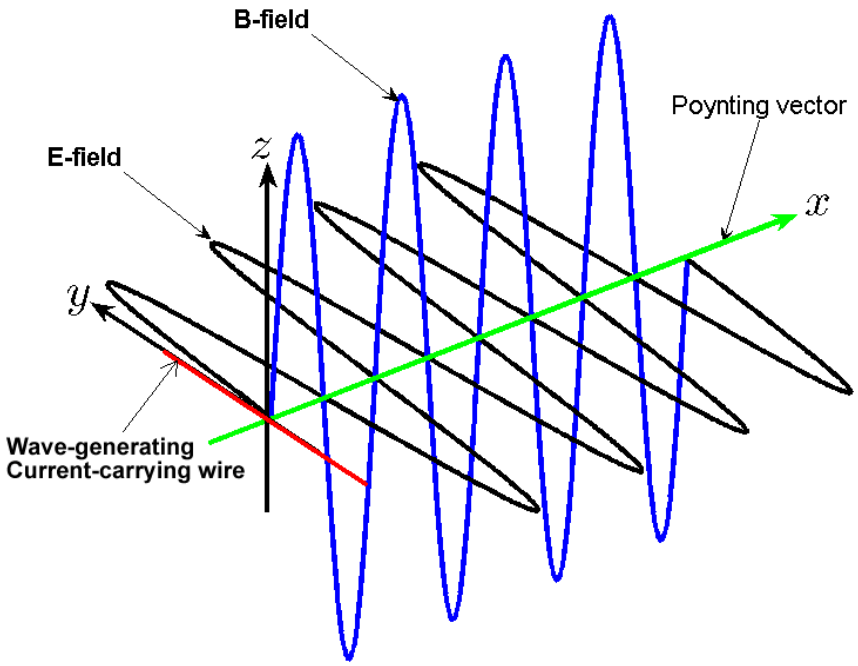

Fig. 11 Horizontally Polarized Electromagnetic Wave's Electric Field

Linear polarization is most commonly associated with antennas whose elements are simple conducting wires. This results directly from the generation of the electromagnetic wave. [2] Electromagnetic waves at any point along the wave's path are described by three mutually orthogonal vectors – the electric and magnetic fields, and the wave's propagation vector. For a wave generated by a wire element, the propagation vector (parallel but not equivalent to Poynting vector, the vector characterizing the direction and rate of energy transfer) shall point normal to the wire's surface, as the wave radiates directly away from the wire. By the Biot-Savart law, the magnetic field shall form concentric rings about the wire, with the field vector tangent to the wire at any given point (assuming straight wire), and superimposed if the wire is curved. The electric field vector must be orthogonal to both of these other vectors, thus it must point parallel to the length of the wire – meaning the electromagnetic wave shall be polarized along the same direction as the length of the wire. Reciprocally, for an incident wave to induce a current in a receiving wire the wire and electric field must again be parallel, else the electric field

could not force electrons to move along the length of the wire, producing a current (and thus, a signal to be received). See Ref. [9] for a more complete discussion of Biot-Savart Law and field orientation relative to current-carrying wires. See Fig. 11 above for an illustration of the waves formed by a straight wire.

Ground planes play a significant role in antenna design as they affect the pattern even without being connected directly to the antenna. Specifically, they act as reflectors. Parallel E-fields across an interface (such as the ground plane) must be equal [10], thus on the surface of a conducting ground plane the E-field tangent to the plane is zero. Since horizontally polarized antennas have the E-field oriented in the horizontal plane, their signal cannot travel along the surface of the horizontal ground plane, and is instead reflected to conserve energy. Vertically polarized waves have zero horizontal E-field, and thus can travel along the surface of the ground plane instead of being reflected. Due to the ground planes' reflective nature for horizontally polarized waves they can be used to transfer some gain from elevation into azimuthal directions.

2.2.2 Oscillating Current Theory

Generally, an oscillating current is any current that varies as a function of time. In context of antennas, and most other engineering applications, an oscillating current on a transmission line is formed by a periodically oscillating voltage across that line. This oscillating voltage varies as a periodic wave about a given zero, which is the potential level of the ground. In a current-carrying RF transmission line one wire is normally labeled "hot", and the other one "ground", with the oscillating voltage varying as a function of that current.

RF transmission lines are commonly drawn using convention shown in Fig. 12 below:

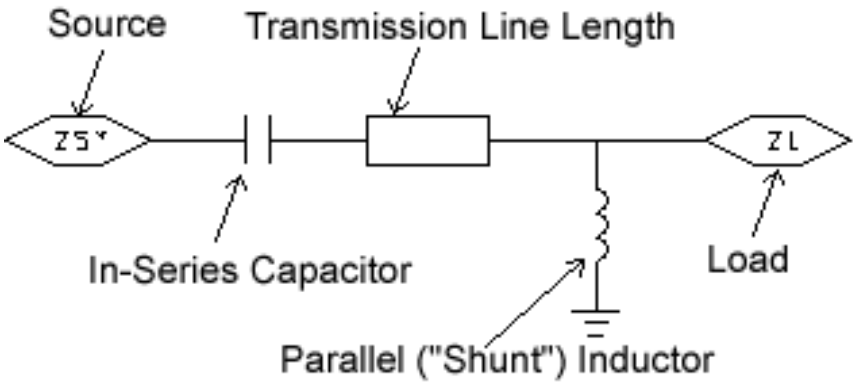

Fig. 12 Transmission Line Illustration
(using ADS 2006a Smith Chart Tool [11])

These schematics are usually used for designing matching networks, as any point on the schematic has an impedance which can be calculated. Normally, impedances toward the load and toward the source at the point right before the load (the antenna) are calculated, as those define the antenna's mismatch (see section 2.1.2 above). All of the shunt elements in the schematic are really in parallel with the load in the circuit.

Sinusoidal periodic oscillating voltage varies as a function of time; see Eq. (2.10):

$$v(t) = V_{peak}\cos(\omega t + \theta) \tag{2.10}$$

In Eq. (2.10), $v(t)$ is voltage as a function of time, V_{peak} is peak voltage, ω is angular frequency of the oscillations and θ is the phase angle. When such a voltage is put across a resistor R, the average power transferred through that resistor is a function of v_{rms}, root-mean-square voltage; see Eq. (2.11):

$$v_{rms} = \sqrt{\frac{1}{T}\int_0^T v^2(t)\,dt} \text{ with } T = \frac{2\pi}{\omega} \tag{2.11}$$

In Eq. (2.11) T is the period of oscillations. For the sinusoidal voltage of Eq. (2.10), v_{rms} becomes Eq. (2.12):

$$v_{rms} = \sqrt{\frac{1}{T}\int_0^T V_{peak}^2 \cos^2(\omega t + \theta)\, dt} = \frac{V_{peak}}{\sqrt{2}} \tag{2.12}$$

Therefore the average power transferred across a resistor is given by Eq. (2.13):

$$P_{avg} = \frac{v_{rms}^2}{R} = \frac{V_{peak}^2}{2R} \tag{2.13}$$

A more detailed discussion of sinusoidal currents and voltages as well as whether or not they lag lead one another (an effect known as transient current) and all of the equations of this section is given in Ref. [4].

It is important to note that all of the current travels only on the surface of the conductor [10], therefore, in modeling and analysis, as well as construction, only surfaces of the solid shapes have to be considered. That leads to using thin hollow copper pipes instead of solid pipes in construction of antennas to save money, as copper is a relatively expensive material used a lot in antenna construction due to good conductivity. Notice, however, that thin strips should not be used in high power applications, as too much heat will be dissipated and they will get thermally damaged.

2.3 Antenna Design and Analysis Methods

Antenna modeling and design is a relatively new (less than 200 years old) and constantly evolving field. This section describes several techniques for antenna modeling that were used in this project. Section 2.3.1 below discusses several charts that are used as illustrative graphical tools in antenna design as they provide insight into various parameters of the antenna. Section 2.3.2 below discusses an FEA (Finite Element Analysis) technique called Method of Moments (MoM) for numerical calculations of antenna performance. Section 2.3.3 below discusses NEC-

2, Numerical Electromagnetics Code, which is a software package that uses MoM for antenna modeling.

2.3.1 Descriptive Charts

Two types of non-standard plots are commonly used in antenna engineering. Radiation pattern plots, the theory of which is discussed in section 2.1.1 above, are the first type. There are three basic ways to present radiation pattern of an antenna: 3D radiation pattern plot, polar radiation pattern plot and rectangular radiation pattern plot. The other plot used to characterize impedance mismatch is the Smith chart. These are discussed in detail in sections below.

2.3.1.1 3D Radiation Pattern Plot

On a 3D plot the pattern is typically shown for only one frequency. It shows a three-dimensional surface defined in terms of direction angles (see section 2.1.1 above and Table 2 above) and gain in dBi or dBd as a function of direction acting as the distance from the origin in that direction. See Fig. 2 above or Fig. 6 above for examples of 3D radiation pattern plots. It is important to note that while antenna gain can be negative (and any real antenna's gain is negative in some direction), distance from the origin is always positive, and the conversion is made by offsetting the gain by a value such that the most negative value of gain is zero. This is illustrated in both Fig. 2 above or Fig. 6 above. 3D radiation pattern plots are used to generally demonstrate where the antenna's radiation goes, and are not typically used to demonstrate antenna's exact performance, as they are (by definition) isometric and thus less accurate.

2.3.1.2 Polar Radiation Pattern Plot

Polar radiation pattern plots show the antenna's performance at one or multiple frequencies, in a specific plane. Gain is represented by the distance from the origin, corrected the same way it is for 3D radiation pattern plots. If the plane is defined in terms of a fixed zenith

angle and a range of azimuthal angles the plot is named "azimuthal pattern at $\theta = \ldots$". If the plane is defined in terms of a fixed azimuthal angle and a range of zenith angles the plot is named "elevation pattern at $\phi = \ldots$". Polar radiation pattern plots can show horizontal, vertical, or total gain.

2.3.1.3 Rectangular Radiation Pattern Plot

Rectangular radiation pattern plots are completely equivalent to polar radiation pattern plots. Gain is typically plotted on the y-axis and variable angle (azimuthal angle for azimuthal pattern and zenith or elevation angle for elevation pattern) on the x-axis. Like polar radiation pattern plots rectangular radiation pattern plots can show horizontal, vertical, or total gain.

2.3.1.4 Smith Chart

Another useful plot that is often seen in RF engineering and matching networks in particular is the Smith chart. The Smith chart is a polar plot of the complex reflection coefficient $\boldsymbol{\Gamma}$, the theory of which is discussed in section 2.1.2 above. Figure 13 below shows an example of a Smith chart demonstrating the matching characteristics of a λ/2 dipole.

The values plotted on the Smith chart are the reflection coefficients as a function of frequency. The frequency is not explicitly shown anywhere on the chart. A well-matched load will have most of its reflection coefficients close to the center of the chart, where $|\boldsymbol{\Gamma}| \approx \mathbf{0}$. $|\boldsymbol{\Gamma}|$ is represented by the distance from the center on the Smith chart. The zone where the load is matched is marked by a green circle about the origin, this is the circle of $\boldsymbol{VSWR \leq 2:1}$ or $|\boldsymbol{\Gamma}| \leq \frac{\mathbf{1}}{\mathbf{3}}$.

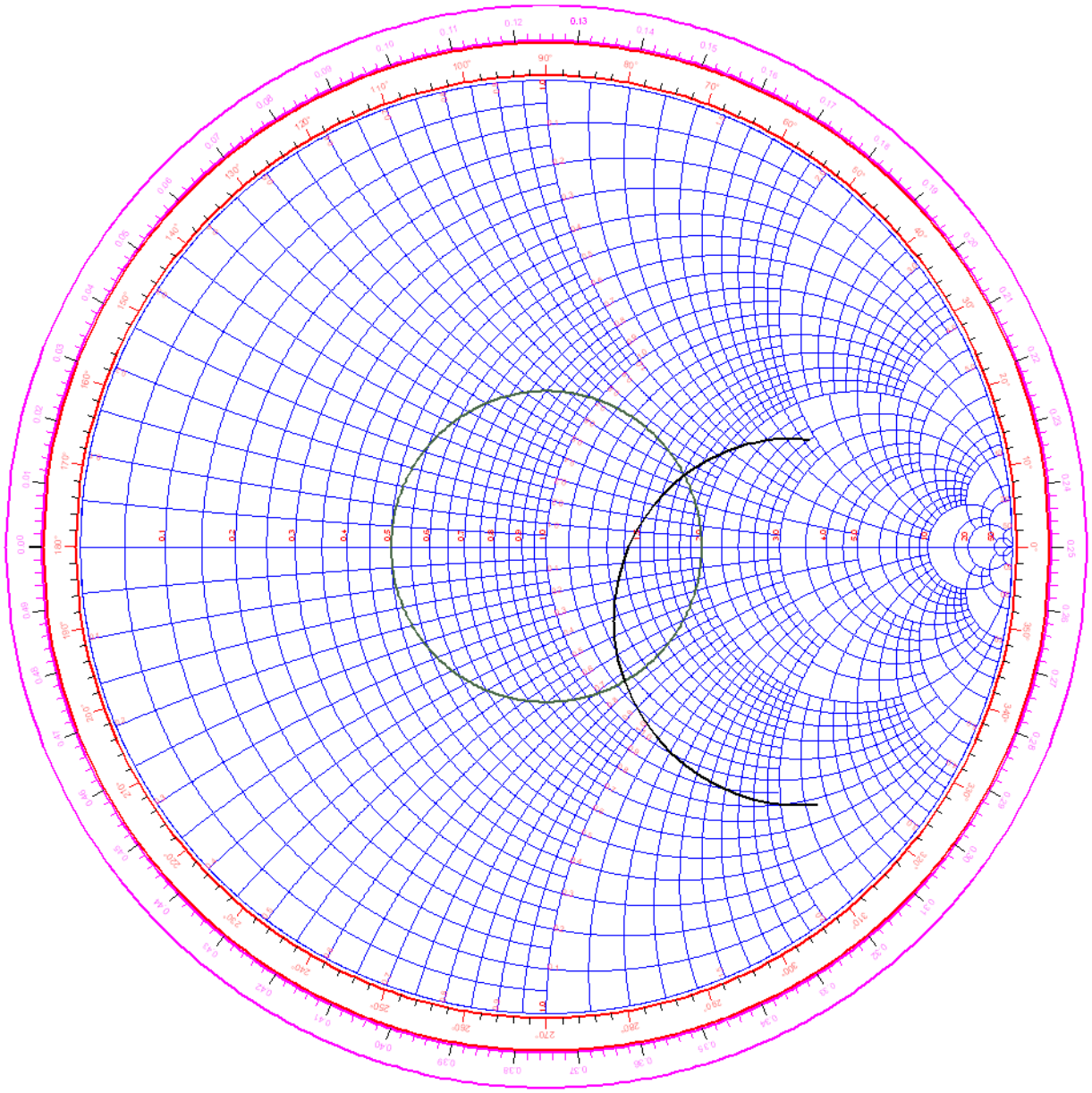

Fig. 13 Half-Wave Dipole Smith Chart
($f \in [350, 550]\,MHz$)

The other curves plotted on the Smith chart represent lines of constant normalized resistance and reactance. A detailed discussion of the nature of these lines is presented in Ref. [12] but is not necessary in this document. Primarily this document makes use of the Smith chart to show the nature of the mismatch (i.e., whether it's due to the load being highly inductive or capacitive, etc.).

2.3.2 Method of Moments

Numerical modeling of antennas is almost always done using a Finite Element Analysis (FEA) method called Method of Moments (MoM). Method of Moments relies on numerically solving the MoM Integral Equation (2.14) over a spherical surface:

$$\boldsymbol{P_{rad}} = \frac{\mathbf{1}}{\mathbf{2}} \oiint_{\boldsymbol{S}} \mathbf{Re}[\,\boldsymbol{E} \times \boldsymbol{H}^{*}\,] \cdot \boldsymbol{ds} \tag{2.14}$$

Where $\boldsymbol{P_{rad}}$ is the average radiated power, $\boldsymbol{E}$ is the electric field vector and $\boldsymbol{H}^{*}$ is the complex conjugate of auxiliary magnetic field. These fields are computed individually based on breaking up antenna's structure into finite size elements and calculating dipole moments between those elements. $\boldsymbol{P_{rad}}$ can then be converted into $\boldsymbol{G(\theta,\phi)}$ (Gain as a function of direction) by Eq. (2.15)

$$\boldsymbol{G(\theta,\phi)} = \frac{\boldsymbol{4\pi U(\theta,\phi)}}{\boldsymbol{P_{in}}} = \boldsymbol{e_{cd}}\left[\frac{\boldsymbol{4\pi U(\theta,\phi)}}{\boldsymbol{P_{rad}}}\right] \tag{2.15}$$

Where $\boldsymbol{U(\theta,\phi)}$ is radiation intensity as discussed in section 2.1.4 above, $\boldsymbol{P_{in}}$ is the power input, and $\boldsymbol{e_{cd}}$ is radiation efficiency which is a function of free space and antenna geometry.

The restrictions of MoM are typically not due to the equations presented in this section, but rather due to the meshing algorithms. Different codes, for example, NEC, RWG, WIPL-D and others, use different meshing algorithms which require varying processing power and thus impose varying limitations. MoM itself is, in theory, limitless in accuracy. [2]

2.3.3 Numeric Electromagnetics Code

NEC-2 is one of the oldest antenna modeling packages. It employs Method of Moments as discussed in section 2.3.2 above, and one of its restrictions is that it requires the user to

manually create the mesh of finite elements. The other, more important restriction, is that NEC's geometry input only accepts straight wires, and thus approximating curves as sequences of straight elements and surfaces as grids is required. Curve approximation is not usually a big problem, however, when surfaces (particularly close together) are parts of an antenna's geometry NEC-2 can fail to accurately model the antenna. Such antennas are better modeled using more modern codes such as WIPL-D, Ansoft HFSS and others which employ automated Delaunay triangulation instead of straight wire segmentation for creating the mesh. [2, 13]

In this project, NEC-Win Pro v1.6 by Nittany Scientific [14] was used to implement NEC-2. NEC compiler accepts ASCII code generated by hand or using MATLAB and then runs NEC's algorithms to execute MoM on the input geometry. It is interesting to note that NEC-2 dates back to mainframe computers so lines in its input files are called "cards".

2.4 Existing Designs

Prior to beginning of this project there existed a design that was claimed by manufacturer to achieve required omnidirectionality. This design was a 3-petal wheel, similar to the one in Fig. 14 below. Tapered chamber measurements indicated that the design does not meet the requirements for omnidirectionality and a similar, better manufactured prototype was manufactured in tested. Figure 14 below shows this prototype.

Fig. 14 Group 39 3-Petal Wheel Prototype Photograph[3]

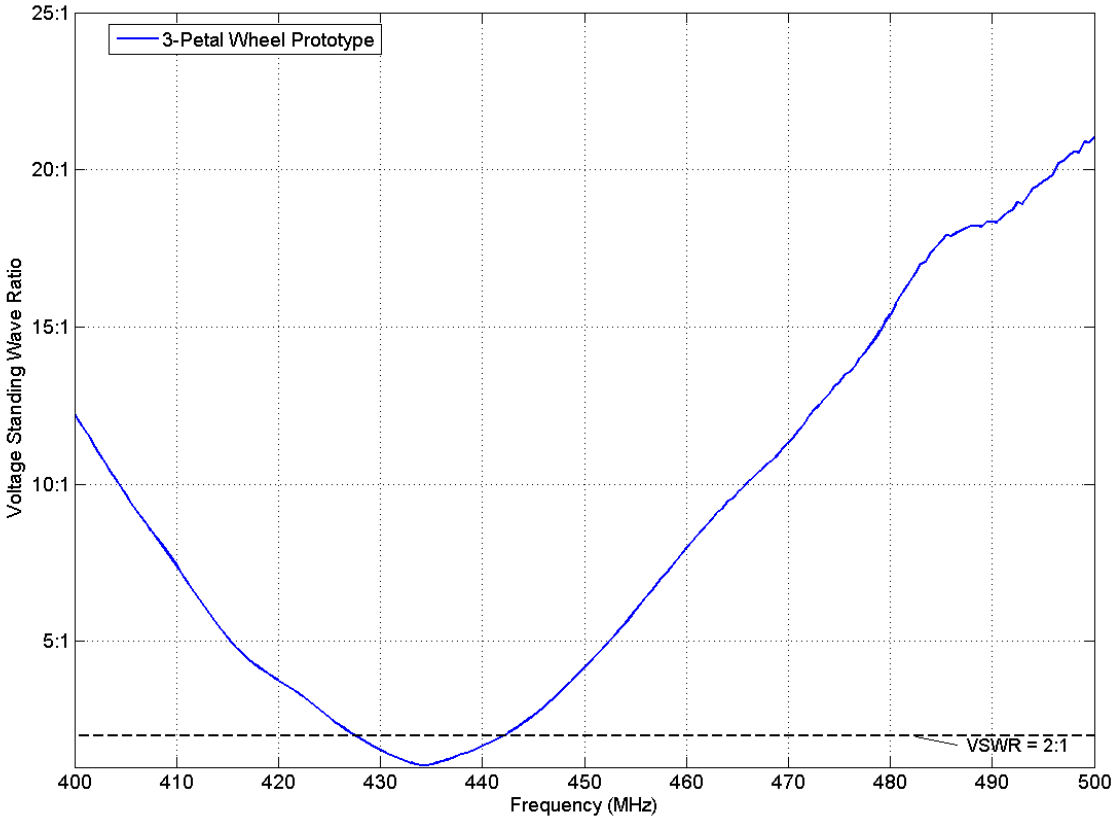

Fig. 15 Group 39 3-Petal Wheel Prototype Measured Match

[3] This photograph was taken by David Bruno of MIT Lincoln Laboratory.

However, this prototype, while matched (see Fig. 15 above) for VSWR vs Frequency plot) did not meet the requirements for omnidirectionality. Figure 16 below shows the prototype's measured pattern. The prototype's measurements were used to confirm modeling accuracy.

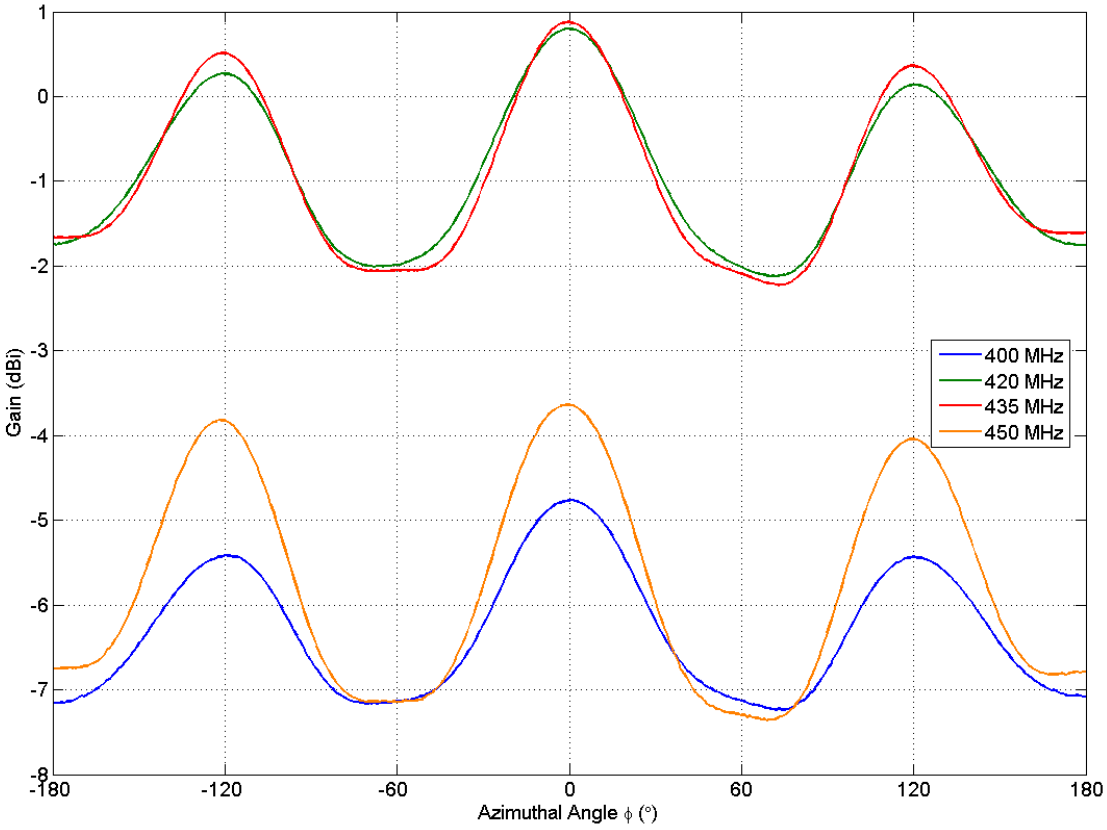

Fig. 16 Group 39 3-Petal Wheel Prototype Measured Azimuthal Pattern

We found several other designs, although none commercially available, that suggested omnidirectionality. However, since they were not commercial samples and were rather just manufactured by radio amateurs, no reliable radiation patterns were available.

2.5 Background Summary

Antenna modeling is a complex and sometimes unreliable discipline. However, it is required prior to prototyping stage to produce an antenna that has approximately right characteristics, although fine-tuning is more of a trial and error process. The background research we conducted prior to this project that is presented in this chapter was used as the basis for nearly all of the procedures conducted throughout this project.

3 Simulation and Measurement Methods

To design the omnidirectional horizontally polarized UHF antenna three objectives were outlined. These are:

1. To simulate potential designs to pick the optimal type.
2. To analyze the optimal type in detail and create prototype dimensions.
3. To manufacture, measure and optimize the prototype.

The methods used to achieve each objective are explained below.

3.1 Potential Designs

The first step of this project involved simul1ating several different antenna designs to pick the optimal type so that detailed design could later be conducted. Simulations were conducted using MATLAB codes that took *structural design parameters* of antennas as inputs and generated NEC-2 code describing the antenna. At this stage, each simulation simplified the antenna geometry to some degree, to make the running and coding of the simulations faster.

Section 2.4 above describes the background data available prior to these simulations. We concluded that the following designs had to be simulated in detail:

- Electrically small circular loop
- Curved dipole cross
- "Big wheel"

Stacked wheel antennas were not simulated at this stage because of potential mechanical difficulties in providing a feed signal to both antennas; instead, stacking was used for curved dipole cross simulation and left as a backup measure for the "big wheel" should the single-element antenna fail to meet specifications. Throughout all initial potential design simulations the following assumptions and were held constant:

Table 3 Constant Design Parameters

Quantity	Symbol	Assigned value
Wavelength[4]	λ	$\lambda_{f=435MHz} = \frac{c}{f} = 0.689m$
Wire diameter[5]	WD	$WD = 1/4\ in$
Material Conductivity	σ	$\sigma_{copper} = 5.8001 \times 10^7 \frac{S}{m}$

Details of each initial simulation are given below.

3.1.1 Electrically small circular loop

One of the difficulties with simulating an antenna with a curved wire element using NEC-2 is that NEC-2 only allows for straight wires. Therefore, regressions of the loop using minimum-length straight wires were used for all curves in all of the models simulated. Wire length was restricted as NEC-2 cannot effectively simulate wires shorter than their diameter [15]. Another difficulty was that the connector for a circular loop (that the coaxial transmission line

---

[4] In every simulation, wavelength λ was corrected with an input correction factor CF (typically $CF \in [0.75, 1.25]$, but for electrically small antenna $CF \leq 0.2$). λ given here is the base λ that was then corrected.

[5] Wire diameter was kept constant because it was planned from the start to make the antenna wires out of $1/4\ in$ diameter copper tubing. The primary reason for this is ease of manufacturing and material availability; the only performance parameter that wire diameter typically affects the most is bandwidth.

would connect to) would have to be installed on a straight segment part of the loop, thus introducing asymmetry into the antenna's geometry.

Appendix A (p. 110) contains the description of MATLAB code for creating the NEC-2 file that describes the electrically small circular loop (ESCL)[6]. Figure 17 below shows the geometry of the simulated model.

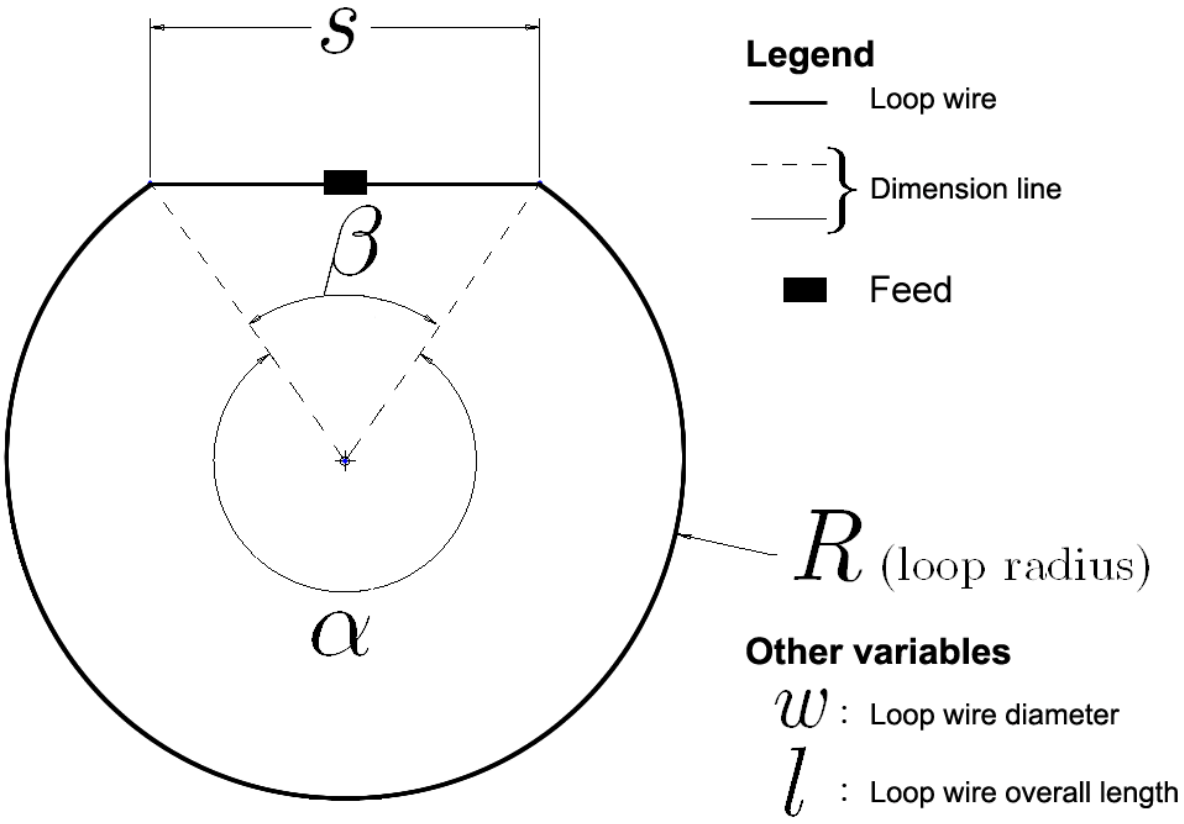

Fig. 17 Electrically Small Circular Loop Geometry

The geometry was computed based on the input variables in Table 4 below:

[6] From this point on, the acronym ESCL is used in this report to refer to an electrically small circular loop.

Table 4 Electrically Small Loop Simulation Values

Variable	Units	Description	Values simulated
l	in	Overall length of the loop together with the straight interval	0.075λ, 0.1λ, 0.2λ
s	in	Length of the straight interval with the feed	1 in

Due to the loop's simple geometry it only had two structural design parameters, and one of them (the length of the straight interval with the feed connector on it) was kept constant at $s = 1in$, because it would very difficult to make a connector that was smaller, and a larger connector would introduce more asymmetry into the antenna geometry.

Appendix A (p. 110) contains the equations used to calculate the geometric variables (α, β and R), which were not design parameters.

Section 4.1 (p. 44 below) contains the results and the outcome of the ESCL simulation.

3.1.2 Curved dipole cross

Originally, a curved monopole cross (CMC)[7] similar to that in Fig. 18 below was considered.

We declined the CMC design due to completely unacceptable impedance match. However, after prototyping has started we (by accident) realized that monopoles and monopole arrays are physically impossible without a reflective and conductive ground. See section 2.1.5.1 (p. 14) for more information about how monopoles operate. This fact rendered CMC physically meaningless.

[7] From this point on, the acronym CMC is used in this report to refer to a curved monopole cross.

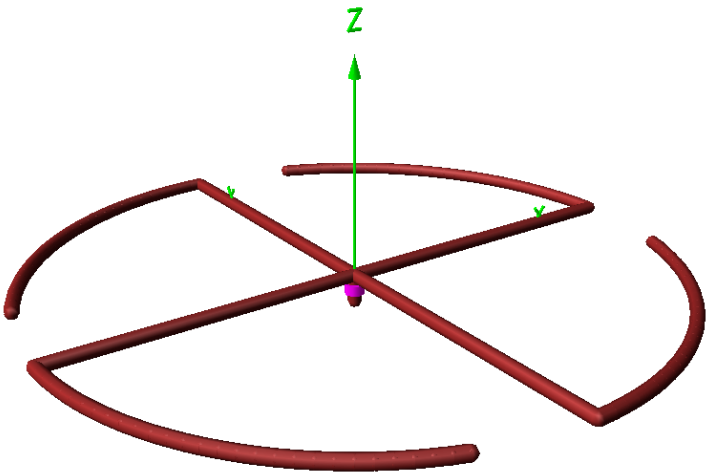

Fig. 18 Curved Monopole Cross 3D Rendering

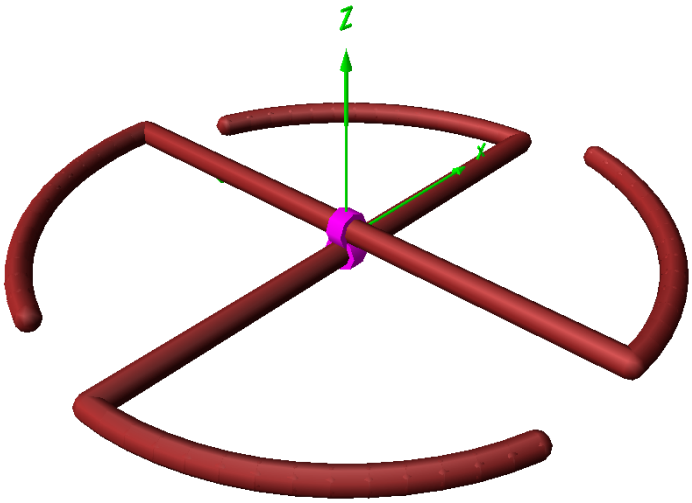

Fig. 19 Curved Dipole Cross 3D Rendering

However, we then modeled a mechanically similar but electrically different configuration which was the curved dipole cross (CDC)[8]. It consists of two curved dipoles stacked on top of each other and fed $\mathbf{90^{\circ}}$ out of phase. Figure 19 above shows the basic geometry of the CDC.

Appendix B (p. 112) contains the description of MATLAB code for creating the NEC-2 file that describes the CDC. Figure 20 below shows the geometry of the simulated model.

[8] From this point on, the acronym CDC is used in this report to refer to a curved dipole cross.

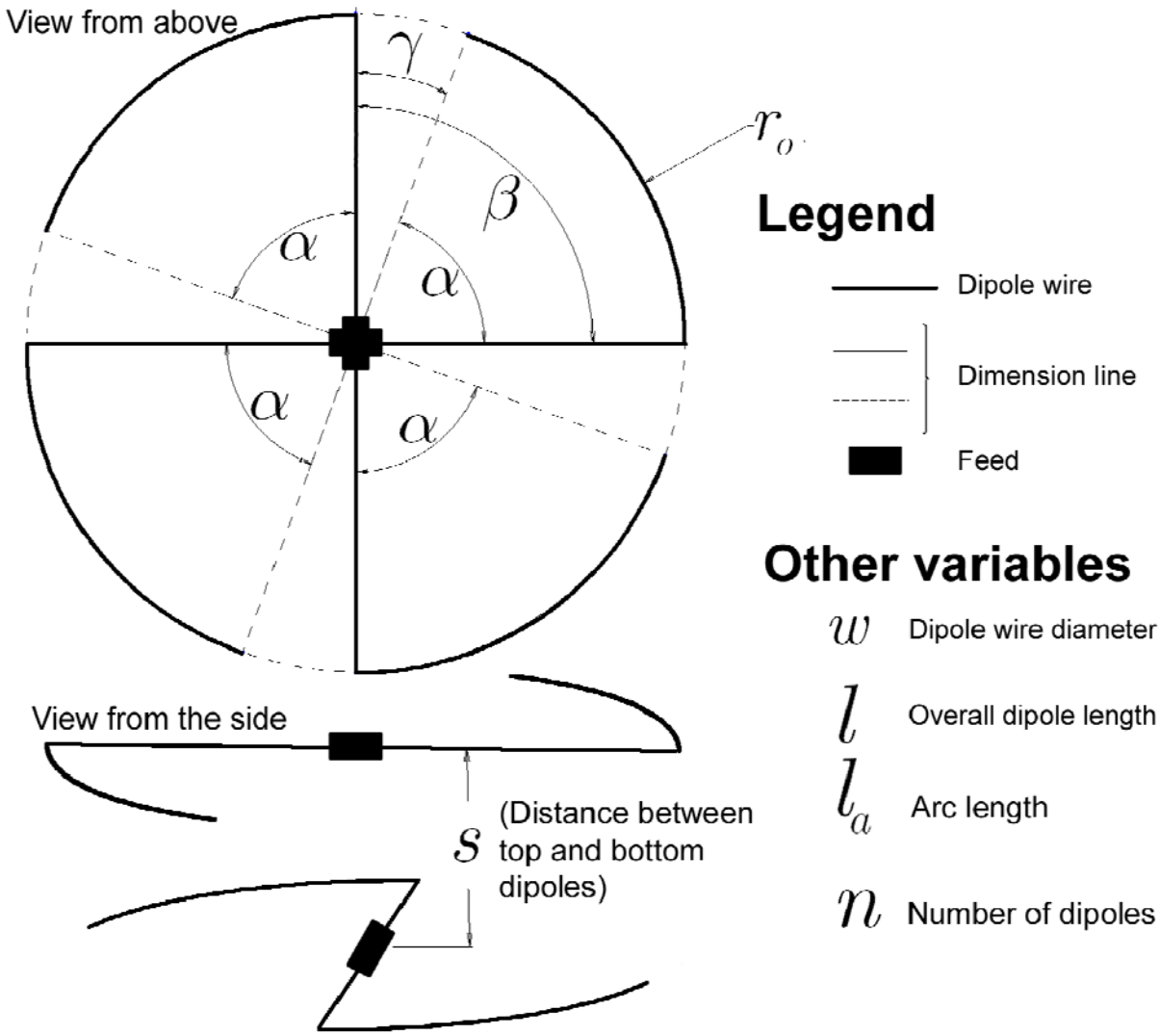

Fig. 20 Curved Dipole Cross Geometry

The geometry was computed based on the input variables in Table 5 below:

Table 5 Curved Dipole Cross Simulation Values

Variable	Units	Description	Values simulated
l	in	Overall length of each dipole	$0.4\lambda, 0.5\lambda, 0.6\lambda$
s	in	Spacing between top and bottom dipole	$1/4\ in$
α	°	Arc angle	$65°, 70°, 75°$
n		Number of dipoles	2

Appendix B (p. 112) contains the equations used to calculate the geometric variables (γ, β and r_o), which were not design parameters.

Section 4.2 (p. 50) contains the results and the outcome of the CDC simulation.

3.1.3 "Big wheel"

An n-petal wheel design was one of the initial potential designs that were looked at. The first simulations were run using "big wheel v1" code a description of which is in Appendix C (p. 114). Figure 21 below shows the geometry of big wheel v1 simulation.

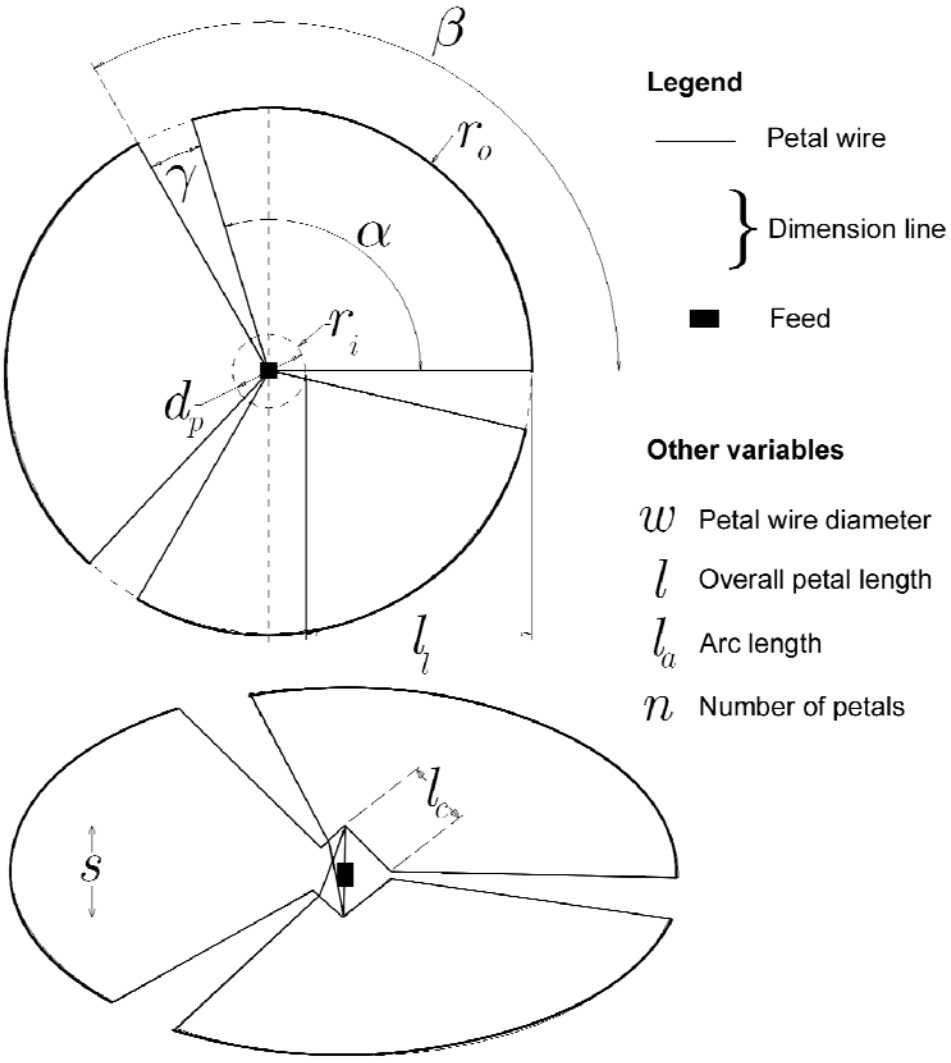

Fig. 21 Big Wheel v1 Geometry

Notice that in it legs and arcs meet at sharp angles (no rounds), and central plates are replaced with connectors. Geometry was computed based on input parameters in Table 6:

Table 6 Big Wheel v1[9] Simulation Values

Variable	Units	Description	Values simulated
l	in	Overall length of each petal	$0.9\lambda,\ 1.0\lambda, 1.1\lambda$
s	in	Spacing between hot and ground connectors	$1/4\ in$
γ	°	Interval angle	$13°$
d_p	in	Central "plate" diameter	$1in$
n		Number of petals	3, 4, 5, 6

Appendix C (p. 114) contains the equations used to calculate the geometric variables that were not design parameters (α, β, r_i, r_o and l_l).

Section 4.3 (p. 59) contains the results and the outcome of big wheel v1 potential design simulations.

3.2 Detailed Design

After we settled on the 5-petal wheel as the type of prototype to develop, we wrote two more simulation codes to more accurately model the wheel. Those codes are big wheel v2 and big wheel v3. Figure 22 below shows the geometry of big wheel v2 simulation; big wheel v3 is similar but has rectangular meshes instead of connectors in place of central plates.

[9] Note that these values are the parameters that only Big Wheel v1 was simulated with. More detailed simulations using a more accurate code were then ran over a much wider range of input design. See chapter 5 (p. 71) for information on these detailed simulations.

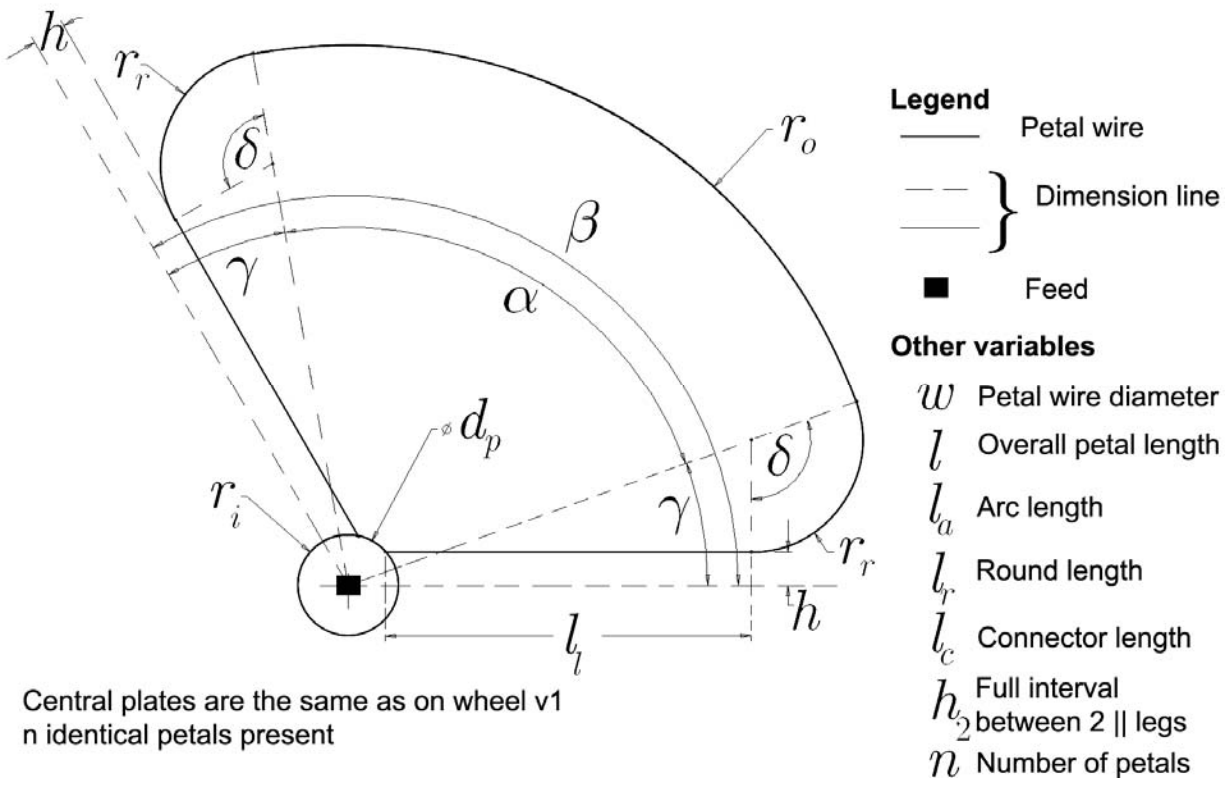

Fig. 22 Big Wheel v2 Geometry

See chapter 5 (p. 70), Appendix D (p. 117) and Appendix E (p. 123) for information on and details of those codes. Geometry for the big wheel v2 simulation was calculated based on input parameters in Table 7 below.

Table 7 Big Wheel v2 Simulation Values

Variable	Units	Description	Values simulated
l	in	Overall length of each petal	$0.9\lambda, 1.0\lambda, 1.1\lambda$
s	in	Vertical spacing between hot and ground connectors	$1/4\ in$
h_2	in	Interval between adjacent parallel legs	$1/2\ in$
r_r	in	Round radius	$5/8\ in$
d_p	in	Central "plate" diameter	$1\frac{11}{16}\ in$
n		Number of petals	3, 4, 5, 6

See Appendix D (p. 117) for derivations of geometric variables that were not input design parameters.

Big Wheel v3's petals and input variables are exactly the same as v2's. However, the central plates, instead of being modeled as connectors, are modeled as circular grids with finite square elements. Appendix E (p. 123) describes Big Wheel v3 in more detail. The input parameters at which big wheel v3 was simulated are listed in Table 8 below.

Table 8 Big Wheel v3 Simulation Values

Variable	Units	Description	Values simulated
l	in	Overall length of each petal	$0.9\lambda,\ 1.0\lambda, 1.1\lambda$
s	in	Vertical spacing between hot and ground connectors	$1/16\ in$
h_2	in	Interval between adjacent parallel legs	$1/2\ in$
r_r	in	Round radius	$5/8\ in$
d_p	in	Central plate diameter	$1\frac{11}{16}in, 3in$
n		Number of petals	3, 4, 5, 6

3.3 Measurements and Analysis

After prototype was manufactured, its S_{11} data was measured using a network analyzer. Different configurations of central plates as well as a tuning stub were tried during these measurements. Also, a gain calibrated measurement of the antenna's azimuthal pattern in tapered anechoic chamber was conducted. See chapter 6 (p. 84) for information on the outcome and details of these measurements.

4 Potential Designs

Sections 4.1 through 4.3 below discuss the potential designs that were simulated prior to choosing a design to optimize. These are: electrically small circular loop (section 4.1), curved dipole cross (section 4.2) and "big wheel" (section 4.3). Section 3.1 (p. 34) describes the general assumptions held constant throughout all of the simulations described in this chapter.

4.1 Electrically Small Circular Loop

Section 3.1.1 (p. 35 above) describes how the ESCL was simulated. The outcome of this simulation was as we had expected. The radiation pattern was very omnidirectional. At optimal values of l the simulated peak to valley difference in azimuthal gain was under 0.25 dB. A more detailed discussion of electrically small circular loop's pattern is in section 4.1.1 below.

The impedance match was unacceptably poor. This is the fundamental problem with electrically small loops – they act as near zero-resistance inductors, and inevitably require strong matching networks. The lowest simulated VSWR was 400:1, which is completely unacceptable. Matching is the primary reason why electrically small circular loop design was rejected. A more detailed discussion of ESCL matching is in section 4.1.2 below.

The ESCL's gain was acceptable. Electrically small loops send most of the power into the azimuthal plane, which is desired. At optimal values of R the average gain along the azimuthal plane was 0.5 dBi.

The ESCL was rejected due to the need for a complicated matching network, and being asymmetrically fed (off-center presence of a feed wire which was not simulated would likely disturb the azimuthal pattern).

4.1.1 Radiation Pattern

As stated above, ESCL produces a very omnidirectional radiation pattern. Figure 23 below shows the antenna's azimuthal radiation pattern at $f = 435MHz$ with $l = 0.075\lambda$.

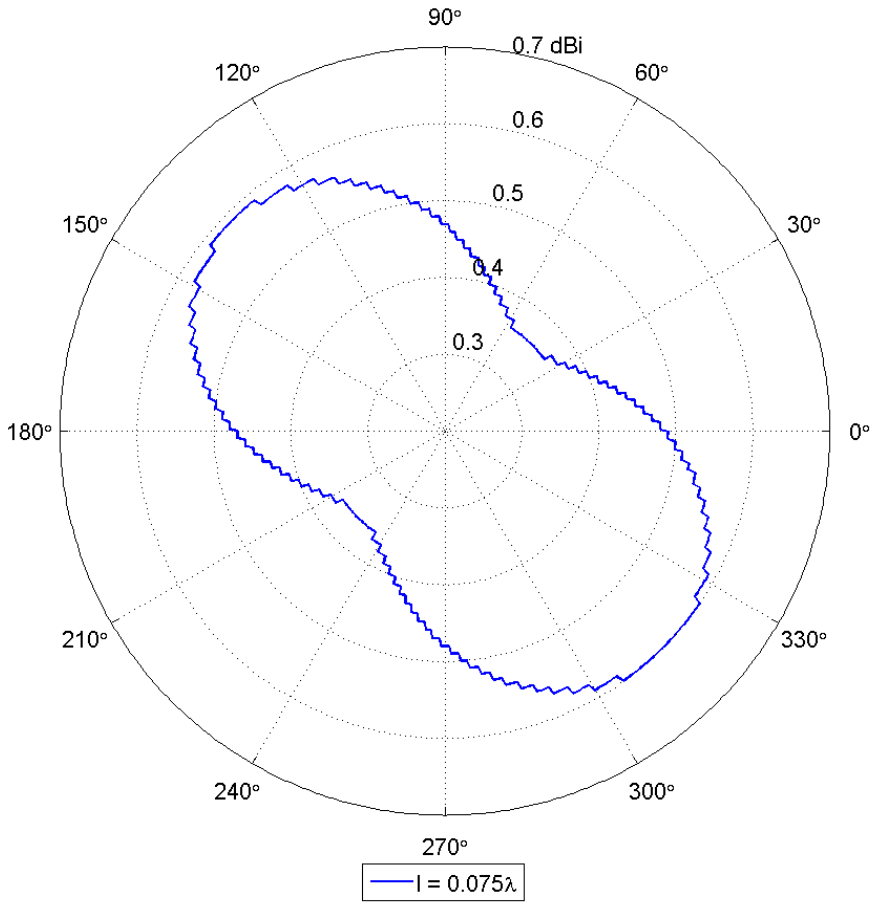

Fig. 23 Electrically Small Circular Loop Best Azimuthal Pattern ($f = 435MHz$)

Most of the energy ESCL radiated went into the azimuthal plane. Figure 24 below shows the elevation pattern at $f = 435MHz$ with $l = 0.075\lambda$.

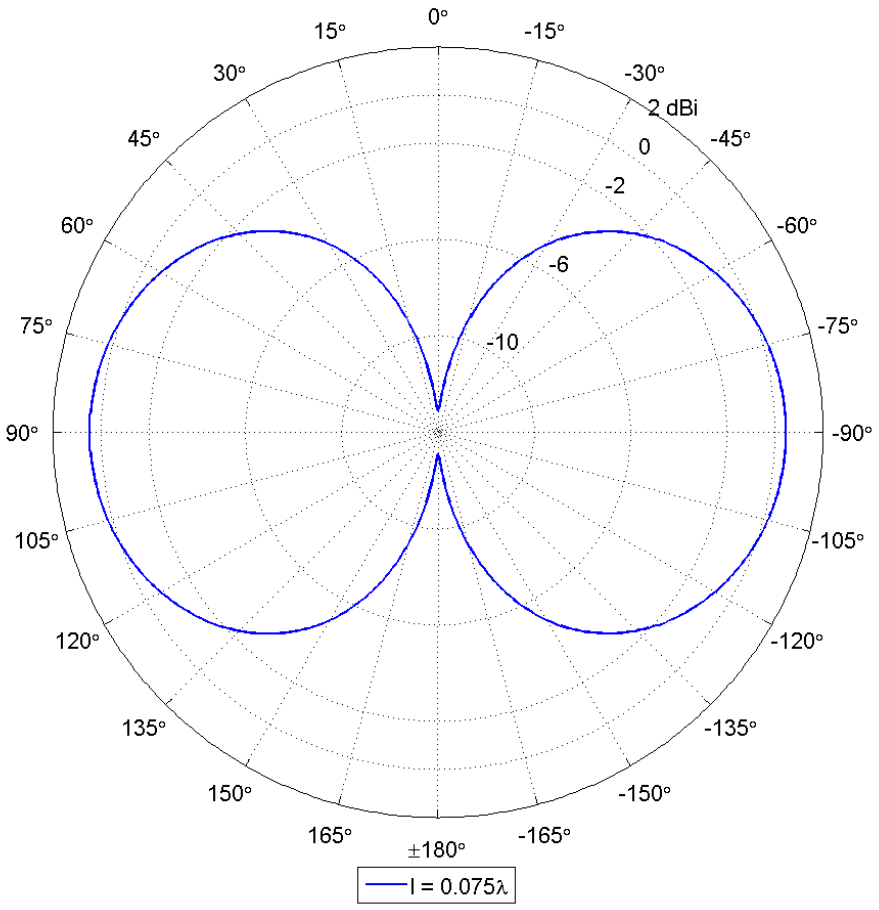

Fig. 24 Electrically Small Circular Loop Best Elevation Pattern
($f = 435MHz$, $\phi = 0°$)

The azimuthal radiation pattern did not vary in shape much with frequency, although gain changed. Figure 25 below shows the antenna's azimuthal radiation pattern over a range of frequencies with $l = 0.075\lambda$.

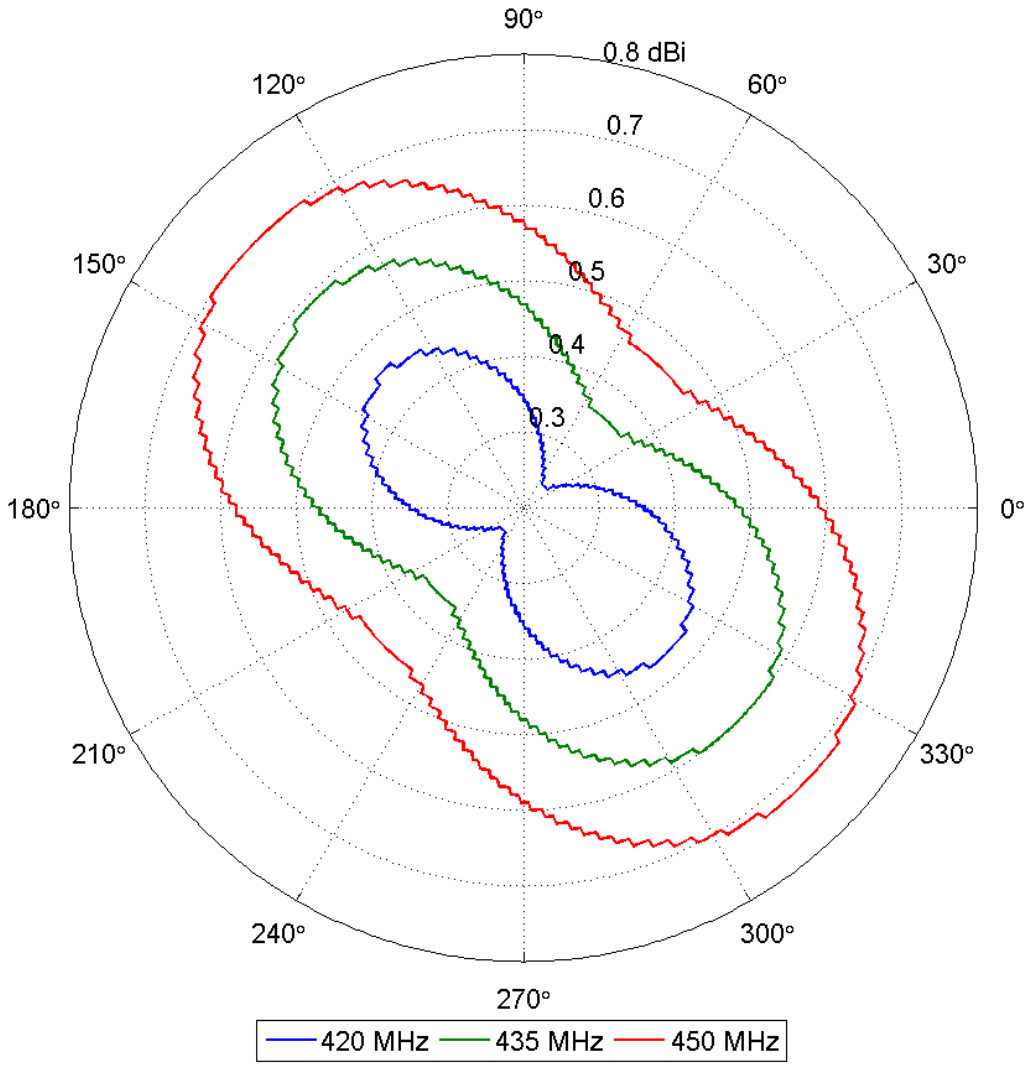

Fig. 25 Electrically Small Circular Loop Azimuthal Pattern vs Frequency ($l = 0.075\lambda$)

Only one design parameter (l) was varied during the simulation of ESCL and so there is no way to state what specific parameter of ESCL's geometry affected the radiation pattern the most. As Fig. 26 below shows, ESCL's azimuthal radiation pattern (at $f = 435MHz$) did vary significantly for $l > 0.1\lambda$, but did not vary significantly for smaller ESCLs. This is in line with the general theory that states that circular loops can be considered electrically small with $l \leq 0.1\lambda$. [13]

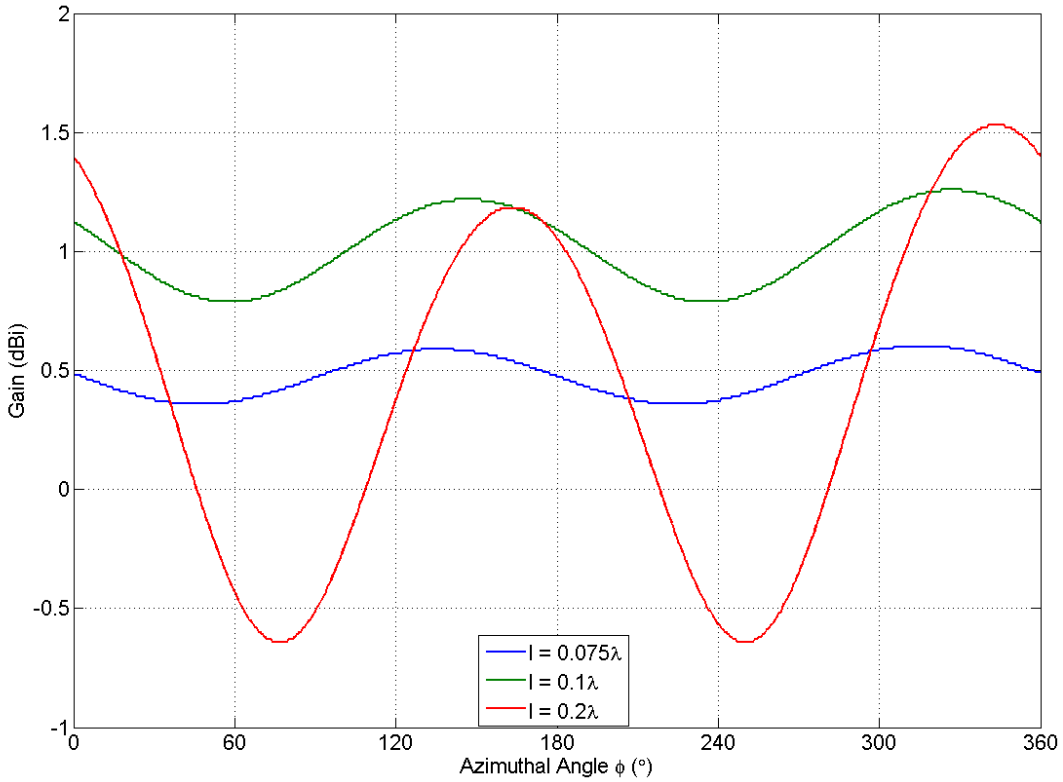

Fig. 26 Electrically Small Circular Loop Azimuthal Pattern vs Loop Length ($f = 435MHz$)

4.1.2 Matching

Fundamentally, electrically small loops tend to be very poorly matched. [2] This was shown to be true in this simulation – as Fig. 27 below shows, the loop was unacceptably poorly matched across bandwidth and any value of l.

The loop was nearly short circuit - at $f = 435MHz$ and $l = 0.075\lambda$ input impedance was $Z = 0.133\Omega + 97.017j\Omega$. Matching was the reason ESCL was rejected.

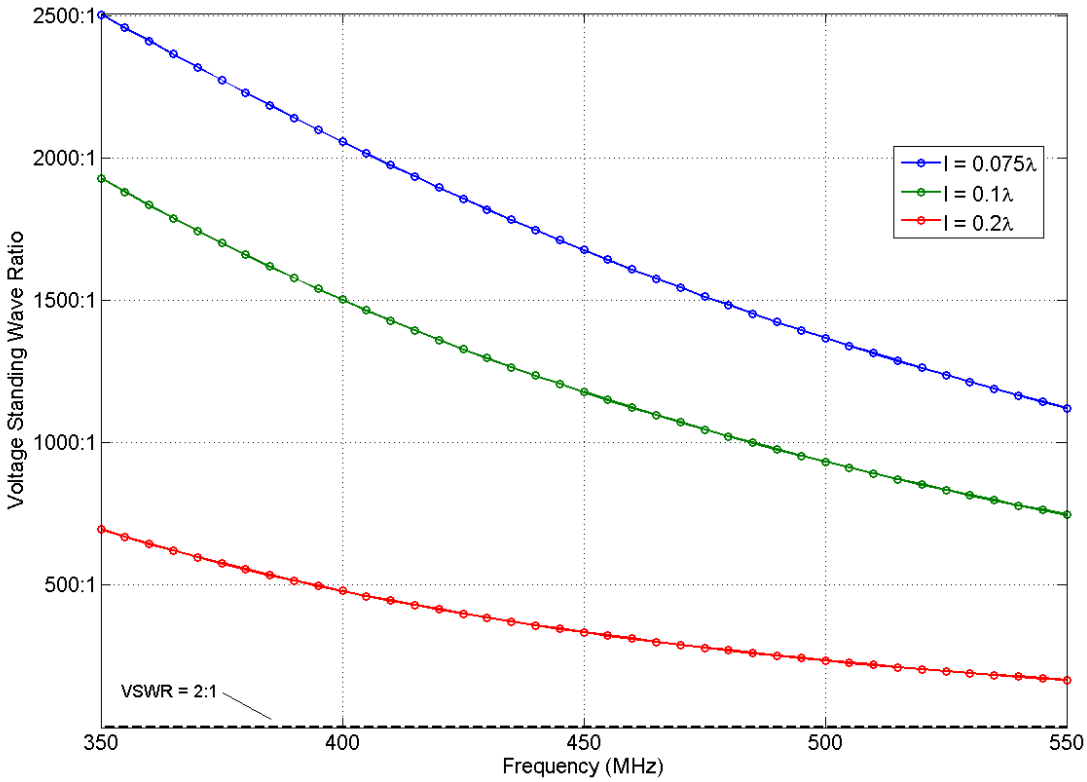

Fig. 27 Electrically Small Circular Loop Match vs Loop Length

4.1.3 Gain

ESCL radiated most of the power into the azimuthal plane. Figures 23 and 24 above show simulated gain distribution at optimal l across both azimuthal and elevation planes. Simulated gain is fully acceptable; however, if absolute gain was accounted for, it would be highly negative, due to complete mismatch.

4.1.4 Summary

ESCL was abandoned due to unacceptably poor matching. However, it provided practice in simulating antennas and also provided a code for approximating arcs with finite length straight elements, which was used in future simulations.

4.2 Curved Dipole Cross

Section 3.1.2 (p. 37) discusses the methods employed in simulating the curved dipole cross (CDC). CDC's geometry and its design parameters are also given in section 3.1.2 (p. 37). As is explained in section 3.1.2, the dipole cross was originally conceived as an arrangement of four curved monopoles (see Fig. 18 (p. 38)).

This geometry, although physically impossible to produce as simulated, had positive simulated gain, omnidirectionality within ± 1dB, but an extremely poor match. The curved dipole cross, which has a mechanically similar (although electrically different) geometry, was expected to perform in a similar manner.

4.2.1 Radiation Pattern

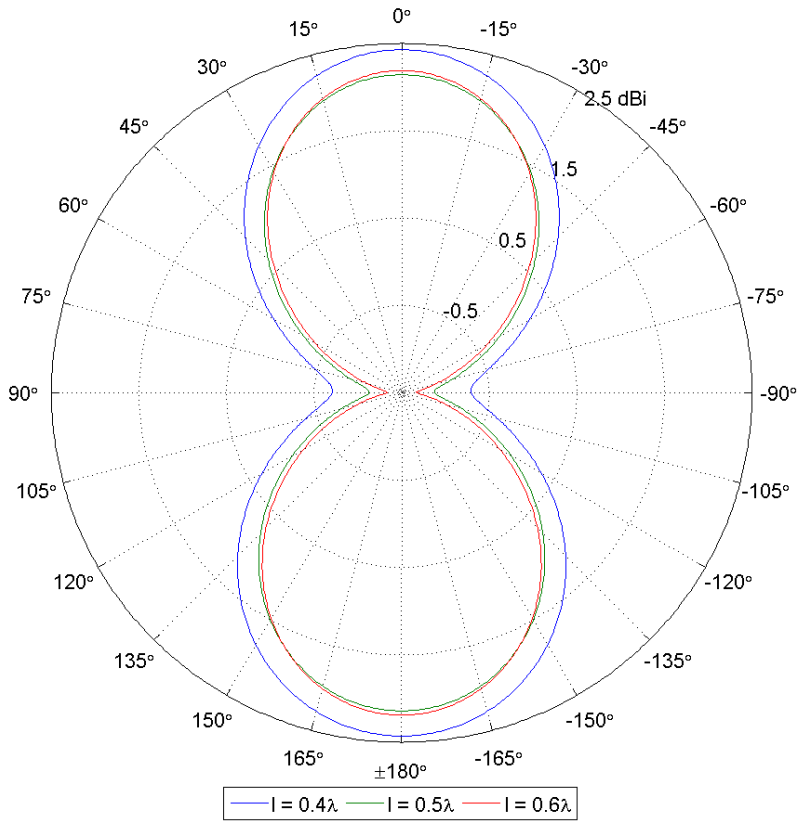

Fig. 28 Curved Dipole Cross Elevation Pattern
($f = 435MHz$, $\alpha = 70°$)

By itself, the curved dipole cross radiates most of its radiation normal to the plane of the antenna, producing very low gain in the azimuth. In this mode, the antenna also operates in both horizontal and vertical polarization. Figure 28 above shows the dipole cross' elevation radiation pattern at $f = 435MHz$ with $l = 0.4\lambda$, 0.5λ, 0.6λ and $\alpha = 70°$.

The addition of circular reflectors located at $d = 0.5\lambda$, where d is the distance from the azimuthal plane to each reflector, above and below the curved dipole cross directed the pattern into the azimuth, as shown in Fig. 29 below which again shows the dipole cross' elevation radiation pattern at $f = 435MHz$ with $l = 0.4\lambda$, 0.5λ, 0.6λ and $\alpha = 70°$, but this time with reflectors.

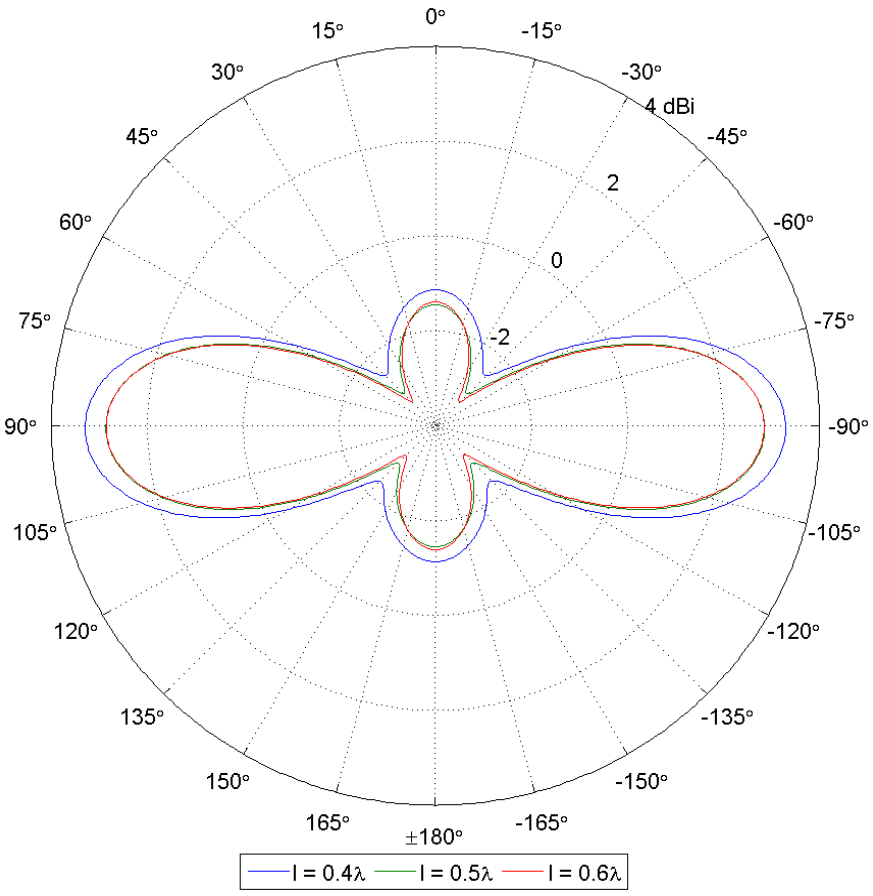

Fig. 29 Curved Dipole Cross with Reflectors Elevation Pattern
($f = 435MHz$, $\alpha = 70°$)

Figure 30 below shows a 3D rendering of the reflectors used in simulation. Reflectors provided a considerable (about 3 dB) improvement in azimuthal gain, as well as improved the omnidirectionality of the radiation pattern. Figure 31 below shows a comparison of azimuthal radiation patterns for the CDC at $\boldsymbol{f = 435MHz}$ with $\boldsymbol{l = 0.5\lambda}$, $\boldsymbol{\alpha = 70°}$ and with both no reflectors as well as reflectors positioned at $\boldsymbol{d = 0.5\lambda}$.

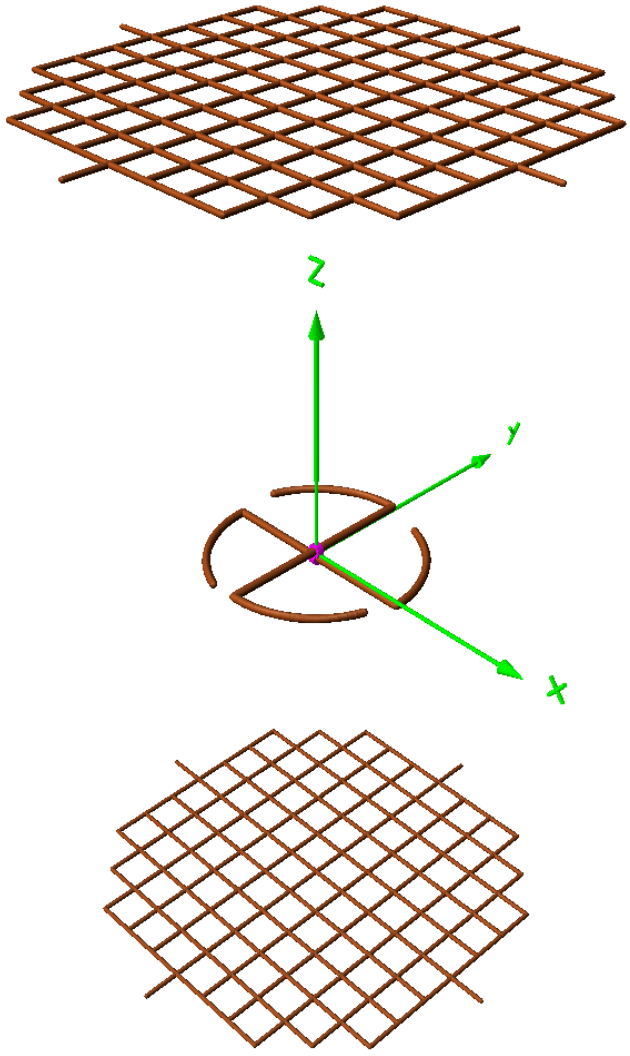

Fig. 30 Curved Dipole Cross with Reflectors 3D Rendering
$(\boldsymbol{d = 0.5\lambda})$

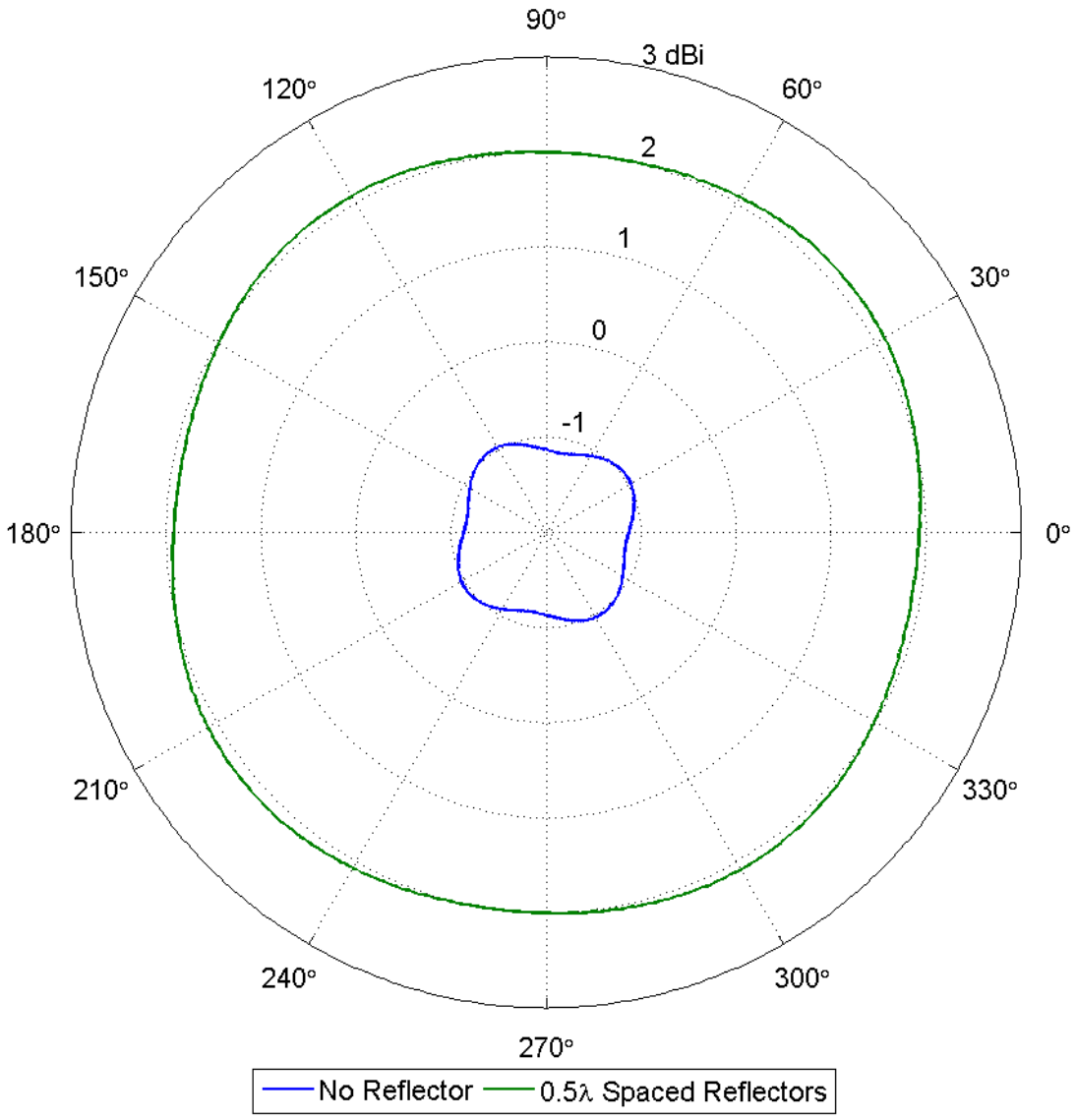

Fig. 31 Curved Dipole Cross Reflector vs No Reflector Azimuthal Pattern Comparison ($f = 435MHz$, $l = 0.5\lambda$, $\alpha = 70°$)

Reflector spacing from the CDC has a significant impact on azimuthal radiation pattern, affecting both the omnidirectionality of the pattern and the gain. Figure 32 below contrasts the radiation patterns in the azimuth for a dipole cross at $f = 435MHz$ with $l = 0.5\lambda$, $\alpha = 70°$ and with reflectors positioned at $d = 0.4\lambda$, 0.5λ and 0.6λ.

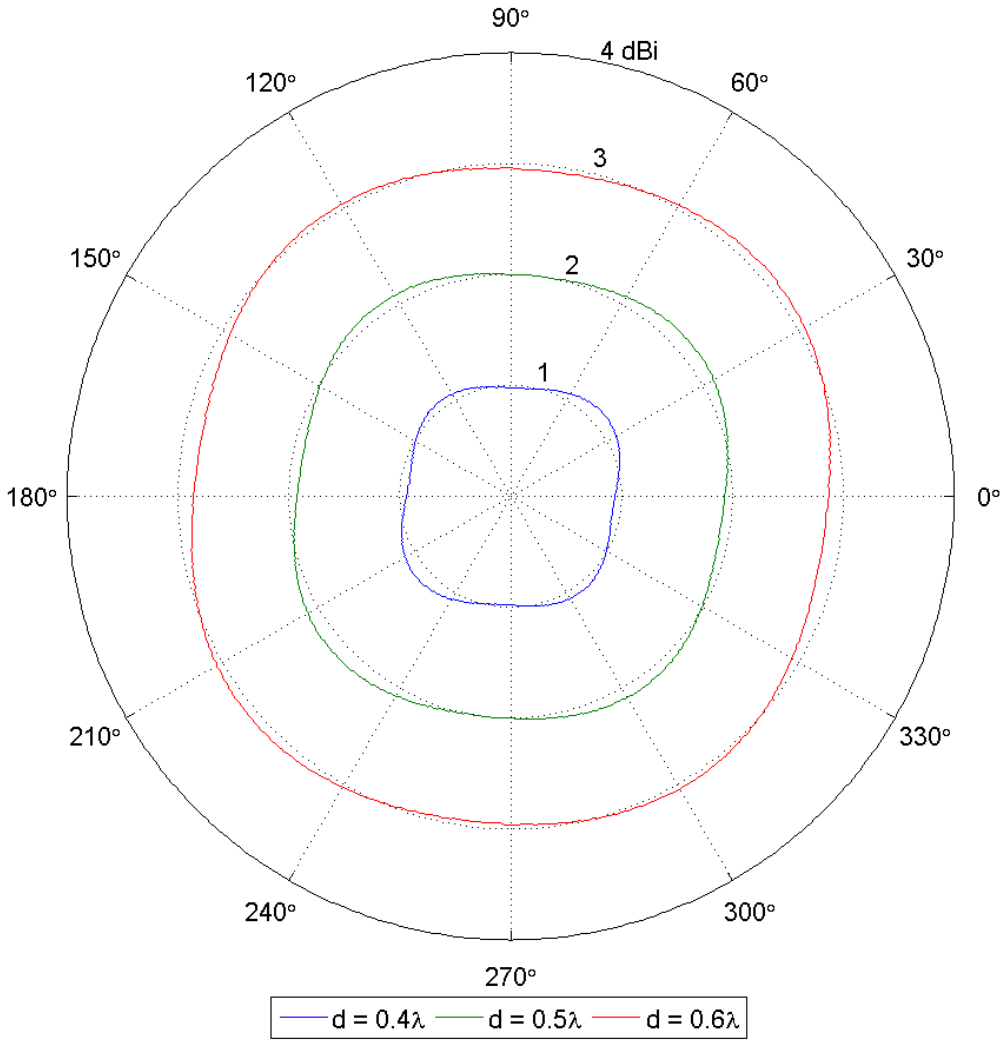

Fig. 32 Curved Dipole Cross Azimuthal Pattern vs Reflector Spacing
($f = 435MHz$, $l = 0.5\lambda$, $\alpha = 70°$)

With reflectors in place, variation in frequency had only minimal impact on pattern but did alter gain. Figure 33 below shows a range of frequencies for $l = 0.5\lambda$, $\alpha = 70°$ and $d = 0.5\lambda$.

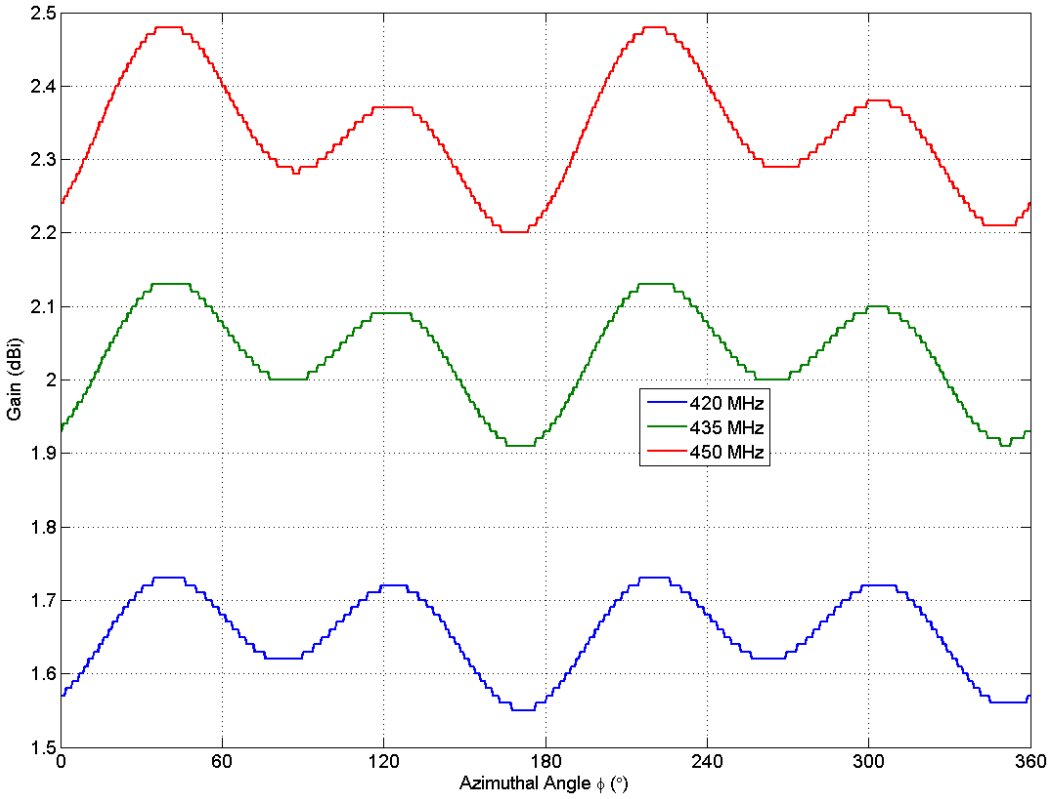

Fig. 33 Curved Dipole Cross Azimuthal Pattern vs Frequency
$(\boldsymbol{l = 0.5\lambda},\ \boldsymbol{\alpha = 70°},\ \boldsymbol{d = 0.5\lambda})$

Two design parameters were varied during simulation of the CDC – the dipole overall length $\boldsymbol{l}$ and the arc angle $\boldsymbol{\alpha}$. Neither were found to have a significant impact on radiation pattern, although both affected the gain. Figures 34 and 35 below show the effect of variation in dipole length ($\boldsymbol{l = 0.4\lambda, 0.5\lambda,\ 0.6\lambda}$) with fixed arc angle ($\boldsymbol{\alpha = 70°}$) and the effect of variation in arc angle ($\boldsymbol{\alpha = 65°,\ 70°,\ 75°}$) with fixed dipole length ($\boldsymbol{l = 0.5\lambda}$). Both figures are at $\boldsymbol{f = 435MHz}$ with circular reflectors spaced $\boldsymbol{d = 0.5\lambda}$ from the antenna.

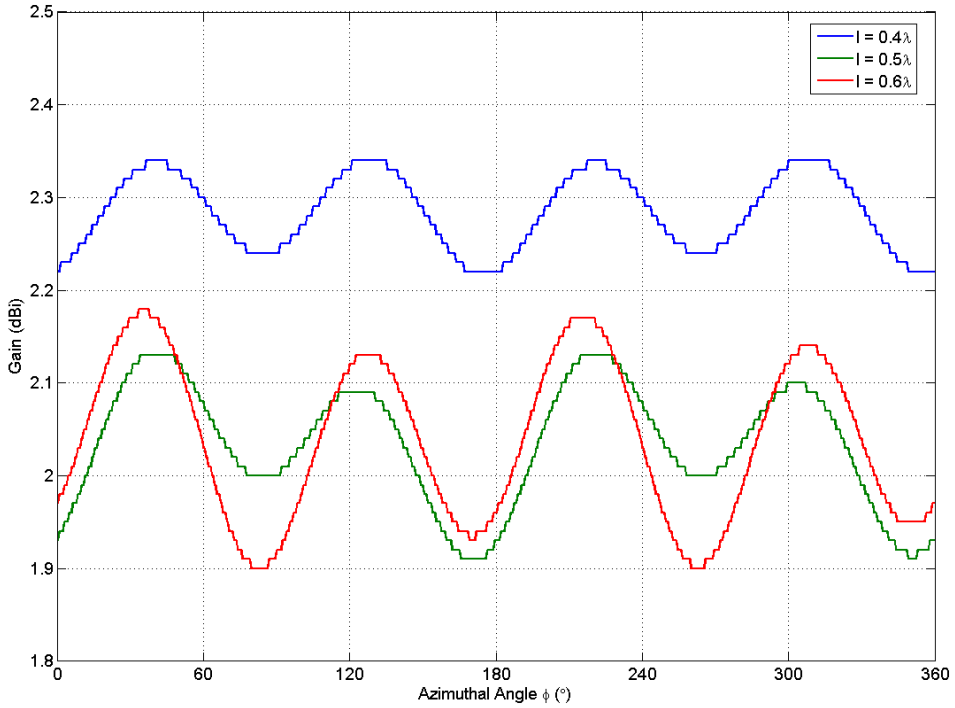

Fig. 34 Curved Dipole Cross Azimuthal Pattern vs Overall Dipole Length
$(f = 435MHz, \alpha = 70°, d = 0.5\lambda)$

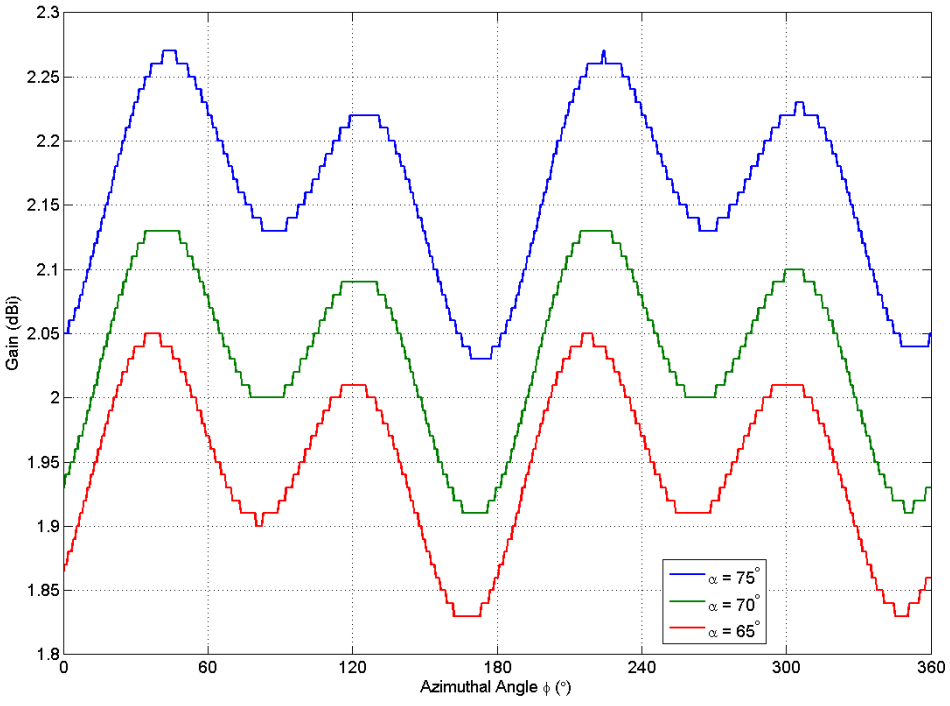

Fig. 35 Curved Dipole Cross Azimuthal Pattern vs Arc Angle
$(f = 435MHz, l = 0.5\lambda, d = 0.5\lambda)$

4.2.2 Matching

The CDC consists of two dipoles stacked one above the other, and thus requires two independent feeds. Further, to prevent destructive interference, the dipoles must be fed $\mathbf{90^\circ}$ out of phase. These factors make impedance matching a complex issue for the CDC. However, the CDC is natively well matched and the presence of reflectors assists in matching the antenna in simulation. Figure 36 below demonstrates this, comparing the match of a dipole cross with $\boldsymbol{l = 0.5\lambda}$, $\boldsymbol{\alpha = 70^\circ}$ with circular reflectors positioned at $\boldsymbol{d = 0.4\lambda}$, $\boldsymbol{0.5\lambda}$, $\boldsymbol{0.6\lambda}$ and no reflectors at all.

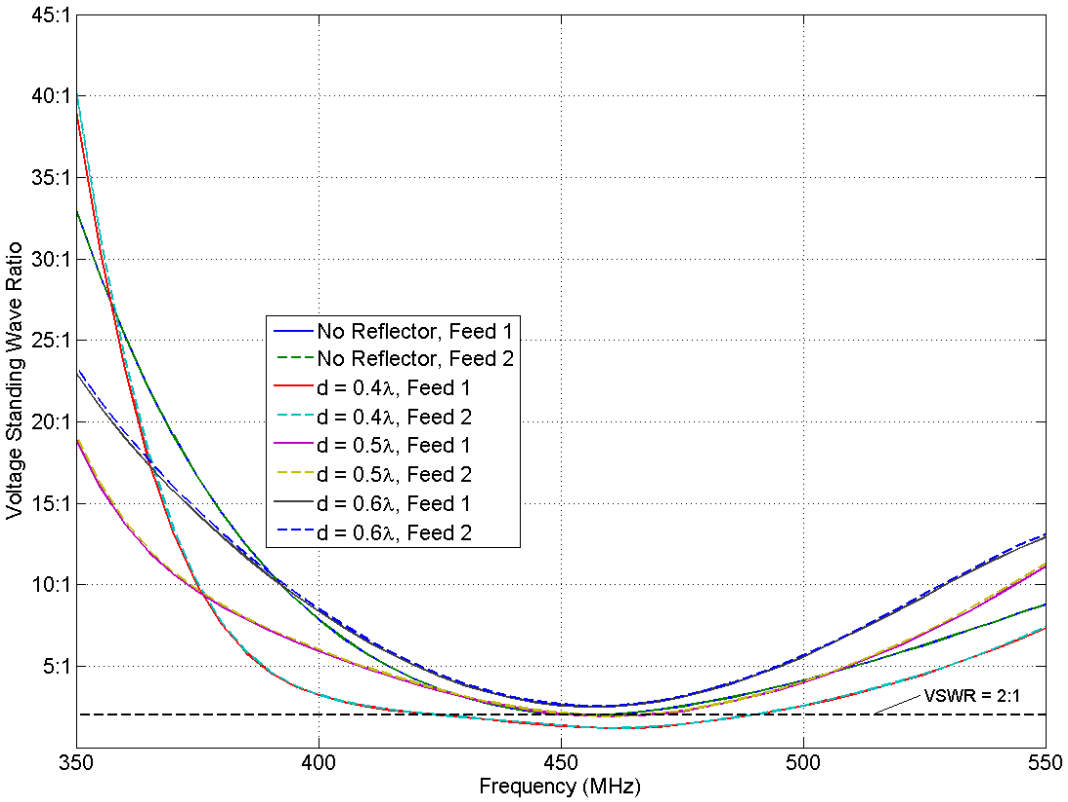

Fig. 36 Curved Dipole Cross Match vs Reflector Spacing
$(\boldsymbol{l = 0.5\lambda}, \boldsymbol{\alpha = 70^\circ})$

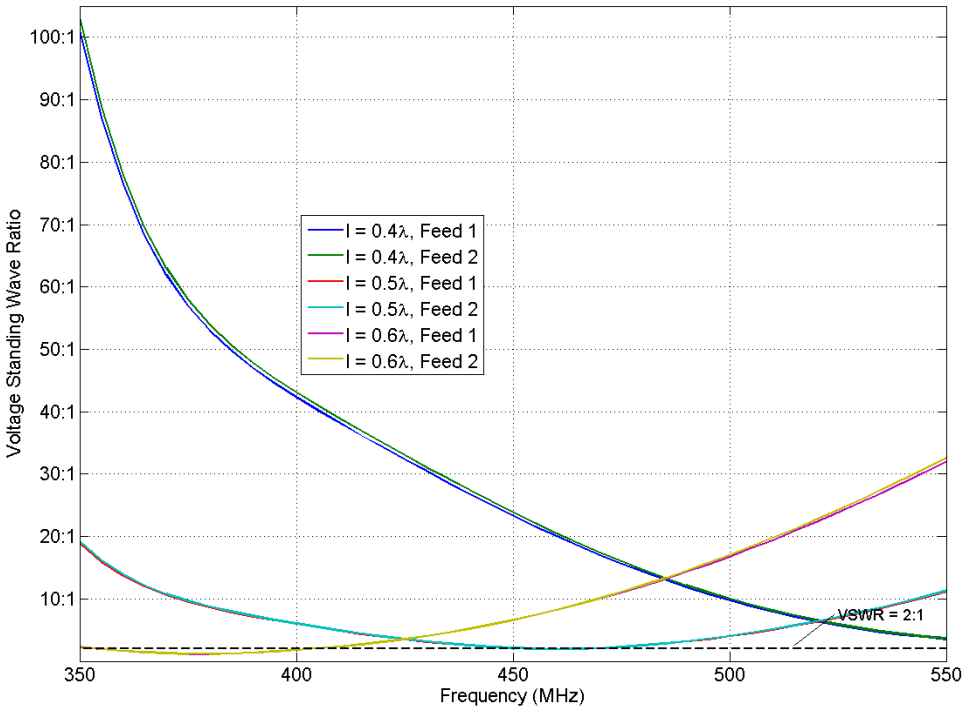

Fig. 37 Curved Dipole Cross Match vs Overall Dipole Length
$(\boldsymbol{\alpha = 70°}, \boldsymbol{d = 0.5\lambda})$

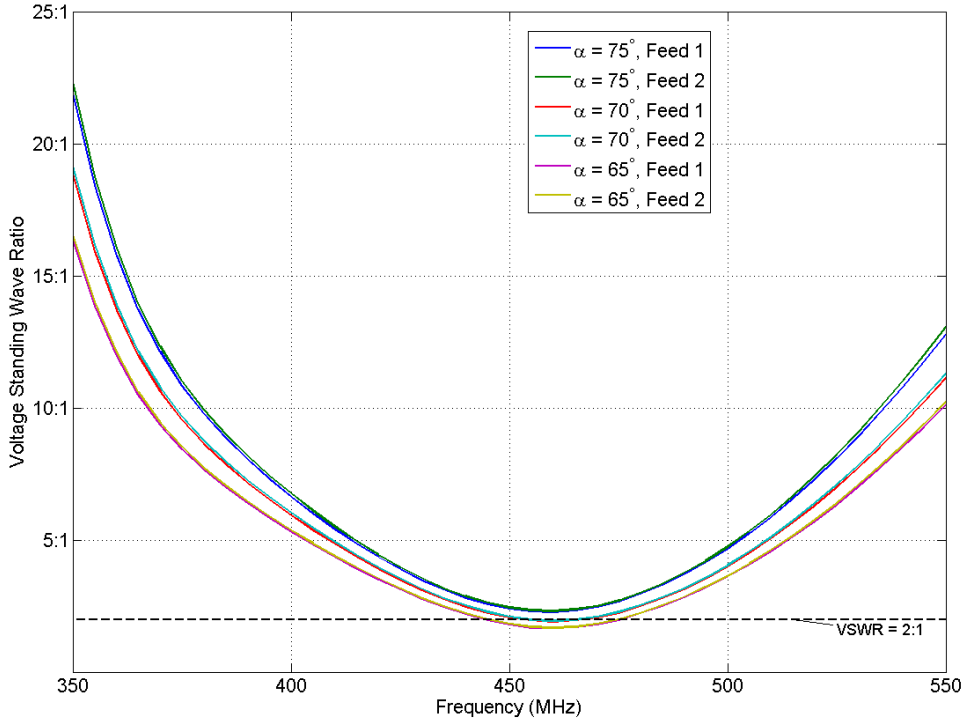

Fig. 38 Curved Dipole Cross Match vs Arc Angle
$(\boldsymbol{l = 0.5\lambda}, \boldsymbol{d = 0.5\lambda})$

The arc angle α had little impact on match; however, the overall length of the dipole l significantly altered the frequency to which the dipole cross was tuned. Figures 37 and 38 above show the impedance match for dipole crosses with dipole length $l = 0.4\lambda$, 0.5λ, 0.6λ with fixed arc angle at $\alpha = 70°$ and arc angle $\alpha = 65°$, $70°$, $75°$ and with fixed dipole length at $l = 0.5\lambda$. Both cases have circular reflectors spaced at $d = 0.5\lambda$.

4.2.3 Gain

As discussed in section 4.1.1 above, without reflectors the CDC has very poor azimuthal gain. The addition of reflectors greatly improves the azimuthal gain, as is shown by Fig. 31 above.

4.2.4 Summary

The curved dipole cross displayed promising radiation pattern, gain, and impedance match in simulation. Unfortunately, time constraints prevented us from building and measuring a prototype of the CDC to confirm simulated performance. Although the complexities in construction resulting from a phased dual feed as well as the necessity of using reflectors make implementation of the dipole cross difficult, its strong performance in simulation warrants future consideration.

4.3 "Big Wheel"

The "big wheel" was the primary antenna geometry considered by our predecessors in Group 39 at MIT Lincoln Laboratory for the application of omnidirectionality with horizontal polarization. As a result, we had experimental data against which we could compare simulations. Thus, in simulating the wheel we could establish the accuracy of our simulation methods and then consider how the configuration of the wheel could be altered to improve its pattern, match,

and gain. Details of our initial wheel simulation code, big wheel v1, were discussed in section 3.1.3 (p. 40). This simulation predicted Group 39's experimental data on the 3-petal big wheel fairly well. Figure 39 below shows the comparison between experiment and simulation for a wheel of comparable geometry and the rough correlation that was seen with both pattern and gain.

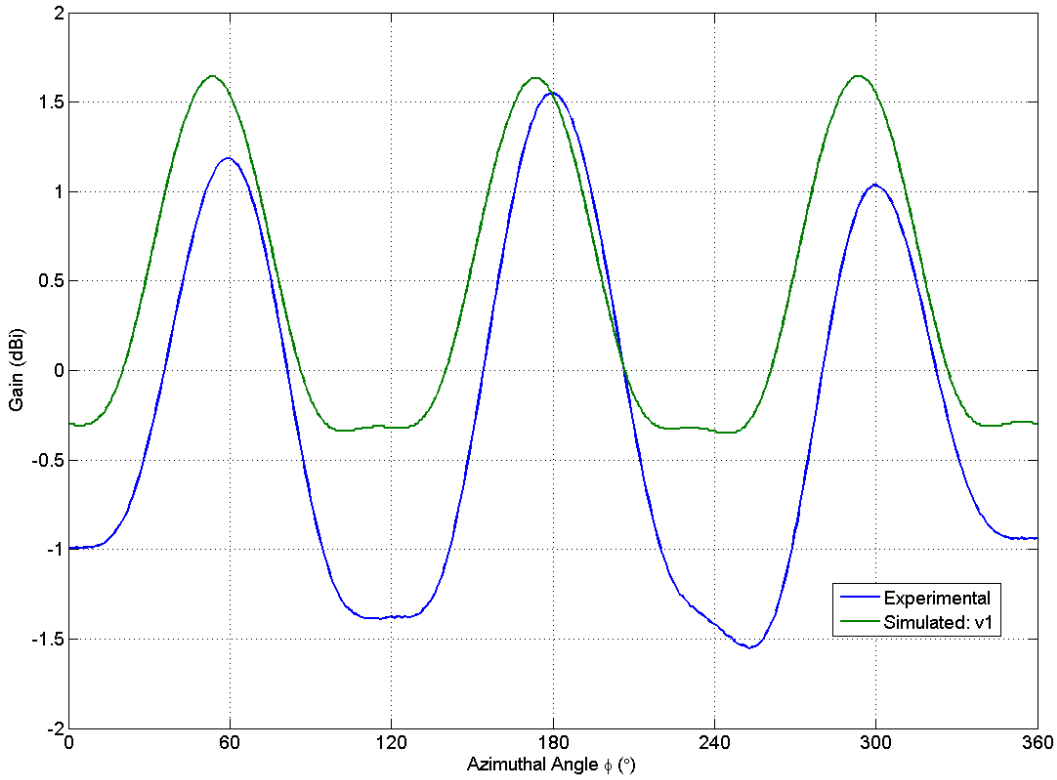

Fig. 39 3-Petal Wheel Measured vs Simulated with v1 Azimuthal Pattern

Simulation using big wheel v1 code failed to accurately predict impedance match. This was expected due to the simplicity of the v1 simulation – which could not accurately model the central plates. Figure 40 below shows the comparison of impedance match between experimental data and simulation for 3-petal wheels of comparable geometry.

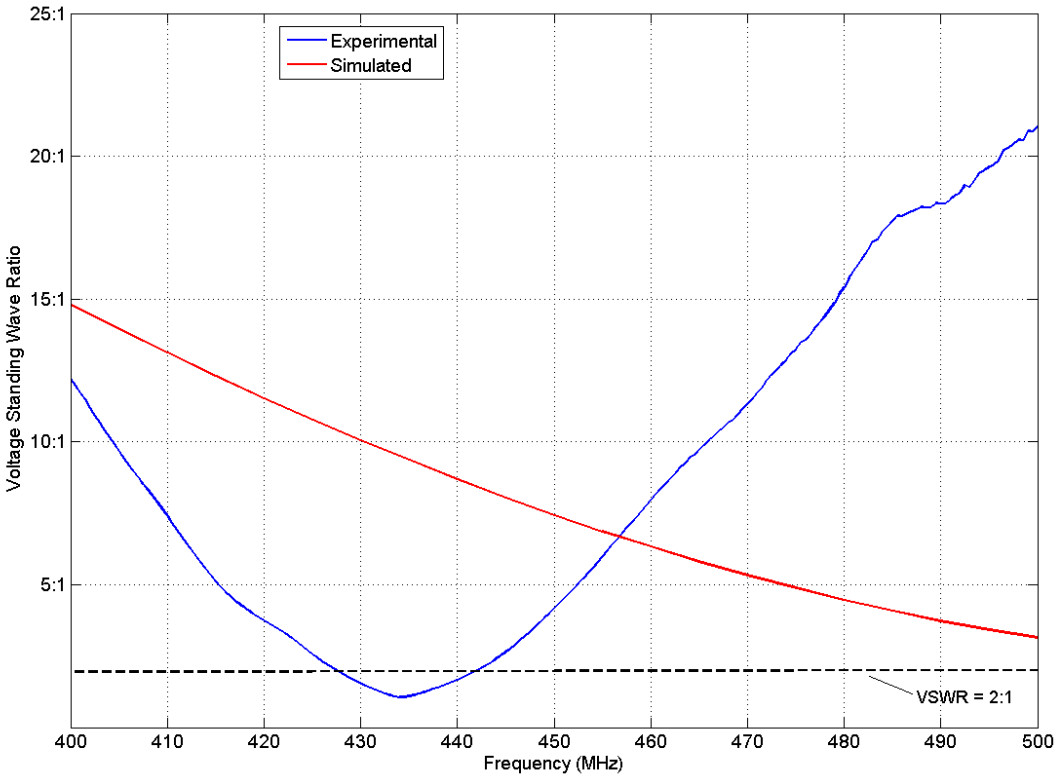

Fig. 40 3-Petal Wheel Measured vs Simulated with v1 Match

4.3.1 Radiation Pattern and Gain

The only parameter which was varied for simulations of the 3-petal big wheel was the total length of each petal l. Total petal length has a significant impact upon both the radiation pattern and gain of the wheel. Figure 41 below compares azimuthal radiation patterns at $f = 435MHz$ for 3-petal wheels having petal lengths of $l = 0.9\lambda, 1.0\lambda, 1.1\lambda$.

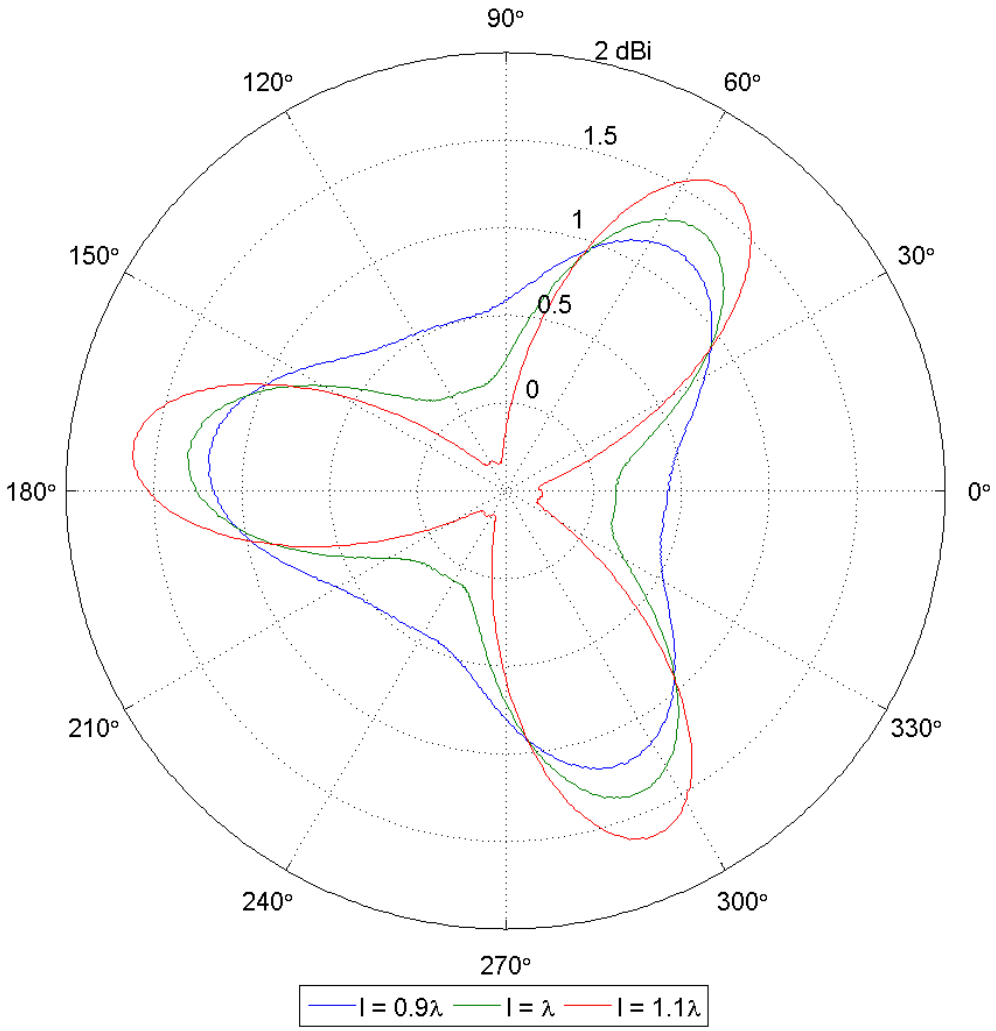

Fig. 41 3-Petal Big Wheel Simulated with v1 Azimuthal Pattern vs Petal Length ($f = 435MHz$)

The peak gain for the 3-petal wheel is in the azimuthal plane for all variations in petal length. This is shown by the elevation radiation patterns of Fig. 42 below which includes loop lengths of $l = 0.9\lambda, 1.0\lambda, 1.1\lambda$ at $f = 435MHz$ and $\phi = 0°$.

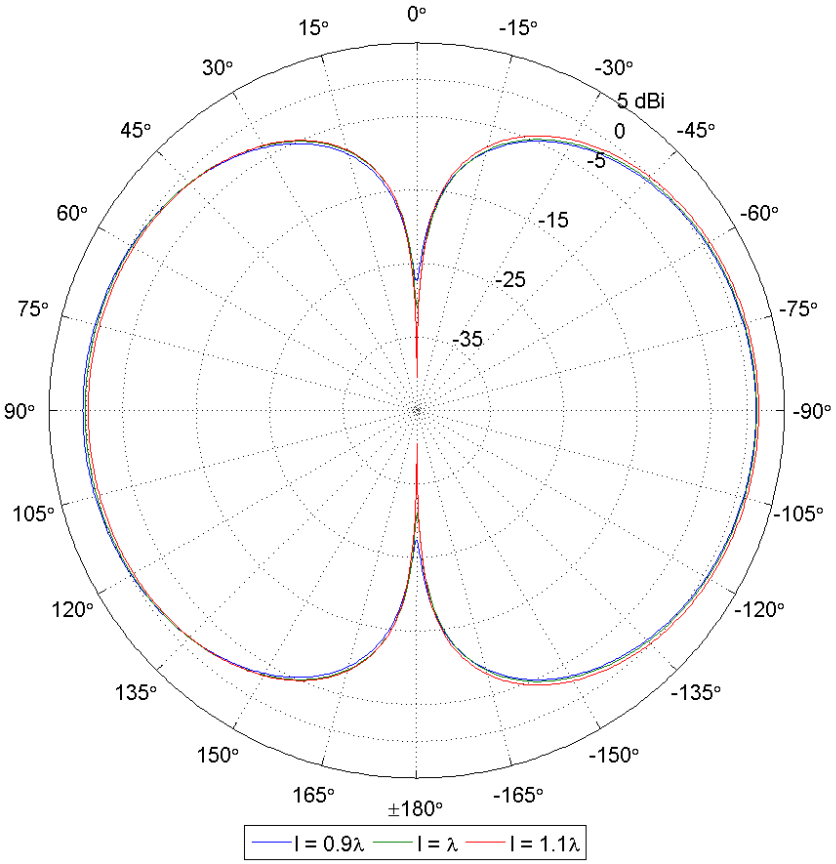

Fig. 42 3-Petal Big Wheel Simulated with v1 Elevation Pattern vs Petal Length ($f = 435MHz, \phi = 0°$)

However, regardless of loop length, these simulations showed that the 3-petal wheel could not produce the omnidirectionality required. Thus, the number of petals n was varied and found to have significant impact upon azimuthal radiation pattern, while having minimal impact on gain. Figure 43 below shows this relation at $f = 435MHz$ for 3, 4, 5 and 6-petal wheels each having petal length $l = 1.0\lambda$.

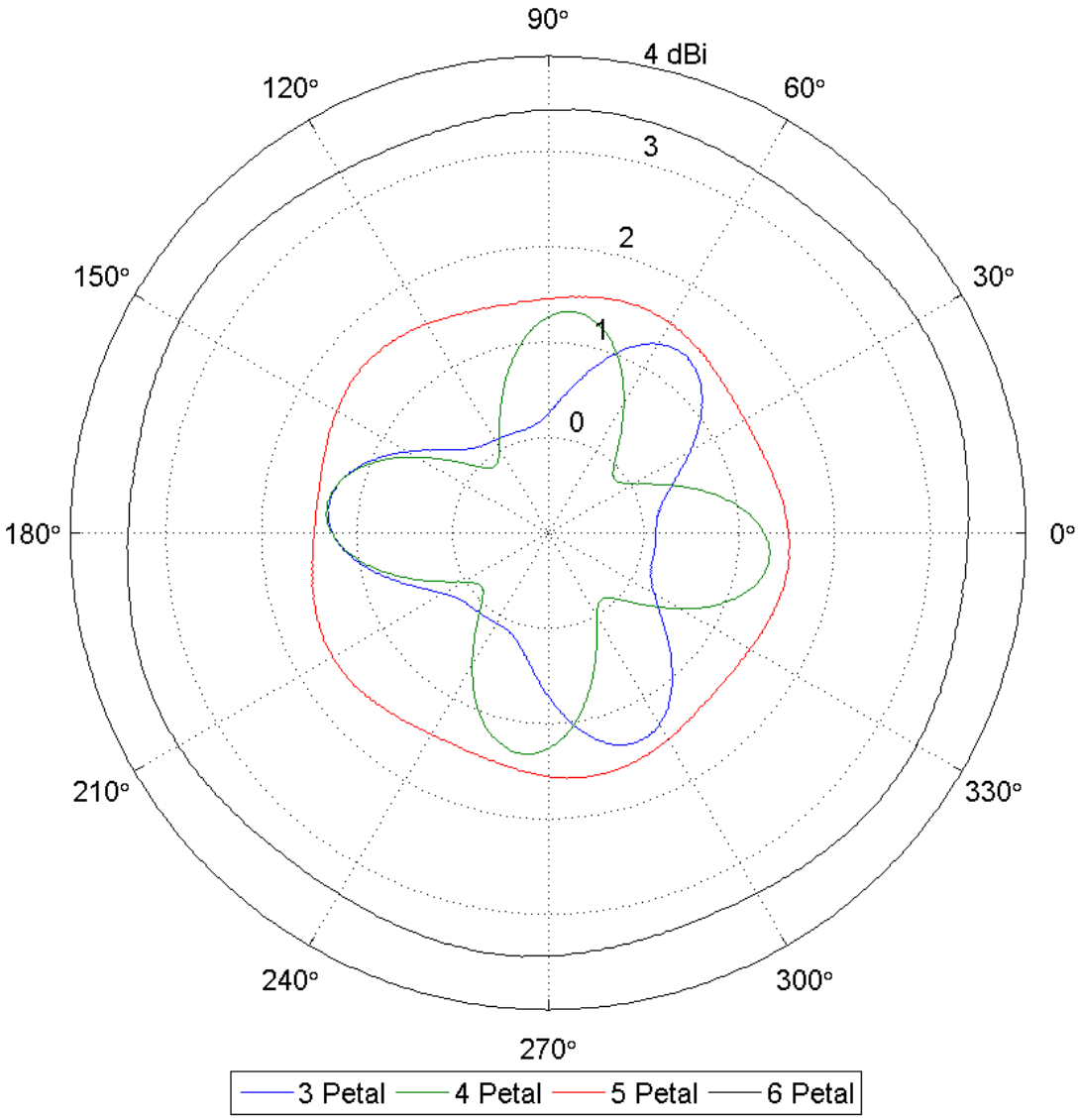

Fig. 43 Big Wheel Simulated with v1 Azimuthal Pattern vs Number of Petals
($f = 435MHz$, $l = 1.0\lambda$)

A 4-petal wheel showed little improvement over a 3-petal wheel, regardless of loop length – as seen in Fig. 44 below which displays azimuthal radiation patterns for 4-petal wheels having loop lengths $l = 0.9\lambda, 1.0\lambda, 1.1\lambda$ at $f = 435MHz$.

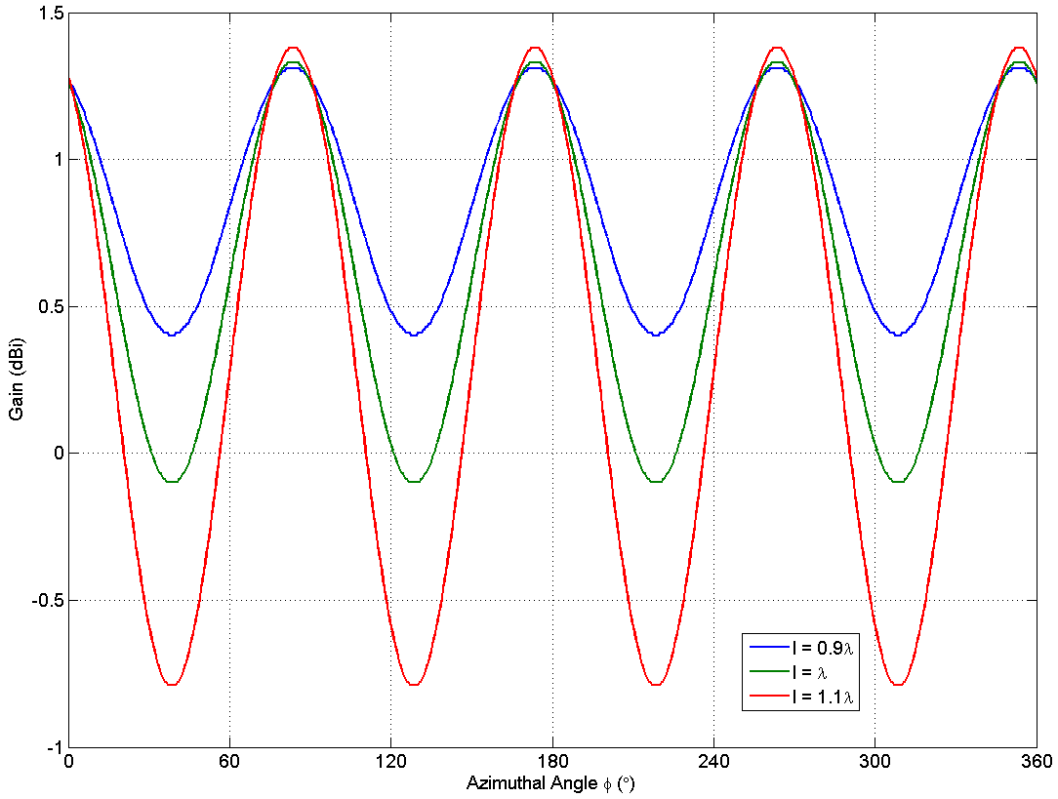

Fig. 44 4-Petal Big Wheel Simulated with v1 Azimuthal Pattern vs Petal Length ($f = 435MHz$)

However, a 5-petal wheel showed dramatic improvement in the pattern. Figure 45 below shows how azimuthal pattern and gain vary for a 5-petal wheel at $f = 435MHz$ as petal length varies with $l = 0.9\lambda, 1.0\lambda, 1.1\lambda$.

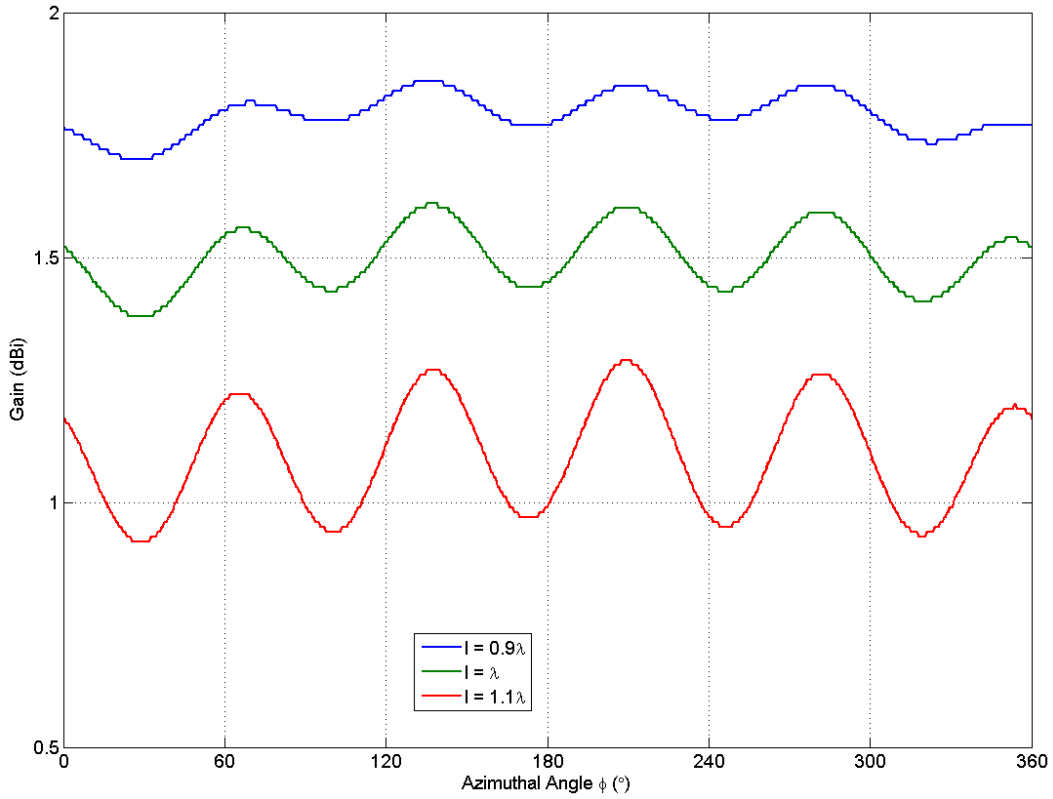

Fig. 45 5-Petal Big Wheel Simulated with v1 Azimuthal Pattern vs Petal Length ($f = 435MHz$)

This trend continued for 6-petal wheels. Figure 46 below shows how azimuthal pattern and gain vary for a 6 petal wheel at $f = 435MHz$ as petal length varies with $l = 0.9\lambda$, 1.0λ, 1.1λ.

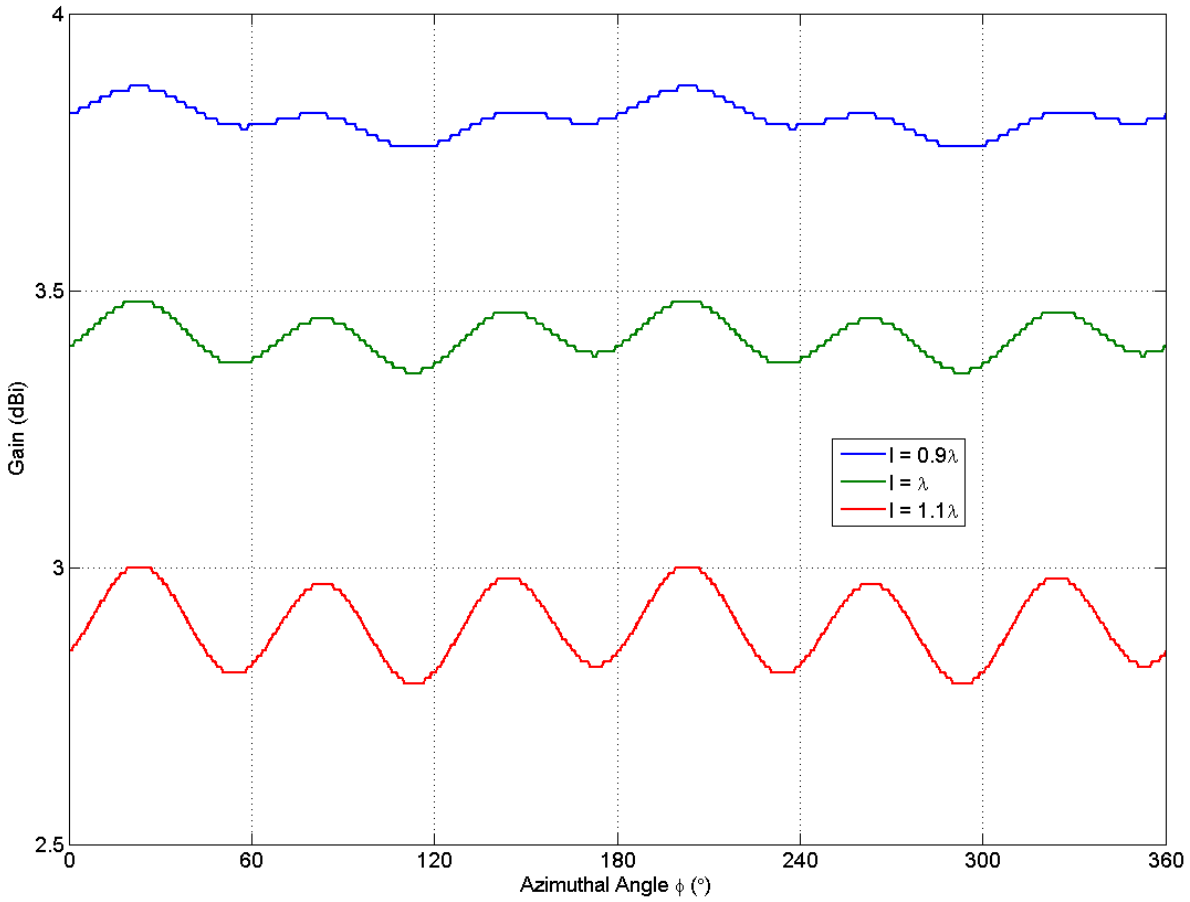

Fig. 46 5-Petal Big Wheel Simulated with v1 Azimuthal Pattern vs Petal Length ($f = 435MHz$)

4.3.2 Matching

Big wheel v1 code was primarily intended for simulating radiation patterns because it relatively accurately models the geometry of the arcs. However, as Fig. 40 above shows, big wheel v1 code cannot be used for accurately simulating match of n-petal wheel antennas because it does not accurately model the geometry of the central plates.

We attempted to use big wheel v1 code to at least identify trends for matching as a function of petal length and number of petals. Figure 47 below shows the trend predicted by big wheel v1. It plots predicted VSWR vs frequency vs number of petals vs petal length. The band of

$f \in [350,550]\,MHz$ is examined for 3 to 6 petals and petal lengths simulated are $l = 0.9\lambda$, 1.0λ and 1.1λ.

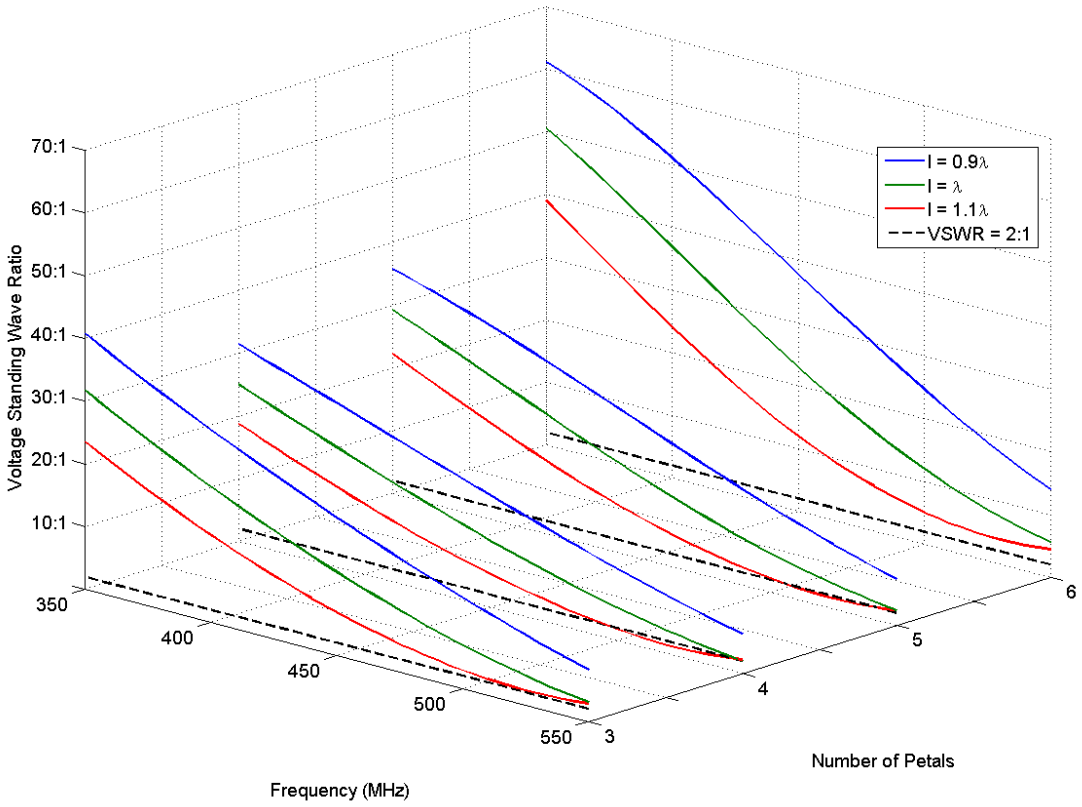

Fig. 47 Big Wheel Simulated with v1 Match vs Number of Petals vs Petal Length

The trend is that more petals is harder to match, and the antennas all appear to be closest to matched a higher than resonant frequency. These are just trends and exact numbers picked out of these simulations will be completely meaningless because of the central plates.

4.3.3 Summary

Based upon early simulations, the big wheel appeared to be a promising candidate for producing an omnidirectional, horizontally polarized radiation pattern. Although the original 3-petal configuration could not satisfy requirements, we determined that through variation of petal length and number of petals an effective pattern could be produced while still being capable of

achieving a proper impedance match. We determined that the 5-petal wheel, being the first geometry to show the desired omnidirectionality, would be the best design to move forward to further consideration and optimization. This would be achieved through the use of more detailed simulations that could account for specific details of the geometry.

5 Detailed Design

This chapter describes and justifies the decisions made in optimizing the simulated 5-petal wheel design a prototype of which was then built.

5.1 Methods and Justification

As discussed in section 4.3.3 (p. 68), we determined that the 5-petal big wheel antenna was the most promising for further consideration and that more detailed simulations were required to accurately determine which configuration to build and experimentally measure. Particularly, we observed that the petal length had a significant effect upon radiation pattern, and thus wanted to more accurately model the petals' actual geometry in simulation. This resulted in the big wheel v2 simulation code, which is described in detail in section 3.2 (p. 41). The code for big wheel v2 is in Appendix D (p. 117). For matching we attempted to simulate central plates as meshes of finite size wire, which resulted in the big wheel v3 simulation code, discussed in greater detail in section 3.2 (p. 41).

As was the case with the big wheel v1 simulation, we compared Group 39's measurements of the 3-petal wheel against results predicted by v2 and v3 simulation codes. Simulations accurately predicted radiation pattern, as is seen in Fig. 48 below. They were not able to accurately predict gain, but pattern was more important than the gain (as long as the maximum gain was in the azimuthal plane and not in elevation). Big wheel v2 simulation was particularly accurate in predicting the radiation pattern. Central plates of the v3 simulation obscured the predicted radiation pattern making v3 more useful for matching simulations and less so for pattern.

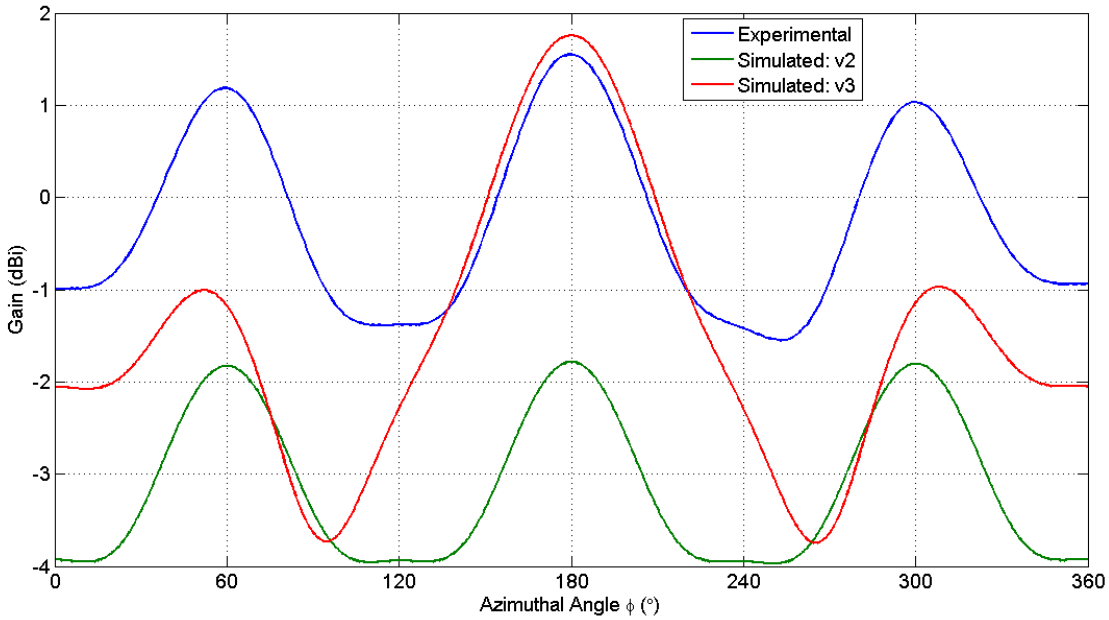

Fig. 48 3-Petal Wheel Measured vs Simulated with v2 and v3 Azimuthal Pattern ($f = 435MHz$)

As stated above, v2 and v3 simulations predicted gain has been substantially lowered as compared to what was predicted by v1 (see Fig. 39, p. 60). Big wheel v2 and v3 simulations show gain shifted by $-4.5dB$ on average compared to results from the v1 simulation. However, the v2 simulation still predicts peak gain within the azimuthal plane, as shown by the elevation radiation pattern of Fig. 49 below, which shows the predicted elevation pattern of a 3-petal wheel wheel at $f = 435MHz$ and $\phi = 0°$ with with petal lengths $l = 0.9\lambda$, 1.0λ, 1.1λ. An antenna cannot have negative gain (not the case for absolute gain) in every direction [2], due to energy conservation. Therefore this shift by $-4.5dB$ was deemed to be an imperfection in NEC-2's algorithm. This result greatly decreases our degree of confidence in the simulation's ability to predict gain. However, based upon the strong correlation of the predicted radiation pattern with that obtained from experimental measurements, we deemed v2 our best simulation to predict omnidirectionality.

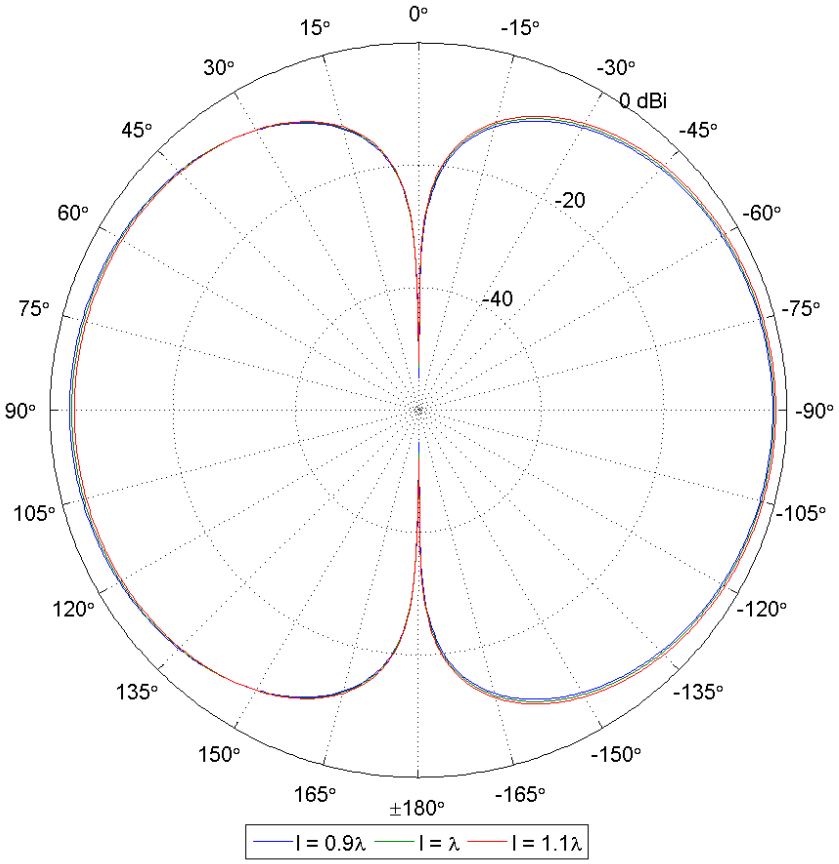

Fig. 49 3-Petal Big Wheel Simulated with v2 Elevation Pattern vs Petal Length ($f = 435MHz, \phi = 0°$)

Predictions of match were also improved by the v2 and v3 simulations. Our v3 simulation, in particular, showed promising correlation to measurements when central plates of the appropriate size were modeled. Figure 50 below shows this relation between measurements and v2 and v3 simulations using 3-petal wheel geometry with $l = 1.1\lambda$ and plate geometry of $d_p = 1\frac{11}{16}\,in$ and $s = \frac{1}{16}\,in$.

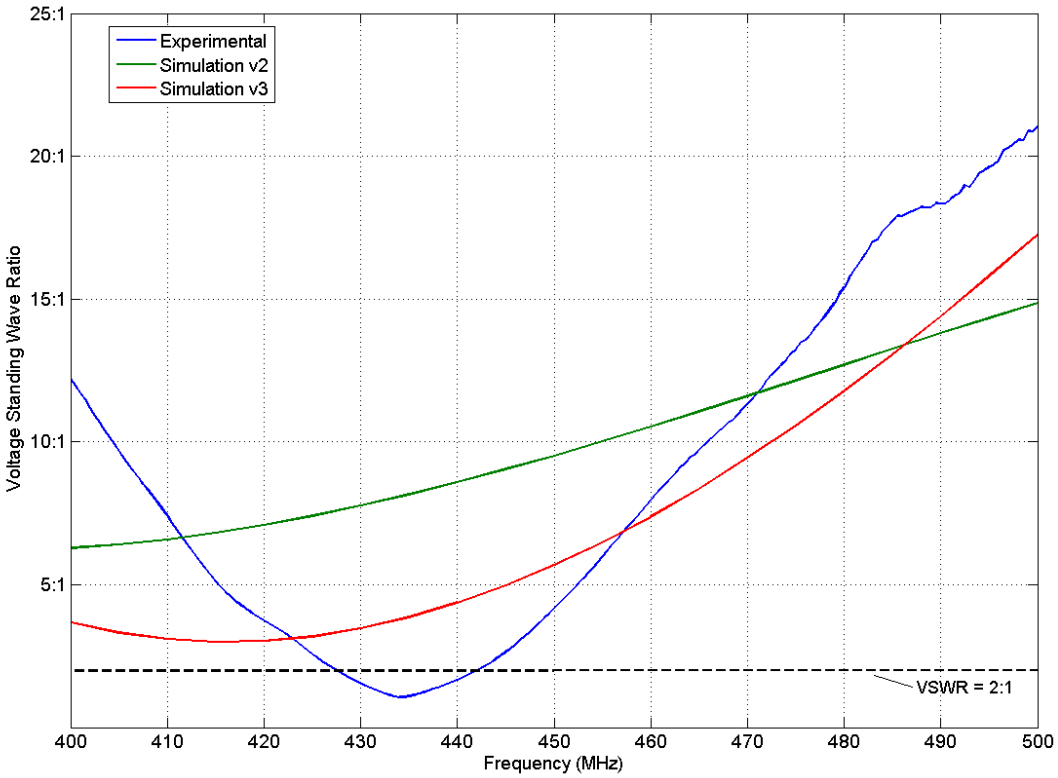

Fig. 50 3-Petal Wheel Measured vs Simulated with v2 and v3 Match

$$(l = 1.1\lambda, d_p = 1\,{}^{11}\!/_{16}\,in, s = {}^{1}\!/_{16}\,in)$$

The detailed simulations (v2) also produced results similar to those predicted by our early v1 simulations, confirming our decision to use a 5-petal wheel and allowing us to move on to design optimization. Figure 51 below shows the relation between v1 and v2 simulations by comparing azimuthal radiation patterns for 3, 4, 5 and 6-petal wheels at $f = 435MHz$ each with $l = 1.0\lambda$.

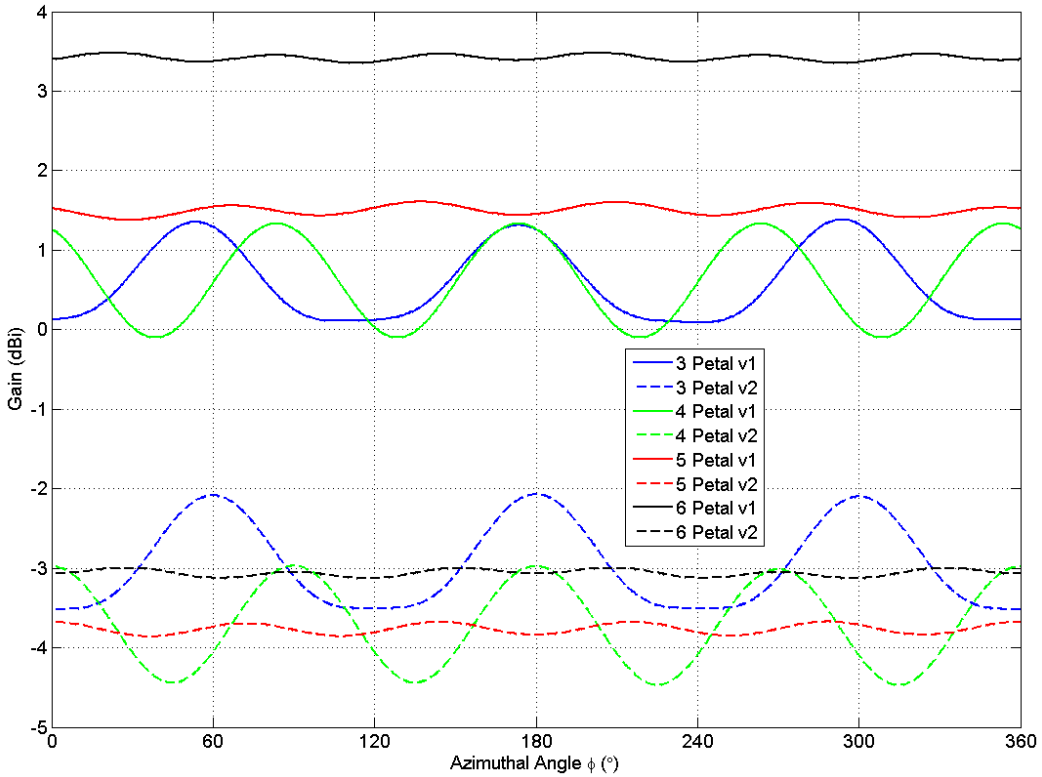

Fig. 51 Big Wheel Simulated with v1 and v2 Azimuthal Pattern vs Number of Petals ($f = 435MHz, l = 1.0\lambda$)

5.2 Design Optimization

Big wheel v2 simulation allowed for the variation of several of parameters defining the geometry of the antenna. However, not all of these were varied in optimization due to manufacturing restrictions. As with previous simulations, we varied only the total length of each petal l, while holding other structural design parameters constant. Table 7 (p. 42) and Table 8 (p. 43) list the structural design parameters over which the antenna was simulated with Big Wheel codes v2 and v3.

Due to the influence of petal length on the characteristics of the antenna, radiation pattern and match were given the greatest weight in determining the final design. This is mostly due to low degree of confidence in the simulation's accuracy in predicting gain and knowing that as long as the maximum gain is in the azimuthal gain and not the elevation, it will be positive (due

to energy conservation [2]). As shown in Fig. 52 below, the azimuthal radiation pattern at $f = 435MHz$ varied with loop length, with the smaller lengths producing the least deviation.

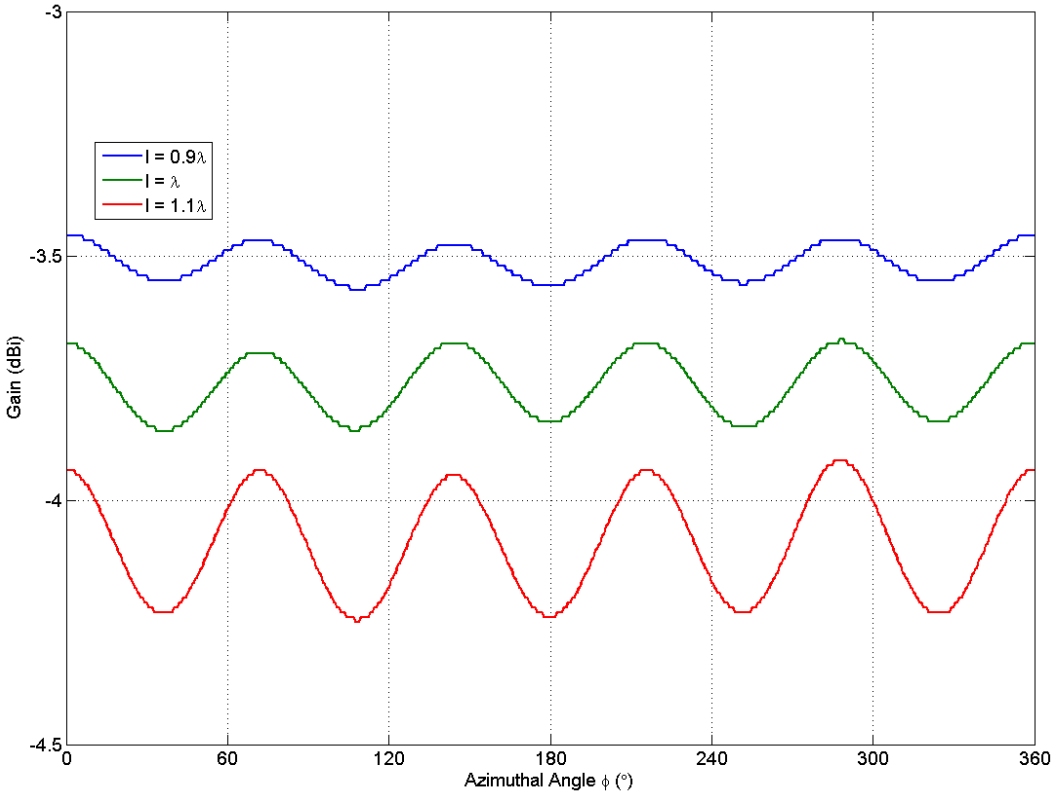

Fig. 52 5-Petal Big Wheel Simulated with v2 Azimuthal Pattern vs Petal Length ($f = 435MHz$)

Matching, and particularly the frequency at which the antenna is best matched, varied significantly as loop length was varied. Figure 53 below shows how impedance match varied for loop lengths of $l = 0.9\lambda$, 1.0λ, 1.1λ using the v2 simulation.

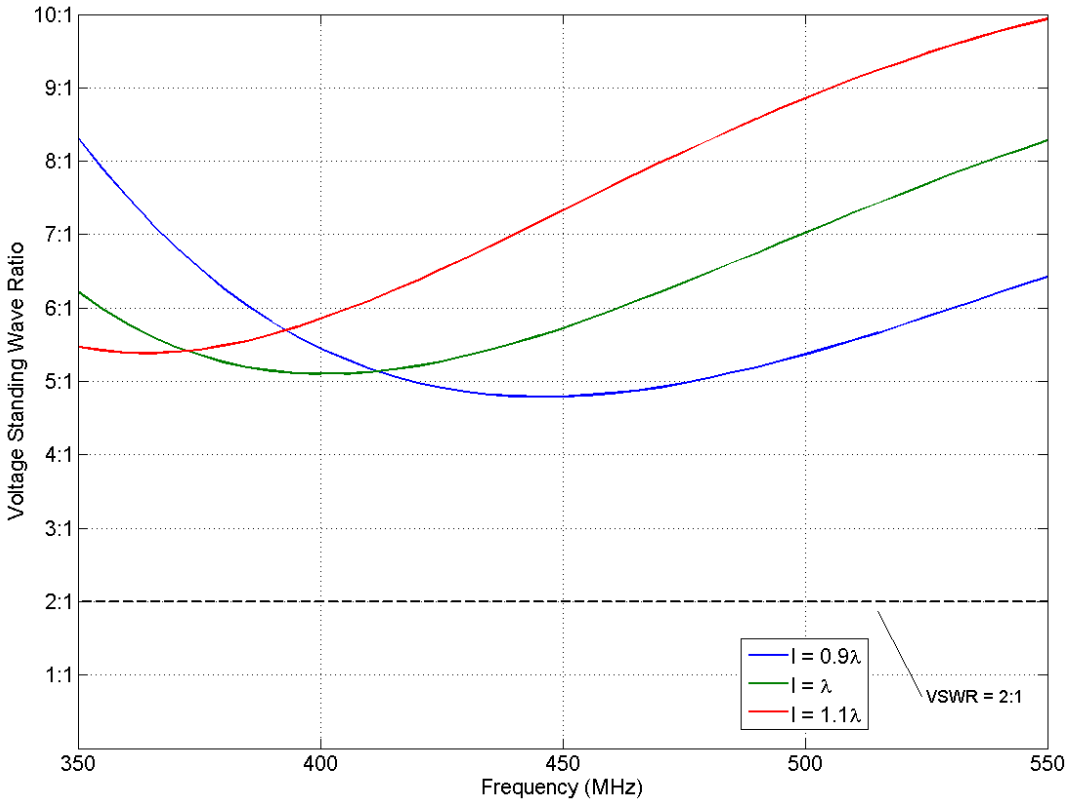

Fig. 53 5-Petal Big Wheel Simulated with v2 Match vs Petal Length

We also needed to determine how varying the size of the central plates might assist matching through use of our v3 simulation. Small plates had been used in Group 39's original prototype, and plates of comparable size $d_p = 1\,^{11}/_{16}\,in$, $s = {}^{1}/_{16}\,in$ were considered first. The impedance match of a wheel with this plate configuration simulated with v3 for $l = 0.9\lambda$, 1.0λ, 1.1λ is shown in Fig. 54 below. The variation with loop length is much the same with this simulation as was seen with the v2 simulation. However, as seen Fig. 50 above, v3 simulation was significantly more accurate than v2.

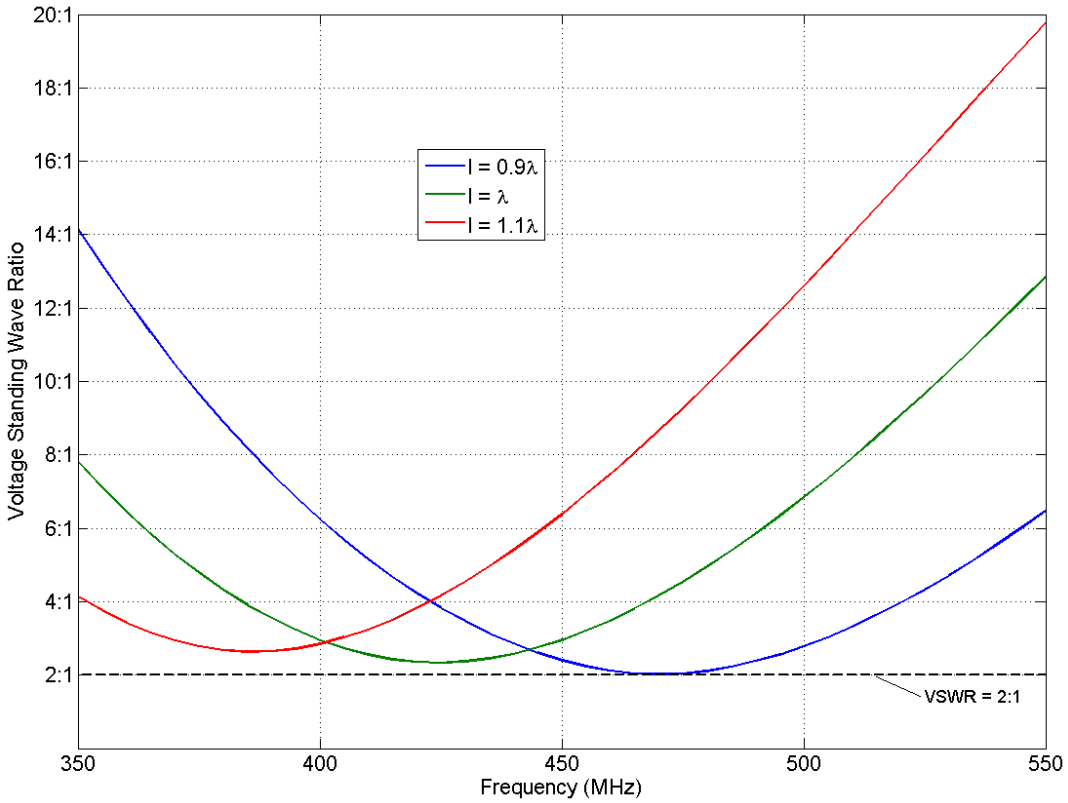

Fig. 54 5-Petal Big Wheel with Small Plates Simulated with v3 Match vs Petal Length ($d_p = 1\frac{11}{16}\,in,\ s = \frac{1}{16}\,in$)

The same simulation was also run for a larger plate size ($d_p = 3in$). Figure 55 below shows the results. The simulation suggests that increasing the size of the plates has the effect of further improving the impedance match of the antenna, as well as shifting the frequency at which it best matched.

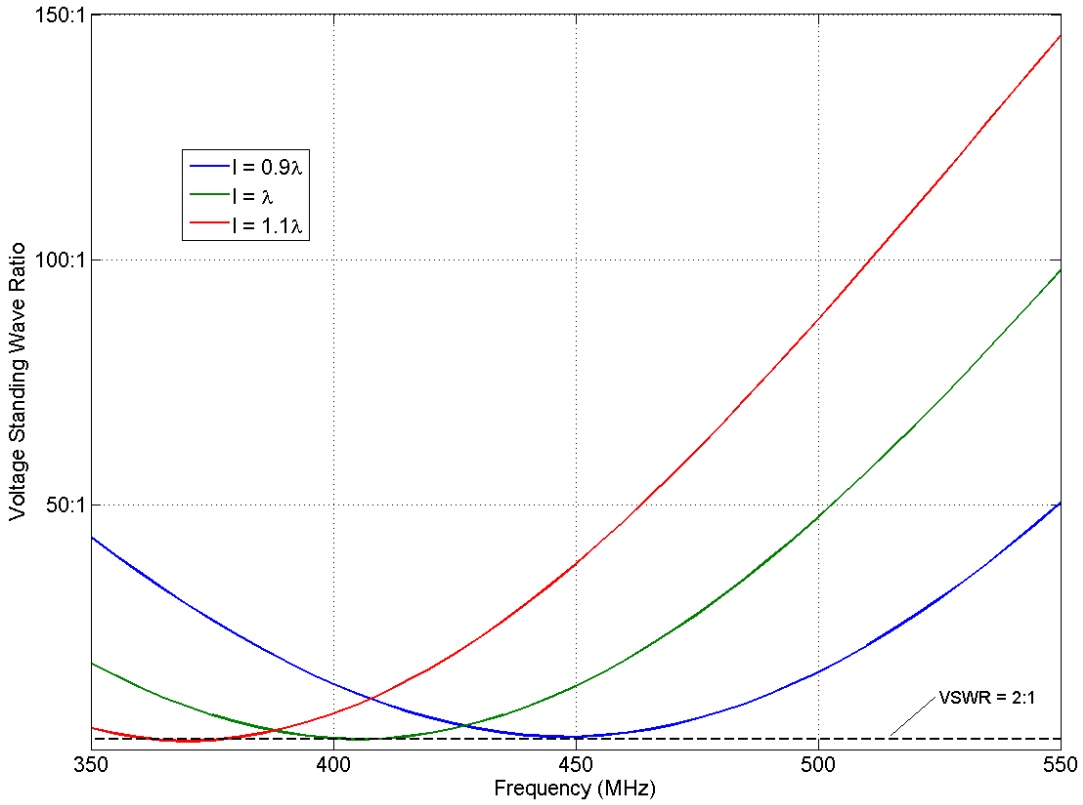

Fig. 55 5-Petal Big Wheel with Large Plates Simulated with v3 Match vs Petal Length

$$(d_p = 3in,\ s = 1/16\ in)$$

Simulated impedances showed the 5-petal wheel antenna to have mostly imaginary inductive input impedance. Its impedance varied significantly with petal size l. Figure 56 below shows 5-petal wheel antenna's Smith chart produced using v3 simulation. From the antenna's location on the Smith chart we can see that in theory a shunt (parallel) capacitor would match the antenna. If the central plates were to behave as parallel-plate capacitor, their size could be adjusted to match the input impedance, because they are in parallel with the petals.

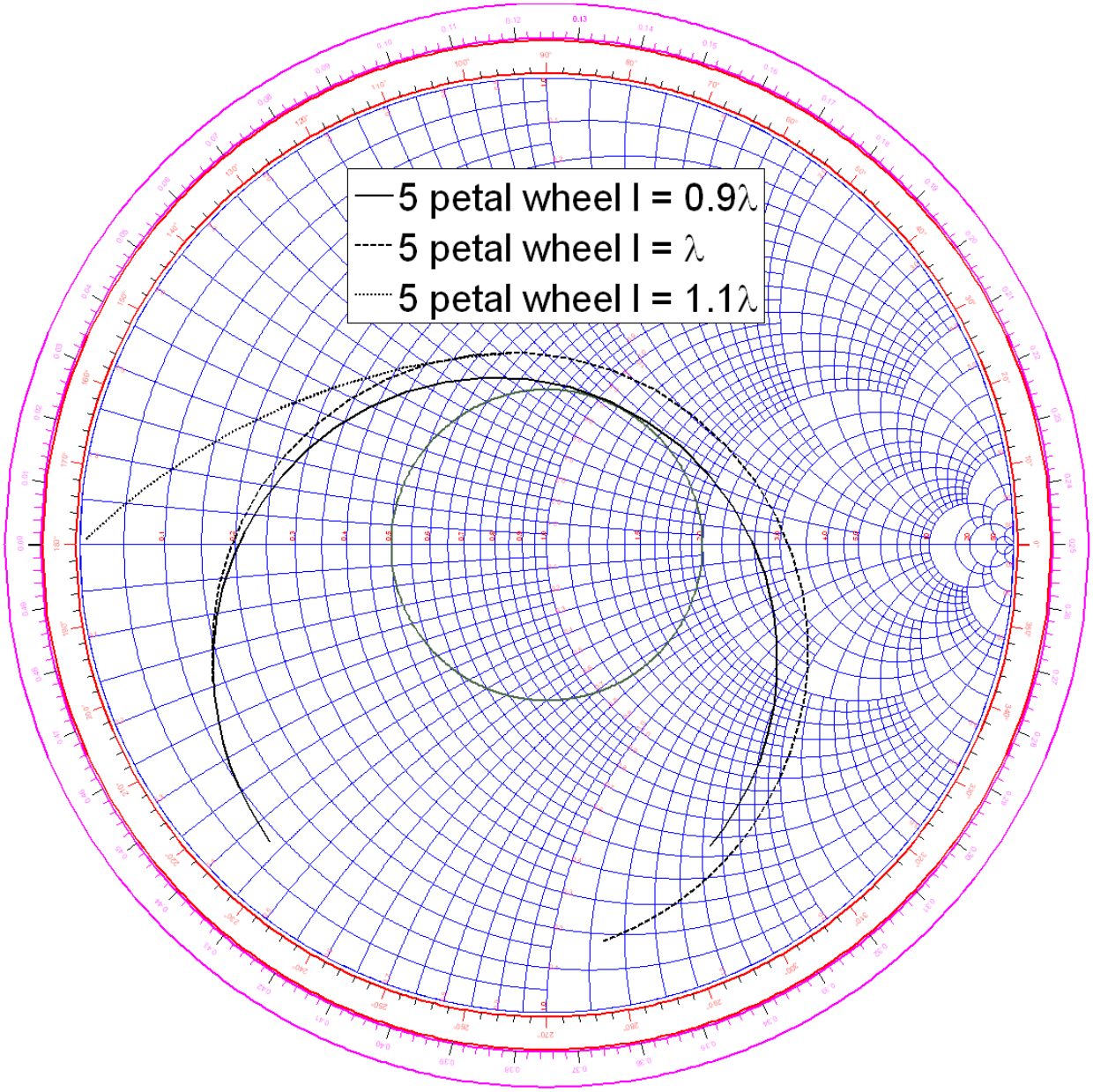

Fig. 56 5-Petal Big Wheel Simulated with v3 Smith Chart with Varying Petal Size

$(d_p = 1\frac{11}{16}\,in,\ s = \frac{1}{16}\,in,\ f \in [350,550]\,MHz)$

5.3 Prototype Dimensions

Based upon trends in simulation results, we concluded that a small petal length would not only provide omnidirectionality well within specifications, but also the highest gain among the 5-petal wheels. Further, both our v2 and v3 big wheel simulations suggested that at $l = 0.9\lambda$

petal length the 5-petal antenna would be matched as well as, if not better than, other petal lengths, and may also be natively tuned to be impedance matched within our desired operation frequency. Therefore, we selected a 5-petal wheel having $\boldsymbol{l = 0.9\lambda}$ as our final design to be built as a prototype and measured.

Simulations suggest that this antenna has its peak gain within the azimuthal plane, as shown by Fig. 57 below, which shows the antenna's simulated (with v2) elevation radiation pattern at $\boldsymbol{f = 435MHz}$.

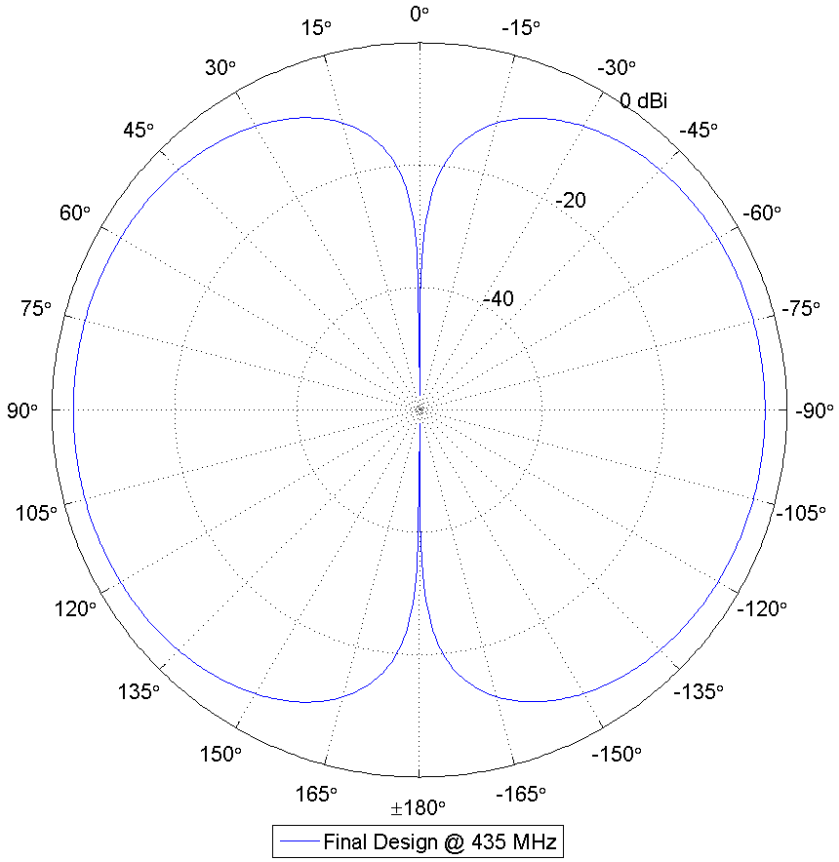

Fig. 57 Prototype Simulated with v2 Elevation Pattern
($\boldsymbol{f = 435MHz}$)

Although the antenna has relatively high gain above and below the azimuth, making it almost isotropic, it shows very good omnidirectionality in the azimuthal plane, having a variation

of only ± 0.06 dB in simulation. Figure 58 below shows the prototype's simulated (with v2) azimuthal radiation pattern for $\boldsymbol{f = 435MHz}$.

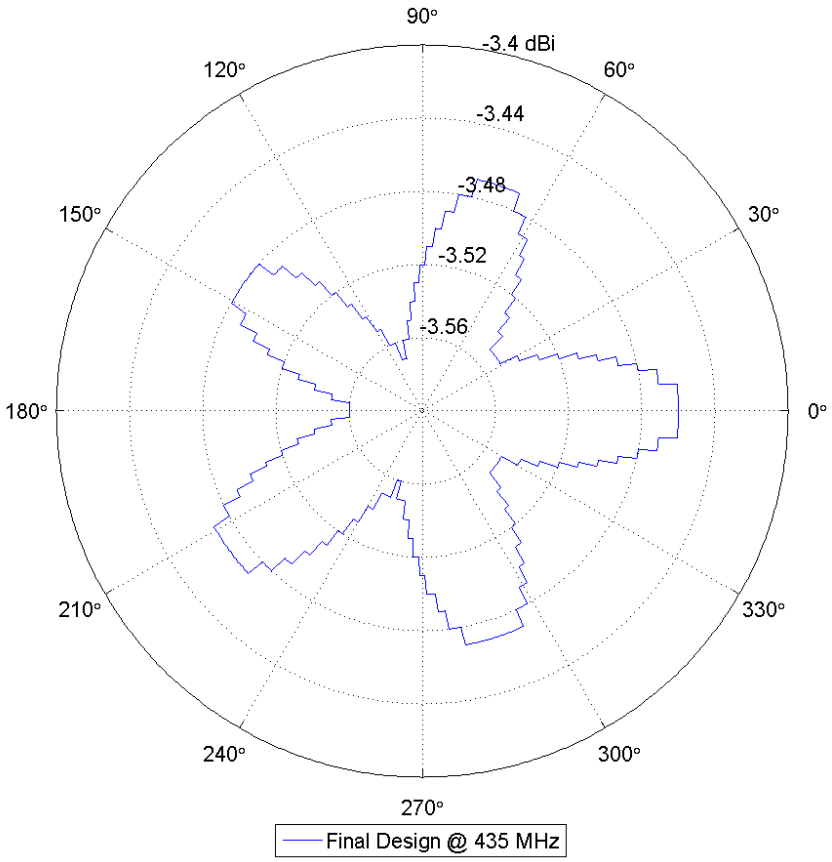

Fig. 58 Prototype Simulated with v2 Azimuthal Pattern
$(\boldsymbol{f = 435MHz})$

The prototype's 3D radiation pattern simulated with v2 is shown at $\boldsymbol{f = 435MHz}$ in Fig. 59 below:

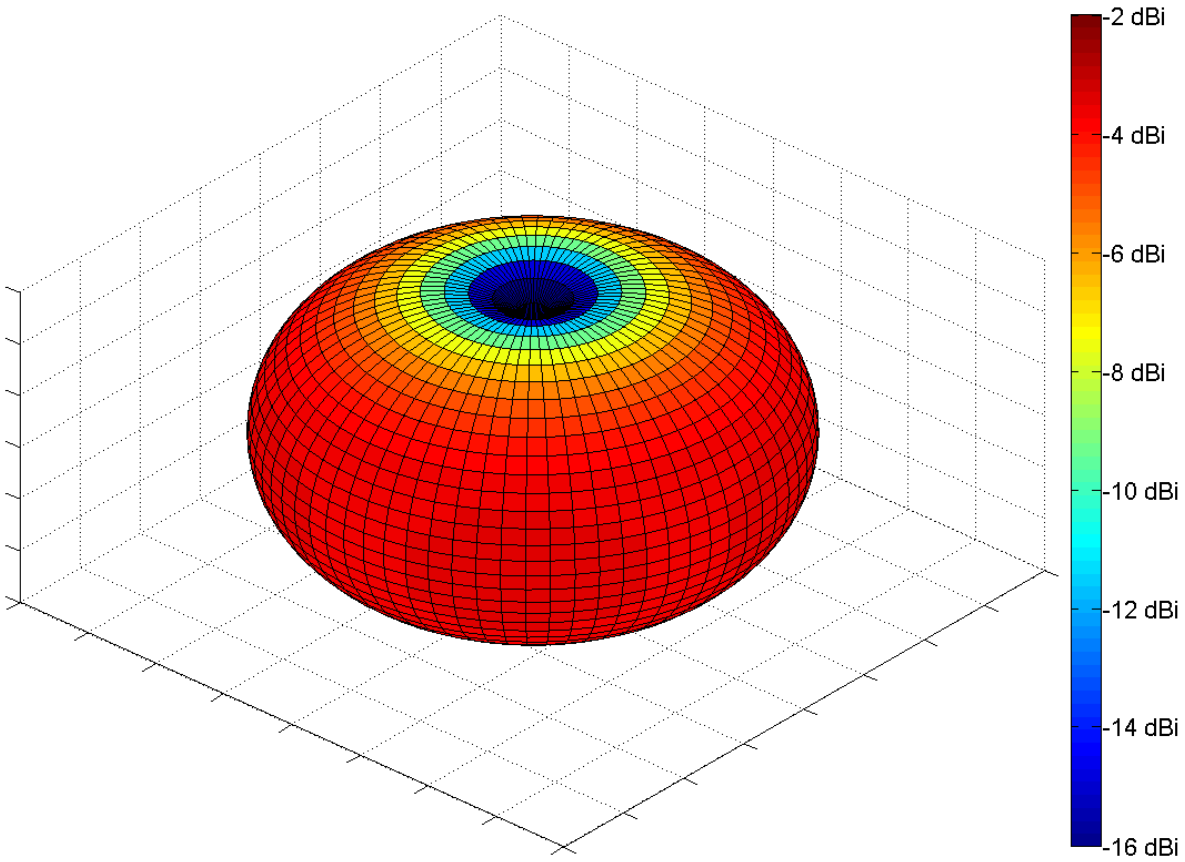

Fig. 59 Prototype Simulated with v2 3D Radiation Pattern
($f = 435MHz$)

As we had only a moderate degree of confidence in the accuracy of the impedance match predicted by simulations, the match was expected to be the main challenge for the prototype. As such, we requested that two sets of central plates be built, one having the dimensions used in the previous 3-petal prototype ($d_p = 1\frac{11}{16} in$), and another of roughly twice the size ($d_p = 3in$). We believed that these plates would act as parallel capacitors, which as discussed in section 5.2 above, would bring the impedance of the antenna to within a close match to its transmission line. By producing two plates, would could confirm this expectation and either match the antenna or determine a more appropriate central plate size for future prototypes.

Table 9 below contains the final dimensions of the produced prototype. See Fig. 22 (p. 42) for definitions of the structural parameters listed in Table 7. Appendix G (p. 126) contains an illustration of how the central plates were constructed.

Table 9 Prototype's Final Dimensions

Parameter	Value
Plate Diameter	$d_p = 1\frac{11}{16} in = 1.68 in$
Antenna Radius	$r_o = 8.34 in$
Interval Between Adjacent Parallel Legs	$h_2 = 1/2 \; in = 0.5 in$
Total Petal Wire Length	$l = 24.42 in$
Leg Length	$l_l = 6.86 in$
Arc Angle Interval	$\gamma = 6.5°$
Arc Angle	$\alpha = 59°$
Round Radius	$r_r = 5/8 \; in = 0.63 in$
Round Angle	$\delta = 97°$

6 Measurements and Analysis

The prototype was built to the general specifications that resulted from the optimization discussed in section 5.2 (p. 74). The exact parameters of the physical prototype can be found in section 5.3 (p. 79); an illustration of the central plates can be found in Appendix G (p. 126). Figure 60 below is a photograph of the prototype, with small ($d_p = 1\frac{11}{16}\,in$) plates.

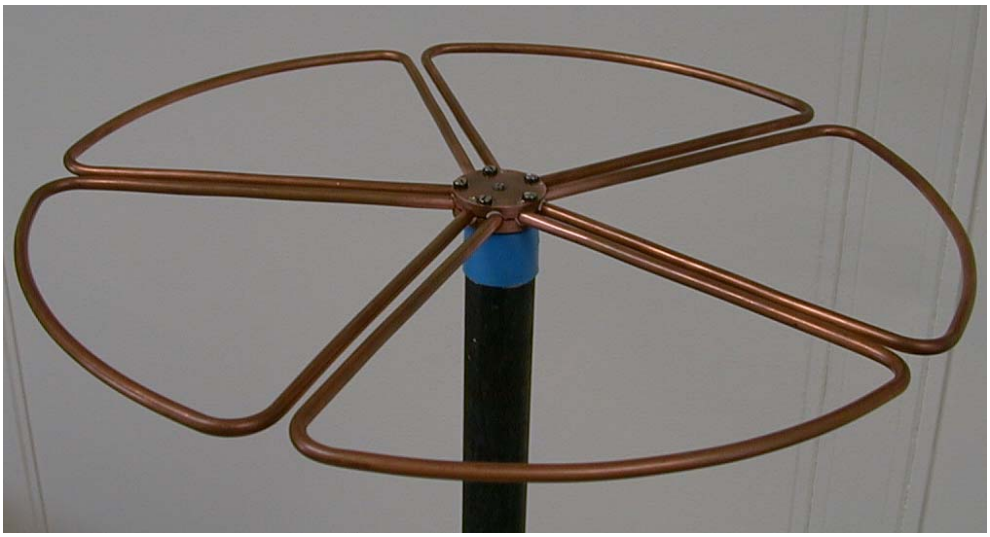

Fig. 60 Prototype with Small Central Plates Photograph[10]

6.1 Measured Impedance Match

Two pairs of central copper plates were manufactured for the prototype, the small pair with diameter $d_p = 1\frac{11}{16}\,in$ and the large pair with diameter $d_p = 3in$. We made S_{11} measurements for the prototype antenna with both sets of plates, and compared to simulation. Figures 61 and 62 below show the results of these measurements as compared to big wheel v3 simulation for appropriately sized plates.

[10] This photograph was taken by Dr. Herbert Aumann of MIT Lincoln Laboratory.

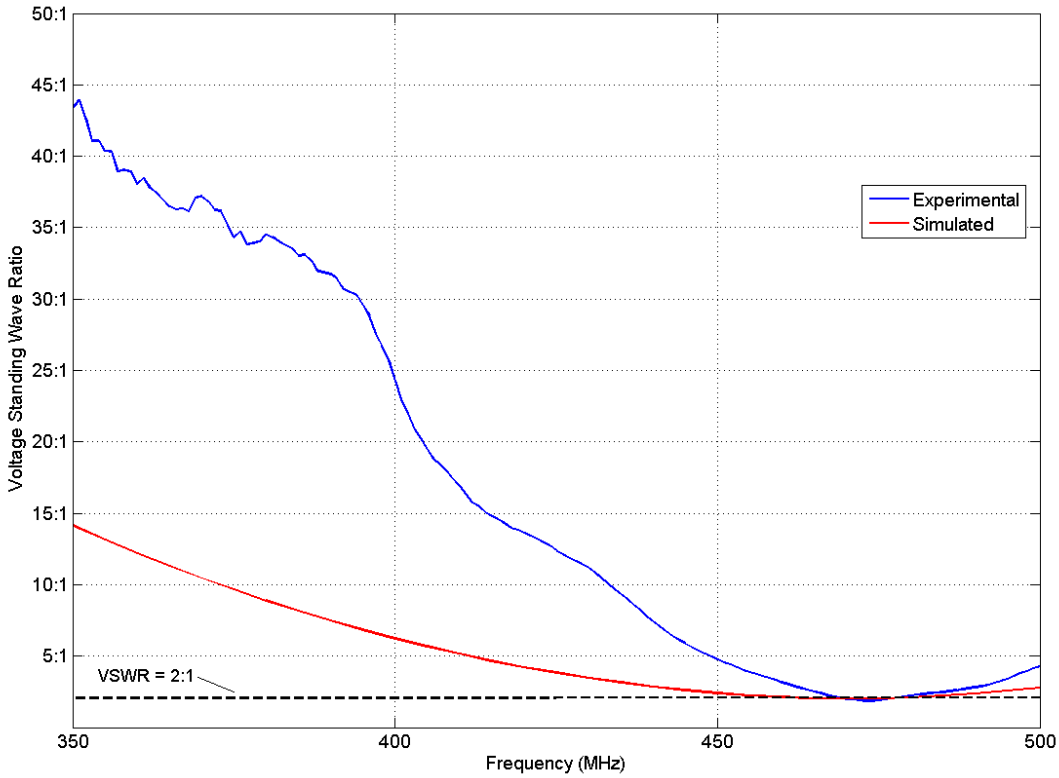

Fig. 61 Prototype with Small Plates Measured vs Simulated with v3 Match

The dependence of the position on the Smith chart on the plates is shown in Fig. 63 below. The large plates did not act as expected at all, instead shifting the impedance away from $\mathbf{50\Omega}$. The spacing between the large plates was also adjusted from $s = \frac{1}{16} in$ to $s = 0.090 in$ but with no observable effect.

Based upon these results and further theoretical research, we determined that the central plates do not act as parallel (shunt) capacitors and instead approximately act as a parallel-plate transmission line.

When used as a transmission line, parallel plates may display both capacitive and inductive behavior. Specifically, for a parallel-plate transmission line configuration in which "the

plate width w is large compared with the plate separation s[11]," and "the skin depth δ is small compared to the thickness t of the plates," [12] the following relations may be applied for the capacitance and inductance of the transmission line respectively:

$$C = \varepsilon \frac{w}{s} \tag{6.1}$$

$$L = \mu \frac{s}{w} \tag{6.2}$$

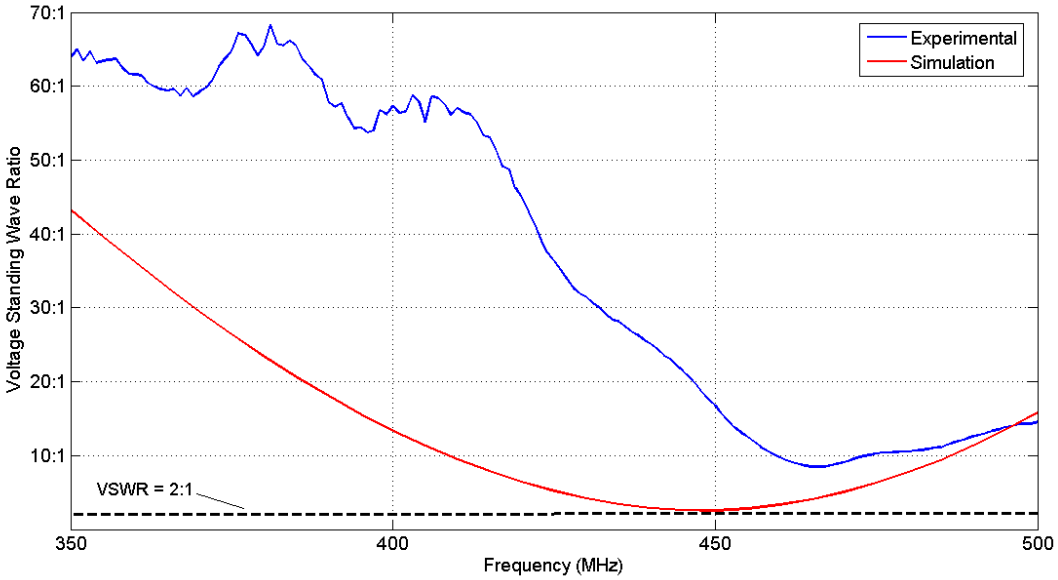

Fig. 62 Prototype with Large Plates Measured vs Simulated with v3 Match

[11] In Ludwig and Bretchko variable d is used, but in this report this variable is s.

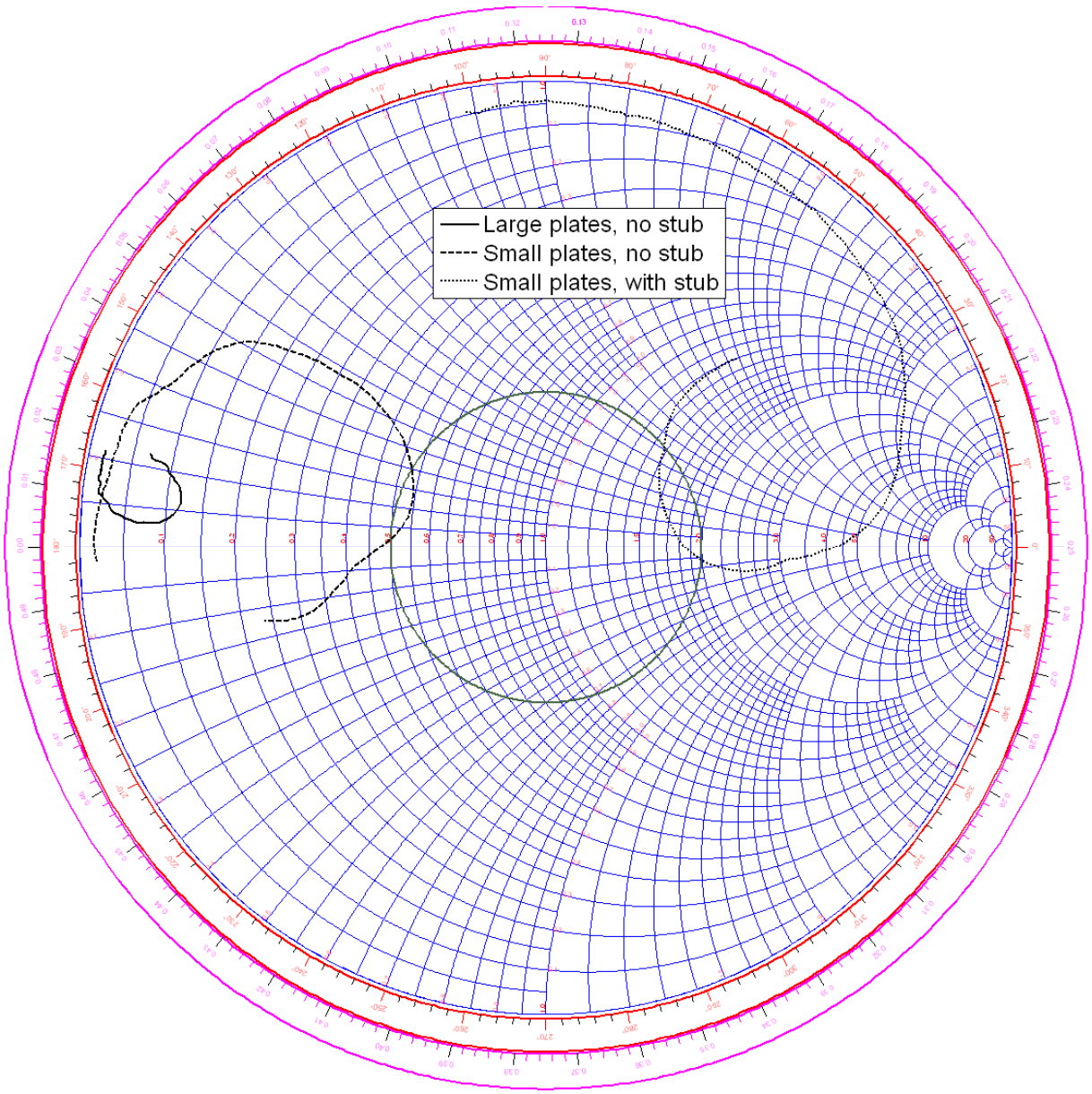

Fig. 63 Prototype Measured Smith Chart Dependence on Plate Size and Stub

Where μ is the permeability of the medium between the plates, ε is the permittivity of the medium between the plates, s is the plate separation and w is the width of the plates. [12]

Although the parallel-plate feed at the center of our prototype is not strictly a parallel-plate transmission line, but rather a highly specific and more complex arrangement of a parallel-plate transmission line, these relations of Eqs. (6.1) and (6.2) still hold to some extent. The width

of the plates is larger than the plate separation by a factor of roughly 25 and the plates have a significant thickness ($t = 0.25in$) which will be much greater than the skin depth.

The complex geometry of the plates and connected elements makes direct application of the equations defining parallel-plate transmission lines inaccurate at best. However, the results may nonetheless provide a generalized view of the interactions in the parallel-plate construction. Applying Eqs. (6.1) and (6.2) theoretically predicts an inductance much higher than its capacitance (by a factor of roughly 250), indicating why the parallel plates of the antenna acted inductively. This means that central plates, at least in their current configuration (central parallel circular plates $d_p = 1/16\ in$ apart with Teflon spacers in between) cannot be used for matching this prototype. Therefore, an alternative central configuration (see chapter 7, p. 99) is required to tune the antenna.

Instead of matching with the plates as planned the antenna had to be single stub-matched instead. An open stub when viewed at its input is a pure susceptance, and thus will move the point clockwise along the line of constant conductance that the point is on. How far it moves the point depends on the frequency of the point, which is why stub-tuning generally increases frequency dependence of the antenna thus widening the Smith chart point group over a given frequency band. Pozar [5] discusses Smith chart application for stub tuning in detail. A longer open stub will move the point more. A shorted (shunt) stub is, when viewed at its input, a pure reactance, and thus will move the point counterclockwise along the line of constant resistance. Again, a longer shunt stub will move the point further and thus increase the antenna's frequency dependence.

Adding a stub means adding a T splitter to the transmission line feeding the antenna close to the input of the antenna and then adding the stub to that T and changing its length. Adding that

T means adding a length of a transmission line, which adds a delay and moves the point clockwise along a circle of constant magnitude (thus not affecting the point's VSWR but moving it clockwise).

The effect of the stub used to tune the prototype can be seen on Fig. 63 above and Fig. 64 below. An very short open stub was used. Figure 65 below is the photograph of the tuning stub used along with the T. The stub consists of an SMA-type gender changer, dual-male and female SMA-T and dual-male SMA-L. An ideal stub would be slightly shorter than the resulting configuration but these were the minimal lengths physically possible. The stub was attached right under the antenna, between the SMA transmission line and type N to SMA converter.

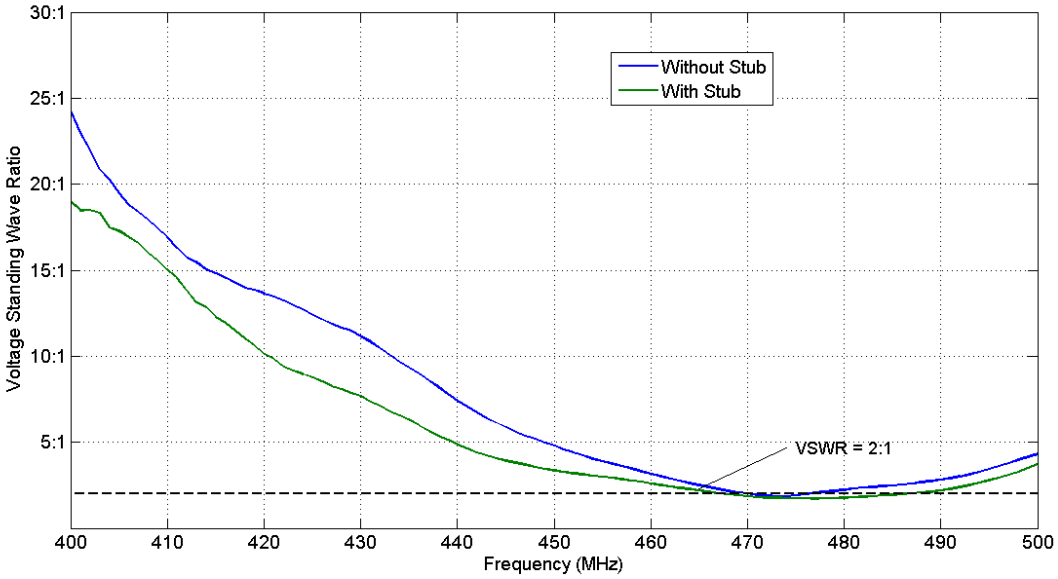

Fig. 64 Prototype Measured Match with Stub and without Stub

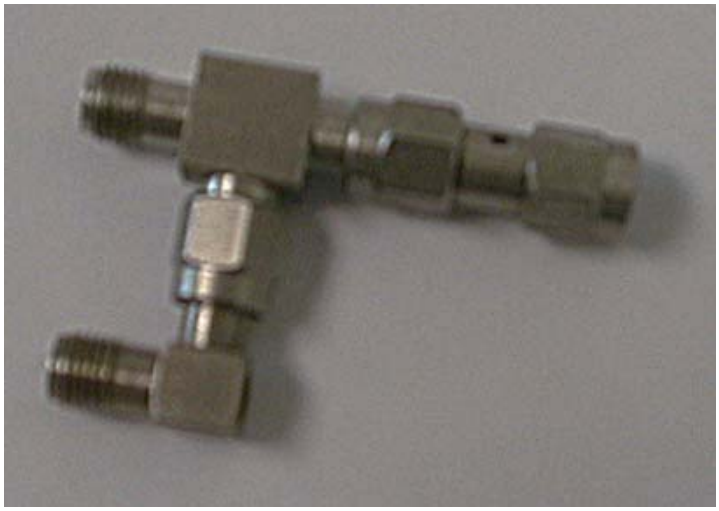

Fig. 65 Prototype's Tuning Stub Photograph[12]

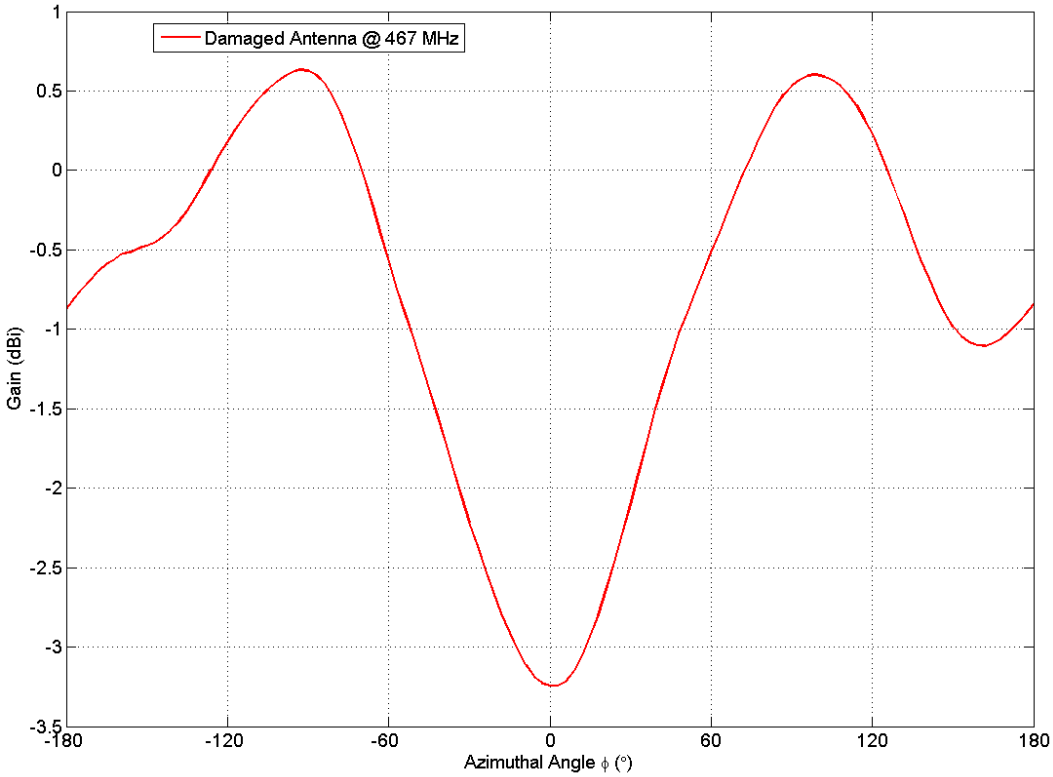

Fig. 66 Damaged Prototype Measured Azimuthal Pattern
($f = 467 MHz$, no stub)

[12] This photograph was taken by Dr. Herbert Aumann of MIT Lincoln Laboratory.

6.2 Measured Radiation Pattern

Measurements of radiation pattern were conducted in a tapered anechoic chamber after a number of measurements of impedance match had been conducted. During these impedance measurements, the prototype was disassembled to vary the size of the central plates, and in this process the antenna was mechanically damaged. Initial measurements were made before we realized that minor defects would have a significant impact upon the antenna's azimuthal radiation pattern. Figure 66 above shows the results of these measurements at $f = 467MHz$. Notice that all gain measurements given in this section are gain-calibrated unless specifically stated otherwise.

Neither the omnidirectionality nor the shape nor the gain of this pattern agreed with simulation. Upon inspection of the prototype, we found that a Teflon spacer used to prevent petals from short circuiting was partially dislodged and that a number of petals were bent slightly out of shape. The defects were repaired and new measurements conducted. Figure 67 below shows a comparison of the new results to the previous results at $f = 465MHz$.

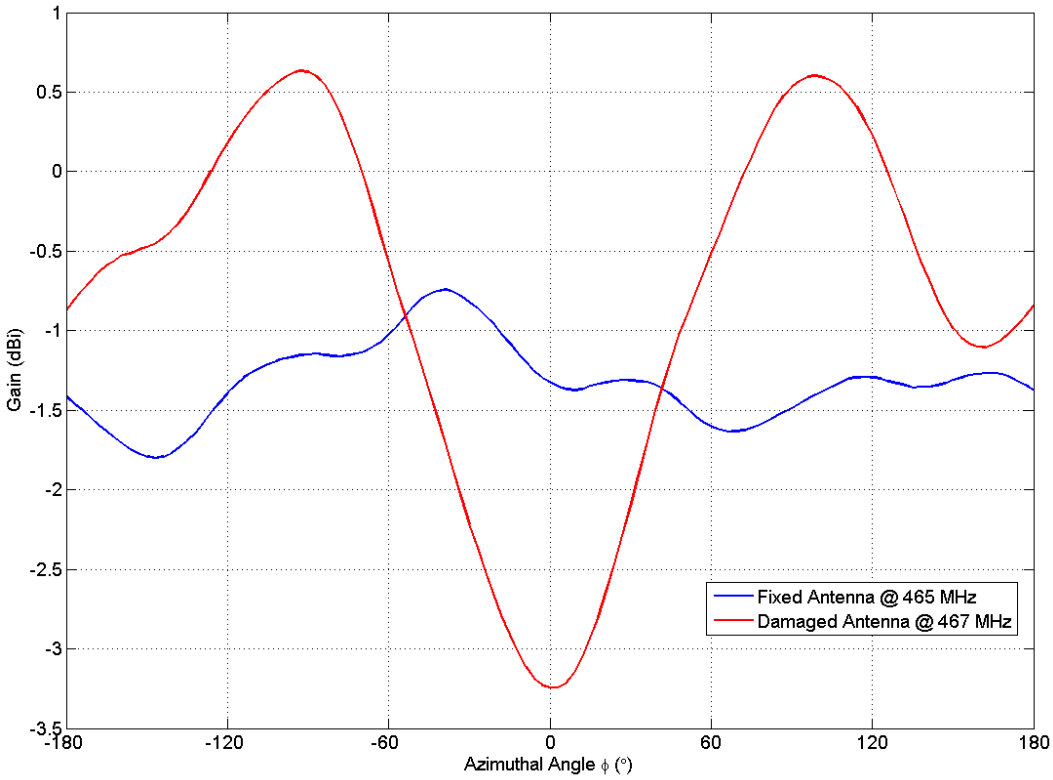

Fig. 67 Damaged vs Repaired Prototype Measured Azimuthal Pattern (no stub)

The repairs resulted in a significant improvement in the antenna's omnidirectionality, although the pattern was still noticeably asymmetric. Figure 68 below shows azimuthal radiation pattern measurements of the repaired antenna over a range of frequencies, $f = 420$, 440, 460, 480 and $500 MHz$. Notice that the average azimuthal gain follows the match (see Fig. 61 above) and maxes out at $f \approx 480 MHz$.

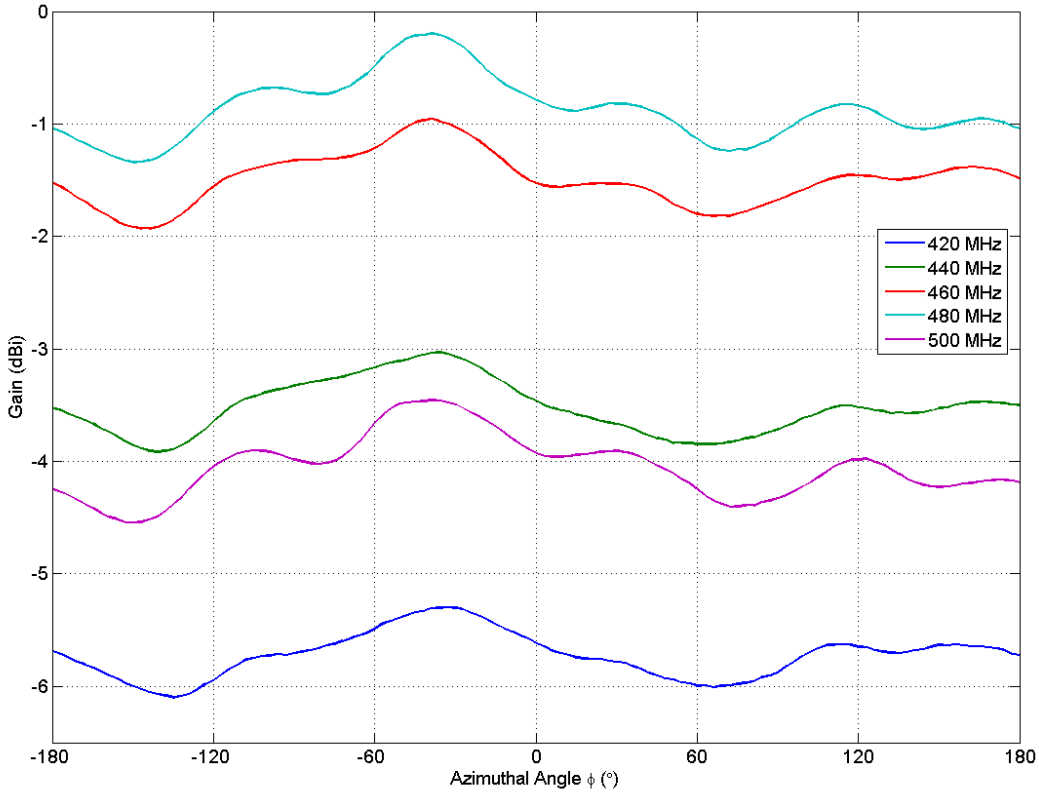

Fig. 68 Repaired Prototype Measured Azimuthal Pattern vs Frequency (no stub)

We found little correlation between our simulations and experimental measurements. Figure 69 below compares both the gain and azimuthal radiation patterns of simulation to experimental results at $f = 435, 450 MHz$.

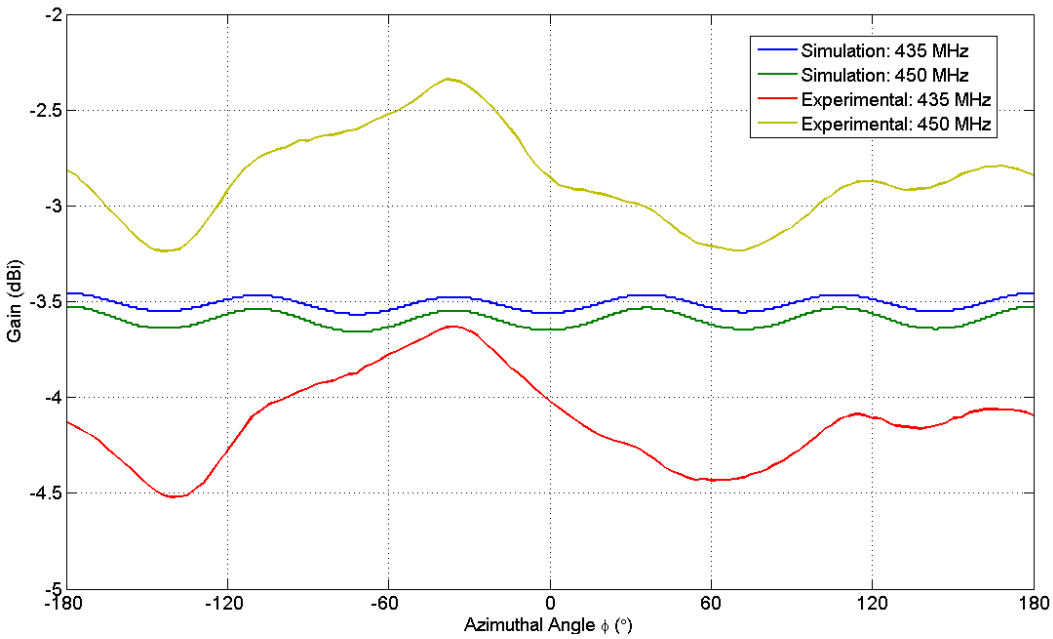

Fig. 69 Repaired Prototype Measured vs Simulated with v2 Azimuthal Pattern (no stub)

It is notable that the measured pattern is not a repetition of five nearly identical ripples across the azimuthal angle range, which would be expected from its geometry. We suspect that this is due to the mechanical imperfections causing the ripple, as opposed to the antenna's electrical structure. Therefore a more precise manufacturing - ideally machining the entire structure out of a big copper workpiece – may be required to get the best omnidirectionality possible.

We also measured the effect of both the stub matching system and a single square reflector on the radiation pattern of the prototype. As shown by Fig. 70 below, the stub greatly disturbed the pattern at $f = 466MHz$, increasing ripple in pattern from $\approx 0.4dB$ to $\approx 1dB$ as compared to a measurement with no stub.

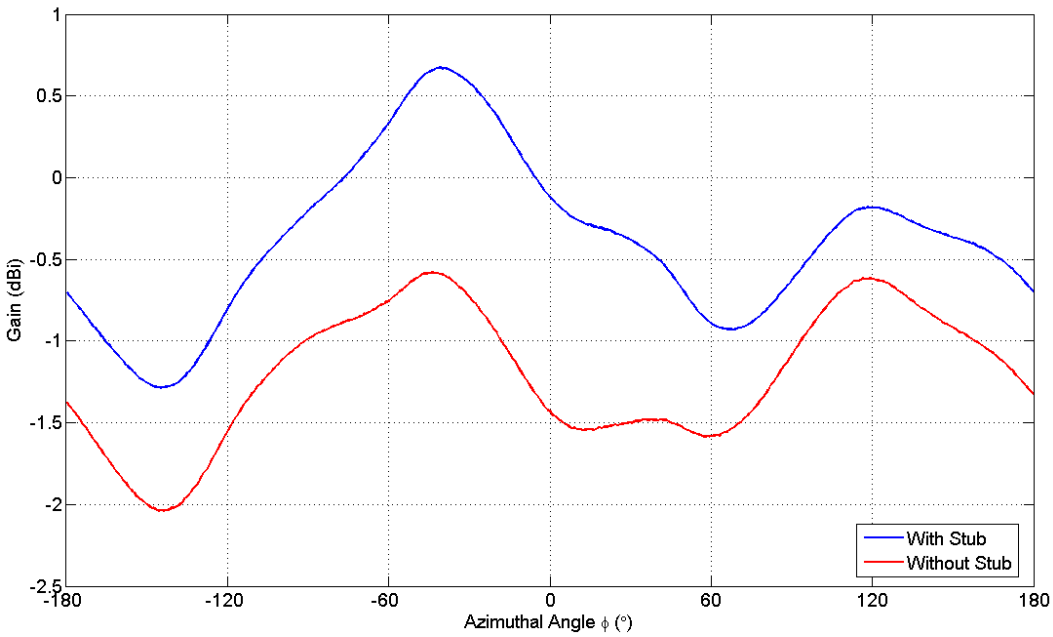

Fig. 70 Repaired Prototype with Stub vs no Stub Azimuthal Pattern
($f = 466MHz$)

Figure 71 below shows a photograph of the metallic rectangular reflector that the antenna was measured with. Due to time constraints, a circular reflector could not be manufactured, and so the reflector the prototype was measured with is highly asymmetric. It was thus less than ideal for an omnidirectional antenna, however, it still provided a way to test the effect of a single reflector on the pattern.

Fig. 71 Repaired Prototype with Rectangular Reflector Photograph[13] ($d = 0.5\lambda$)

Figure 72 below compares the results of a single square reflector placed a distance $d = 0.5\lambda$ below the antenna to results with no reflector at $f = 465MHz$. The reflector performed as expected, increasing gain by $\approx 1dB$, although at the cost of pattern. This was expected, as not only was a single reflector used, but it was square and thus introduced asymmetry of its own. A more accurate consideration of the effect of reflectors upon the azimuthal radiation pattern would require circular reflectors placed both above and below the antenna. Also note that the reflector used was not grounded, just like the reflectors in simulation.

Prototype's measured azimuthal gain as a function of frequency and azimuthal angle is shown in Fig. 73 below.

[13] This photograph was taken by David Bruno of MIT Lincoln Laboratory.

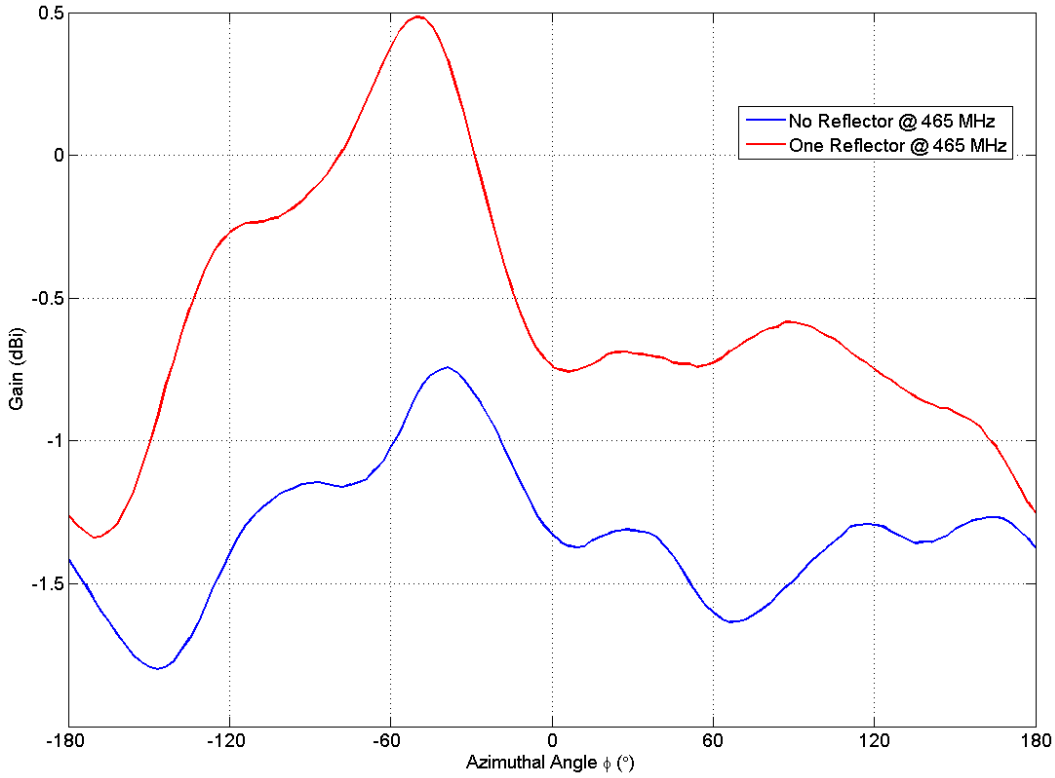

Fig. 72 Repaired Prototype Rectangular Reflector Effect on Azimuthal Pattern ($d = 0.5\lambda$)

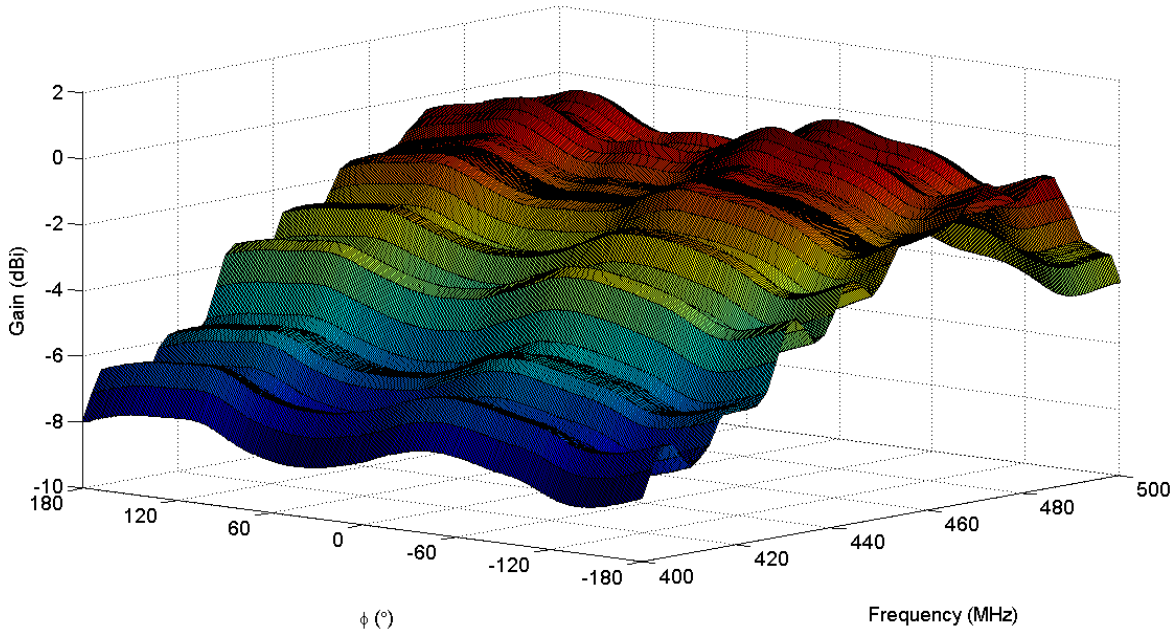

Fig. 73 Repaired Prototype Gain vs Frequency vs Azimuthal Angle (no stub)

6.3 Prototype Performance Summary

The manufactured prototype's geometry was somewhat different from the simulated model due to central plates and unavoidable mechanical imperfections introduced in manufacturing and tweaking. However, its azimuthal pattern was still very omnidirectional, having ripple of only $\approx 0.4dB$. More precise manufacturing and handling of the antenna should help reduce ripple even more. Stub and reflector both increased the gain (due to match and geometry variation respectively), both damaging the pattern. The prototype was measured to be best matched at higher frequencies than expected: $VSWR \leq 2:1$ at $f \in [470,476]MHz$ with no stub and $f \in [468,486]MHz$ with stub. However, with VSWR limit lifted to $VSWR \leq 2.5:1$ the antenna was measured to be matched at $f \in [466,485]MHz$ with no stub and $f \in [462,492]MHz$ with stub.

The prototype's measured azimuthal gain peaked at just under $0dBi$, which was expected, as the antenna's simulated radiation pattern is nearly isotropic. It also follows the match, and thus increasing the match will increase the gain.

A single square reflector increased the gain but disturbed the pattern, increasing the ripple. A circular reflector should increase the gain without disturbing the pattern, and dual reflectors above and below the prototype should increase the gain even more.

7 Conclusions and Recommendations

This chapter summarizes the outcome of this project.

7.1 Conclusions

After extensive consideration of antenna geometries and optimization of design parameters, we produced a prototype 5-petal "big wheel" antenna with each petal length of $l = 0.9\lambda$ and parallel circular plates central configuration. According to all of our simulations, 5-petals is the minimum number of petals that can produce the omnidirectional pattern required.

The prototype antenna's impedance match, azimuthal radiation pattern and gain were measured experimentally. The antenna was found to be natively matched in a narrow band and at a higher frequency than in simulation. Without a tuning stub the prototype had $VSWR \leq 2:1$ at $f \in [470, 476]MHz$, but it also had $VSWR \leq 2.5:1$ at $f \in [466, 485]MHz$. Tuning stub matched the antenna at $f \in [468, 486]MHz$ for $VSWR \leq 2:1$ and $f \in [462, 492]MHz$ for $VSWR \leq 2.5:1$.

This match could be improved with a parallel capacitor, and it was expected that the central plates would act as one. However, these plates were found to be parallel-plate transmission lines acting highly inductively instead.

The radiation pattern of the prototype was found to be highly sensitive to very minor defects in construction. Although the measured pattern had little correlation to those predicted our simulations, it was still very omnidirectional with a ripple of only $\pm 0.4dB$.

The prototype's gain was measured to be just under $0dBi$ at frequency of best match. This agrees with simulation which predicts the 3D pattern to be nearly isotropic with the highest gain being in the azimuthal plane. This gain was measured to improve by about $1dB$ after an

addition of a rectangular reflector half a wavelength under the antenna's azimuthal plane. The rectangular reflector also increased the ripple to $\approx \pm 1 dB$.

7.2 Recommendations

The prototype's measured performance proves that an optimized 5-petal big wheel antenna can achieve the high omnidirectionality required. The biggest problem with this configuration is the inherently poor match which requires added shunt capacitance to match the antenna. Good match should also bring the antenna's azimuthal gain to be positive.

It was found that parallel plate configuration used with the prototype did not help the match but instead made it worse. The parallel plates added shunt inductance instead of acting capacitively. Therefore, a central configuration is required that acts capacitively, and does not require such high tolerances for both design manufacturing as the parallel plates do.

Figure 74 below shows one design that may have such properties. It has not been manufactured and tested, and so we recommend that Group 39 does manufacture and test a prototype with such central configuration. Assuming this configuration does act as a cylindrical capacitor it can be easily tuned by adjusting the size of the cylinders and also adding and removing dielectric rings (not shown in the figure) between the central cylinder and the grounded shell. We think it will act as a cylindrical capacitor because in it the legs are oriented normally to the potential-carrying surfaces, as opposed to parallel as is the case with the parallel central plates that the prototype had. Here the size and the thickness of the shell can be varied more easily than with the plates which will change the reactance of this configuration. If any matching network is still required it can be placed between the grounded shell and the central cylinder and thus will not affect the pattern as much as a stub located under the antenna's azimuthal plane.

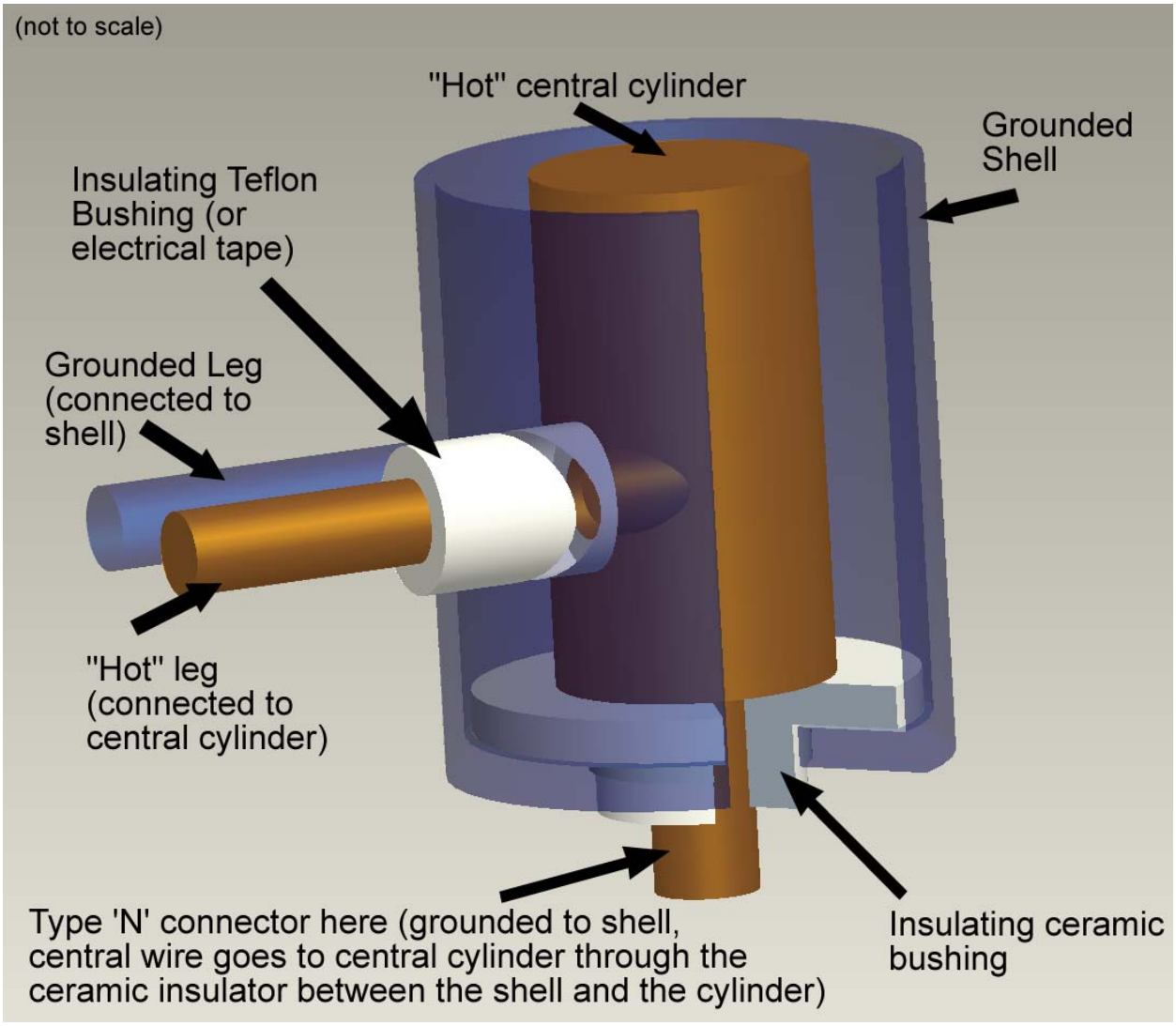

Fig. 74 Suggested Capacitive Central Configuration for Future Prototype (cutting section view)

Simulations suggested that increasing petal size tunes the antenna to a lower frequency without considerably affecting the ripple as long as the petal length l stays about one design wavelength. Therefore, the next prototype should have larger petals since this project's prototype was tuned to a higher frequency than desired.

It may also be worth it to investigate other designs, particularly the curved dipole cross, due to its phenomenal simulated performance. Dual reflector effect is worth investigating on the 5-petal prototype (even the currently existing one), as dual reflectors (especially if brought closer

to the antenna than half a wavelength) can act capacitively and help match the antenna while decreasing the ripple by redirecting more energy into the azimuthal plane. The reflectors have to be circular as a rectangular reflector was found to disturb the pattern.

Finally, a design that was suggested at the beginning of the project although never considered is two stacked 60° offset 3-petal wheels. This design was not considered due to complexity and bulkiness, but given the highly periodic shape of 3-petal wheels' measured performance it is worth investigating. Alternatively, the wheels can be placed without offset and fed 180° out of phase. However, 5-petal wheel with a different central configuration than parallel plates should be given higher priority since it is mechanically simpler, requires only 1 feed, and is much more omnidirectional than a single 3-petal wheel.

8 Glossary

This section contains a collection of terms common in RF circuit and antenna design which are used in this project. When a term is first used in the main text it is *italicized*.

Absolute Gain: A measure of the radiation intensity, in a given direction, obtained over that expected from an isotropic radiator, while taking into account losses endured due to impedance polarization mismatches. [2] (See **Gain** below). Absolute gain is given as:

$$G_{abs}(\theta,\phi) = e_0 G(\theta,\phi) \tag{7.1}$$

Where $G(\theta,\phi)$ is gain and e_0 is total antenna efficiency.

Anechoic Chamber: "The walls, ceiling and floor of an anechoic chamber are covered completely with absorbing material. An anechoic chamber simulates a reflectionless free space and allows all-weather antenna measurements in a controlled laboratory environment. In an anechoic chamber, the test area is isolated from interfering signals much better than at outdoor ranges. The isolation can be improved further by shielding." [16]

Antenna: "That part of a transmitting or receiving system that is designed to radiate or to receive electromagnetic waves." [1]

Beamwidth: "The angular separation between two identical points on opposite side of the pattern maximum." [1, 2]

Half-Power Beamwidth (HPBW): "In a radiation pattern cut containing the direction of the maximum of a lobe, the angle between the two directions in which the radiation intensity is one-half the maximum value." [1]

Bandwidth of an Antenna: "The range of frequencies within which the performance of an antenna, with respect to some characteristic, conforms to a specified standard." [1]

Decibel (dB): "One tenth of the common logarithm of the ratio of relative powers, equal to 0.1 B (bel). The decibel is the conventional relative power ratio, rather than the bel, for expressing relative powers because the decibel is smaller and therefore more convenient than the bel." [6] The relative power in decibels is determined as:

$$dB = 10\log_{10}(\dim) \tag{7.2}$$

Where $\dim$ is the dimensionless ratio of powers and dB is the relative power in decibels.

Directivity: "The ratio of the radiation intensity in a given direction from the antenna to the radiation intensity averaged over all directions." [2] Directivity is given as:

$$D(\theta,\phi) = 4\pi\frac{U(\theta,\phi)}{P_{rad}} \tag{7.3}$$

Where $U(\theta,\phi)$ is radiation intensity and P_{rad} is total radiated power.

Far-Field (Fraunhofer) Region: "That region of the field of an antenna where the angular field distribution is essentially independent of the distance from the antenna. For an antenna focused at infinity, the far-field region is sometimes referred to as the Fraunhofer region on the basis of analogy to optical terminology." [2]

Field Vector:

Circularly Polarized Field Vector: "At a point in space, a field vector whose extremity describes a circle as a function of time." [1]

Elliptically Polarized Field Vector: "At a point in space, a field vector whose extremity describes an ellipse as a function of time." [1]

Linearly Polarized Field Vector: "At a point in space, a field vector whose extremity describes a straight line segment as a function of time." [1]

Gain: "The ratio of the intensity, in a given direction, to the radiation intensity that would be obtained if the power accepted by the antenna were radiated isotropically." "Gain does not include losses arising from impedance mismatches (reflection losses) and polarization mismatches (losses)." [2] (See: **Absolute Gain** above). Gain is given as:

$$G(\theta,\phi) = 4\pi\frac{U(\theta,\phi)}{P_{in}} \tag{7.4}$$

Where $U(\theta,\phi)$ is radiation intensity and P_{in} is total input power.

Ground Plane: "A conducting or reflecting plane functioning to image a radiating structure." [1]

Impedance: "The total passive opposition offered to the flow of electric current. Impedance is determined by the particular combination of resistance, inductive reactance, and capacitive reactance in a given circuit. Impedance is a function of frequency, except in the case of purely resistive networks." [4] Complex impedance is a phasor given by:

$$Z = R + jX \tag{7.5}$$

Where Z is the total impedance phasor, R is the resistance, and X is the reactance of the circuit. (See Reactance below).

Input Impedance: "The impedance presented by an antenna at its terminals or the ratio of the voltage to current at a pair of terminals or the ratio of the appropriate components of the electric to magnetic fields at a point." [2]

Isotropic Radiator: "A hypothetical lossless antenna having equal radiation in all directions." [1]

Omnidirectional Antenna: "An antenna having an essentially non-directional pattern in a given plane of the antenna and a directional pattern in any orthogonal plane." [1]

Omnidirectivity: The degree to which an antenna approximates an ideal omnidirectional antenna. (See: **Omnidirectional Antenna** above).

Polarization Loss Factor (PLF): A measure of the energy loss associated with the mismatch in polarization between a transmitting and receiving antenna. [2] For a perfectly matched arrangement, the loss factor is unity. PLF is a dimensionless quantity. Polarization Loss Factor is given as:

$$PLF = \left|\cos\left(\psi_p\right)\right|^2 \tag{7.6}$$

Where ψ_p is the angle between the unit vectors of the receiver's and the wave's electric fields.

Polarization of an Antenna: "In a given direction from the antenna, the polarization of the wave transmitted by the antenna." [1] (See: **Polarization of a Wave** below)

Polarization of a Wave: "That property of an electromagnetic wave describing the time-varying direction and relative magnitude of the electric-field vector; specifically, the figure traced as a function of time by the extremity of the vector at a fixed location in space, and the sense in which it is traced, as observed along the direction of propagation." [2]

Polarization Pattern: "The spatial distribution of the polarizations of a field vector excited (radiated) by an antenna taken over its radiation sphere." [1]

Radiating Near-Field (Fresnel) Region: "That region of the field of an antenna between the reactive near-field region and the far-field region wherein radiation fields predominate and wherein the angular field distribution is dependent upon the distance from the antenna. If the antenna has a maximum dimension that is not large compared to the wavelength, this region may not exist. For an antenna focused at infinity, the radiation near-field region is sometimes referred to as the Fresnel region on the basis of analogy to optical terminology." [1]

Radiation Intensity: "The power radiated from an antenna per unit solid angle." [2] The radiation intensity is given as:

$$U(\theta,\phi) = \frac{r^2}{2\eta}|\mathbf{E}(r,\theta,\phi)|^2 \tag{7.7}$$

Where η is the intrinsic impedance of the medium and $\mathbf{E}(r,\theta,\phi)$ is the far-zone electric-field intensity of the antenna.

Radiation Lobe: "A portion of the radiation pattern bounded by regions of relatively weak radiation intensity." [2]

Back Lobe: "A radiation lobe whose axis makes an angle of approximately 180° with respect to the beam of an antenna. By extension, a radiation lobe in the half-space opposed to the direction of peak directivity." [1]

Major Lobe: "The radiation lobe containing the direction of maximum radiation." May also be called a main lobe. [1]

Minor Lobe: "Any radiation lobe except a major lobe." [1]

Side Lobe: "A radiation lobe in any direction other than the intended lobe." [2] Most commonly found adjacent to the major lobe and occupying the hemisphere containing the direction of primary radiation. [2]

Reactance: The imaginary component of impedance due to inductive and capacitive elements. [4] (See Impedance above). Inductive elements add imaginary impedance and capacitive elements subtract imaginary impedance. Inductive reactance is given by:

$$X_L = \omega L \tag{7.8}$$

Where X_L is the inductive reactance, ω is the angular frequency of the signal, and L is the inductance of the inductor. Inductive reactance is always positive. Capacitive reactance is given by:

$$X_C = -\frac{1}{\omega C} \tag{7.9}$$

Where X_C is the capacitive reactance, ω is the angular frequency of the signal, and C is the capacitance of the capacitor. Capacitive reactance is always negative. Overall reactance of the circuit is given by:

$$X = X_L + X_C \tag{7.10}$$

Reactive Near-Field Region: "That portion of the near-field region immediately surrounding the antenna wherein the reactive field predominates." [1]

Reflection Coefficient: "The amplitude of the reflected voltage wave normalized to the amplitude of the incident voltage wave." [5] Reflection coefficient is given by:

$$\Gamma = \frac{Z_L - Z_S}{Z_L + Z_S} \tag{7.11}$$

Where Z_L is the impedance towards the source at the interface, and Z_S is the impedance towards the source. Power reflected is expressed in terms of $|\Gamma|$, absolute reflection coefficient. $|\Gamma| = 1$ means total energy propagation, and $|\Gamma| = 0$ means total reflection.

RF: Radio frequency, refers to the spectrum of electromagnetic waves that can be generated and received using antennas. Specifically, it's the spectrum of frequencies between $10^4\,Hz$ to $10^{11}\,Hz$. An RF-circuit is a circuit used to generate and / or process signals in that frequency spectrum. [9]

Ripple: Maximum variation in an antenna's omnidirectional pattern across a plane. For example, if an antenna's azimuthally omnidirectional to within $\pm 0.5 dB$, it is said that its ripple is $0.5 dB$ and thus the peak to valley variation is $1.0 dB$

Structural Design Parameters: A structural design parameter is a quantity that describes the shape of the antenna (more generally – of any structure). The number of design parameters needed to unambiguously describe the antenna's shape corresponds to the number of degrees of freedom in that antenna's shape. Antenna's geometry is calculated from its design parameters. [17]

Transmission Line: "The material medium or structure that forms all or part of a path from one place to another for directing the transmission of energy, such as electric currents, magnetic fields, acoustic waves, or electromagnetic waves. Examples of transmission lines include wires, optical fibers, coaxial cables, rectangular closed waveguides, and dielectric slabs." [6]

Ultra High Frequency (UHF): "Frequencies from 300 MHz to 3000 MHz." [6]

Voltage Standing Wave Ratio (VSWR): "In a transmission line, the ratio of maximum to minimum voltage in a standing wave pattern. VSWR is a measure of impedance mismatch between the transmission line and its load. The higher the VSWR, the greater the mismatch. The minimum VSWR, that which corresponds to a perfect impedance match, is unity." [6]

$$VSWR = \frac{1 + |\Gamma|}{1 - |\Gamma|} \tag{7.12}$$

Where $|\Gamma|$ is the absolute value of the reflection coefficient (see **Reflection Coefficient** above).

Appendix A: MATLAB Code for Electrically Small Circular Loop NEC File Generation

See sections 3.1.1 (p. 35) and 4.1 (p. 44) for information on how this code was used in this project. See Fig. 17 (p.36) for definition of all the geometric input and calculated variables.

The geometric variables that were not design parameters were calculated from the design parameters based on the following equations (all derived from how the geometry of the loop was restricted):

$$\begin{cases} r_o = \dfrac{l}{\pi} \\ \beta = \dfrac{2s}{2r_o} = \dfrac{s \cdot \pi}{l} \\ \alpha = 2\pi - \beta = 2\pi - \dfrac{s \cdot \pi}{l} \end{cases} \tag{A.1}$$

Notice that angles are measured in radians in all of the above equations.

MATLAB file loop.m provided with this report can be used to create NEC file describing the ESCL. Inputs that the simulation requires are listed in Table 4 (p. 37). Table 10 below contains the variable names used in loop.m MATLAB code.

See the comments in the loop.m code file for more details on Electrically Small Circular Loop simulation.

Notice that this code, like the rest of the simulation codes written over the course of this project, allows for an addition of a module that adds reflectors of different geometries. See Appendix F (p. 124) for a description of the reflector code.

The variables described here are geometric. All curved wires are regressed by finite size straight wire elements; see the loop.m file for details on how this is done.

Table 10 Variable Names Used in Electrically Small Circular Loop Code

Variable Symbol	Variable Name in MATLAB Code
r_o	lrad
λ	wavel
l	looplength
α	2*pi-aint
β	aint
w	wdiam
s	lengthint

Appendix B: MATLAB Code for Curved Dipole Cross NEC File Generation

See sections 3.1.2 (p. 37) and 4.2 (p. 50) for information on how this code was used in this project. See Fig. 20 (p. 39) for definition of all the geometric input and calculated variables.

The geometric variables that were not design parameters were calculated from the design parameters based on the following equations (all derived from how the geometry of the crossed dipoles was restricted):

$$\begin{cases} n\beta = \pi \\ \gamma + \alpha = \beta \\ 2r_o + 2l_a = l \\ l_a = \alpha r_o \end{cases} \tag{B.1}$$

Solving Eqs. (B.1) yields:

$$\begin{cases} \beta = \dfrac{\pi}{n} \\ \gamma = \beta - \alpha = \dfrac{\pi}{n} - \alpha \\ r_o = \dfrac{l}{2 \cdot (1 + \alpha)} \\ l_a = \alpha r_o = \dfrac{\alpha l}{2 \cdot (1 + \alpha)} \end{cases} \tag{B.2}$$

Notice that angles are measured in radians in all of the above equations.

MATLAB file cdc.m provided with this report can be used to create NEC file describing the Curved Dipole Cross. Inputs that the simulation requires are listed in Table 5 (p. 39). Table 11 below contains the variable names used in cdc.m MATLAB code.

Table 11 Variable Names Used in Curved Dipole Cross Code

Variable Symbol	Variable Name in MATLAB Code
r_o	orad
n	ndipoles
λ	wavel
l	dipolelength
l_a	arclength
α	arcangle
γ	aint
β	adipolestep
w	wdiam
s	platespace

See the comments in the cdc.m code file for more details on Curved Dipole Cross simulation.

Notice that this code, like the rest of the simulation codes written over the course of this project, allows for an addition of a module that adds reflectors of different geometries. See Appendix F (p. 124) for a description of the reflector code.

The variables described here are geometric. All curved wires are regressed by finite size straight wire elements; see the cdc.m file for details on how this is done.

Appendix C: MATLAB Code for "Big Wheel" v1 NEC File Generation

See sections 3.1.1 (p. 35) and 4.3 (p. 59) for information on how this code was used in this project. See Fig. 21 (p. 40) for definition of all the geometric input and calculated variables.

The geometric variables that were not design parameters were calculated from the design parameters based on the following equations (all derived from how the geometry of the wheel was restricted in v1 simulation):

$$\begin{cases} r_i = \dfrac{d_p}{2} \\ l_c^2 = r_i^2 + \left(\dfrac{s}{2}\right)^2 \\ 2l_c + 2l_l + l_a = l \\ \alpha + \gamma = \beta \\ l_a = r_o \cdot \alpha \\ \beta = \dfrac{2\pi}{n} \end{cases} \tag{C.1}$$

Solving Eqs. (C.1) yields Eqs. (C.2):

$$
\begin{cases}
r_i = \dfrac{d_p}{2} \\
\beta = \dfrac{2\pi}{n} \\
\alpha = \dfrac{2\pi}{n} - \gamma \\
l_c = \sqrt{\left(\dfrac{d_p}{2}\right)^2 + \left(\dfrac{s}{2}\right)^2} \\
l_l = \dfrac{\left(l - 2\sqrt{\left(\dfrac{d_p}{2}\right)^2 + \left(\dfrac{s}{2}\right)^2}\right) - \left(\dfrac{d_p}{2}\right)\cdot\left(\dfrac{2\pi}{n} - \gamma\right)}{\left(\dfrac{2\pi}{n} - \gamma\right) + 2} \\
r_o = \dfrac{\left(l - 2\sqrt{\left(\dfrac{d_p}{2}\right)^2 + \left(\dfrac{s}{2}\right)^2}\right) + 2\left(\dfrac{d_p}{2}\right)}{\left(\dfrac{2\pi}{n} - \gamma\right) + 2} \\
l_a = \dfrac{\left(l - 2\sqrt{\left(\dfrac{d_p}{2}\right)^2 + \left(\dfrac{s}{2}\right)^2}\right)\cdot\left(\dfrac{2\pi}{n} - \gamma\right) + 2\cdot\left(\dfrac{d_p}{2}\right)\cdot\left(\dfrac{2\pi}{n} - \gamma\right)}{\left(\dfrac{2\pi}{n} - \gamma\right) + 2}
\end{cases}
\tag{C.2}
$$

Notice that angles are measured in radians in all of the above equations.

MATLAB file bigwheel1.m provided with this report can be used to create NEC file describing the Big Wheel v1. Inputs that the simulation requires are listed in Table 6 (p. 41) Table 12 below contains the variable names used in bigwheel1.m MATLAB code.

See the comments in the bigwheel1.m code file for more details on Big Wheel v1 simulation.

Notice that this code, like the rest of the simulation codes written over the course of this project, allows for an addition of a module that adds reflectors of different geometries. See Appendix F (p. 124) for a description of the reflector code.

The variables described here are geometric. All curved wires are regressed by finite size straight wire elements; see the bigwheel1.m file for details on how this is done.

Table 12 Variable Names Used in Big Wheel v1 Code

Variable Symbol	Variable Name in MATLAB Code
r_i	irad
r_o	orad
d_p	platediam
n	npetals
λ	wavel
l	looplength
l_c	conlength
l_a	arclength
l_l	leglength
α	arcangle
γ	aint
β	apstep
w	wdiam
s	platespace

Appendix D: MATLAB Code for "Big Wheel" v2 NEC File Generation

See sections 3.2 (p. 41) and 5.1 (p. 70) for information on how this code was used in this project. See Fig. 22 (p. 42) for definition of the geometric input and calculated variables.

There are several other geometric variables that are not in Fig. 22 (p. 42). These variables are not useful for construction but help in simulation; they are given in Fig. 75 below:

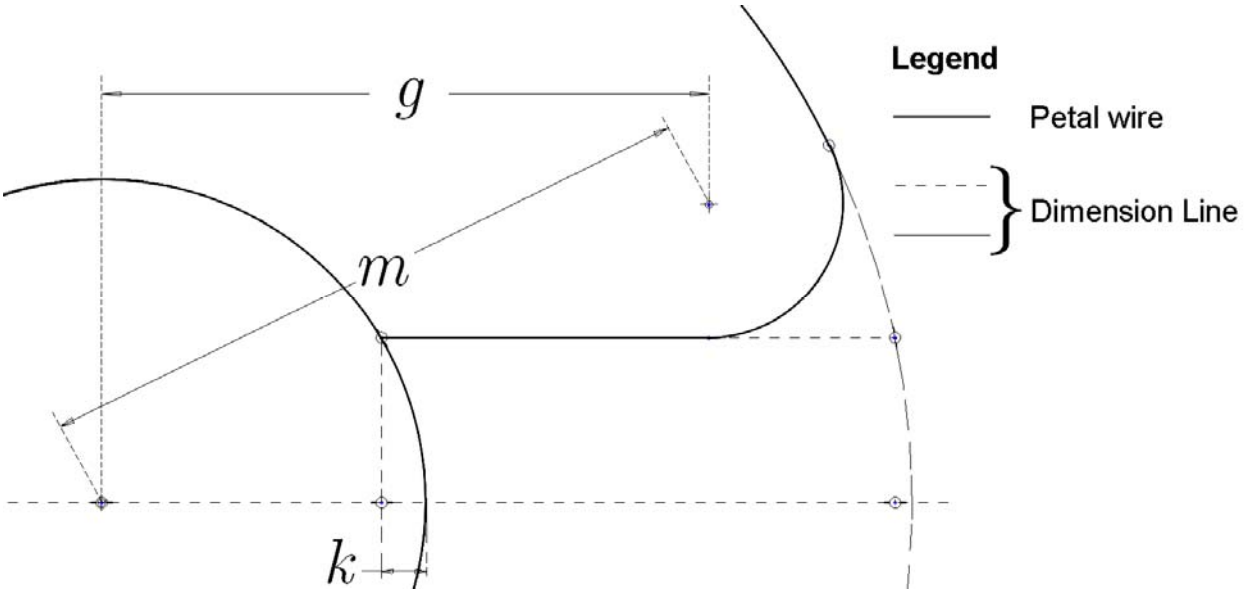

Fig. 75 Big Wheel v2 Supplementary Geometric Variables

The geometric variables that were not design parameters were calculated from the design parameters based on Eqs. (D.1), all derived from how the geometry of the wheel was restricted in v2 simulation).

$$
\begin{cases}
2l_l + 2l_r + l_a = l \\
l_a = \alpha \cdot r_o \\
2\gamma + \alpha = \beta \\
\beta = \dfrac{2\pi}{n} \\
r_i = \dfrac{d_p}{2} \\
l_r = \delta \cdot r_r \\
h = \dfrac{h_2}{2} \\
r_i^2 = h^2 + \left(r_i - k\right)^2 \\
\gamma + \dfrac{\pi}{2} = \delta \\
\left(\left(r_i - k\right) + l_l\right)^2 + \left(h + r_r\right)^2 = \left(r_o - r_r\right)^2 \\
g = \dfrac{h + r_r}{\tan\left(\gamma\right)} \\
g - \left(r_i - k\right) = l_l \\
l_c^2 = r_i^2 + \left(\dfrac{s}{2}\right)^2 \\
m^2 = g^2 + \left(r_r + h\right)^2
\end{cases}
\tag{D.1}
$$

The following variables can be immediately calculated from the given variables:

$$
\begin{cases}
\beta = \dfrac{2\pi}{n} \\
r_i = \dfrac{d_p}{2} \\
h = \dfrac{h_2}{2} \\
l_c = \sqrt{\left(\dfrac{d_p}{2}\right)^2 + \left(\dfrac{s}{2}\right)^2} \\
k = r_i - \sqrt{r_i^2 - h^2} = \dfrac{d_p}{2} - \sqrt{\left(\dfrac{d_p}{2}\right)^2 - \left(\dfrac{h_2}{2}\right)^2}
\end{cases}
\tag{D.2}
$$

Which after substitution and simplification reduces the system to:

$$\begin{cases} 2l_l + 2\left(\left(\gamma + \frac{\pi}{2}\right)\cdot r_r\right) + \alpha \cdot r_o = l \\ 2\gamma + \alpha = \frac{2\pi}{n} \\ \left(\left(\frac{d_p}{2} - \left(\frac{d_p}{2} - \sqrt{\left(\frac{d_p}{2}\right)^2 - \left(\frac{h_2}{2}\right)^2}\right)\right) + l_l\right)^2 + \left(\frac{h_2}{2} + r_r\right)^2 = \left(r_o - r_r\right)^2 \\ \frac{h + r_r}{\tan(\gamma)} - \left(\frac{d_p}{2} - \left(\frac{d_p}{2} - \sqrt{\left(\frac{d_p}{2}\right)^2 - \left(\frac{h_2}{2}\right)^2}\right)\right) = l_l \\ m = \sqrt{\left(\frac{h + r_r}{\tan(\gamma)}\right)^2 + \left(r_r + h\right)^2} \end{cases} \tag{D.3}$$

Further substitution eventually yields the following equation with one unknown γ:

$$\begin{aligned} 2\left(\frac{\frac{h_2}{2} + r_r}{\tan(\gamma)} - \sqrt{\left(\frac{d_p}{2}\right)^2 - \left(\frac{h_2}{2}\right)^2}\right) + 2r_r\left(\gamma + \frac{\pi}{2}\right) + \dots \\ \dots + \left(\frac{2\pi}{n} - 2\gamma\right)\cdot\frac{r_r\sin(\gamma) + r_r + \frac{h_2}{2}}{\sin(\gamma)} \end{aligned} = l \tag{D.4}$$

Equation (D.4) is not solvable analytically. Therefore, MATLAB's numerical function `fminbnd()` was implemented to minimize the following function $f(\gamma)$:

$$\begin{aligned} f(\gamma) = \Bigg| 2\left(\frac{\frac{h_2}{2} + r_r}{\tan(\gamma)} - \sqrt{\left(\frac{d_p}{2}\right)^2 - \left(\frac{h_2}{2}\right)^2}\right) + 2r_r\left(\gamma + \frac{\pi}{2}\right) + \dots \\ \dots + \left(\frac{2\pi}{n} - 2\gamma\right)\cdot\frac{r_r\sin(\gamma) + r_r + \frac{h_2}{2}}{\sin(\gamma)} - l \Bigg| \end{aligned} \tag{D.5}$$

`fminbnd()` is based on golden section search and parabolic interpolation, and always converges as it does not use derivatives. [18, 19] This is why it was used instead of regular

solving functions – due to the nature of $f(\gamma)$, most algorithms are not guaranteed to converge for it. This method approximates the location of the function's minimum which approximates γ. After finding γ the following equations can be used to find the rest of the variables:

$$\begin{cases} \alpha = \dfrac{2\pi}{n} - 2\gamma \\ l_l = \dfrac{\left(\dfrac{h_2}{2} + r_r\right)}{\tan(\gamma)} - \sqrt{\left(\dfrac{d_p}{2}\right)^2 - \left(\dfrac{h_2}{2}\right)^2} \\ g = l_l + \sqrt{\left(\dfrac{d_p}{2}\right)^2 - \left(\dfrac{h_2}{2}\right)^2} \\ m = \sqrt{\left(l_l + \sqrt{\left(\dfrac{d_p}{2}\right)^2 - \left(\dfrac{h_2}{2}\right)^2}\right)^2 + \left(r_r + \dfrac{h_2}{2}\right)^2} \\ \delta = \gamma + \dfrac{\pi}{2} \\ l_r = \left(\gamma + \dfrac{\pi}{2}\right) \cdot r_r \\ r_o = \dfrac{r_r \sin(\gamma) + r_r + \dfrac{h_2}{2}}{\sin(\gamma)} \\ l_a = \left(\dfrac{2\pi}{n} - 2\gamma\right) \cdot \left(\dfrac{r_r \sin(\gamma) + r_r + \dfrac{h_2}{2}}{\sin(\gamma)}\right) \end{cases} \tag{D.6}$$

To summarize, Eqs. (D.2) and (D.6) can be used to compute all the geometric variables which are not design parameters when design parameters are given and γ is found using the method of Eq. (D.5).

Notice that angles are measured in radians in all of the above equations.

MATLAB file bigwheel2.m provided with this report can be used to create NEC file describing the Big Wheel v2. Inputs that the simulation requires are listed in Table 7 (p. 42). Table 13 below contains the variable names used in bigwheel2.m MATLAB code.

Table 13 Variable Names Used in Big Wheel v2 Code

Variable Symbol	Variable Name in MATLAB Code
l	looplength
n	npetals
d_p	platediam
r_r	roundrad
h_2	legint
s	platespace
w	wdiam
l_l	leglength
l_r	roundlength
l_a	arclength
α	arcangle
r_o	orad
r_i	irad
γ	arcinitangle
β	apstep
δ	roundangle
k	ldiff
h	halflegint
g	roundleglength
l_c	conlength
m	crad

See the comments in the bigwheel2.m code file for more details on Big Wheel v2 simulation.

Notice that this code, like the rest of the simulation codes written over the course of this project, allows for an addition of a module that adds reflectors of different geometries. See Appendix F (p. 124) for a description of the reflector code.

The variables described here are geometric. All curved wires are regressed by finite size straight wire elements; see the bigwheel2.m file for details on how this is done.

Appendix E: MATLAB Code for "Big Wheel" v3 NEC File Generation

See sections 3.2 (p. 41) and 5.1 (p. 70) for information on how this code was used in this project. See Fig. 22 (p. 42) for definition of the geometric input and calculated variables.

Big Wheel v3 geometry is the same as v2's (see Appendix D, p. 117), except for the variable l_c which does not get used. This is because instead of connectors there are parallel central plates approximated with finite square element circular grids. See the MATLAB file bigwheel3.m for more details.

Figure 76 below shows the prototype antenna (see the description of it in section 5.3, p. 79) simulated using Big Wheel v3 code.

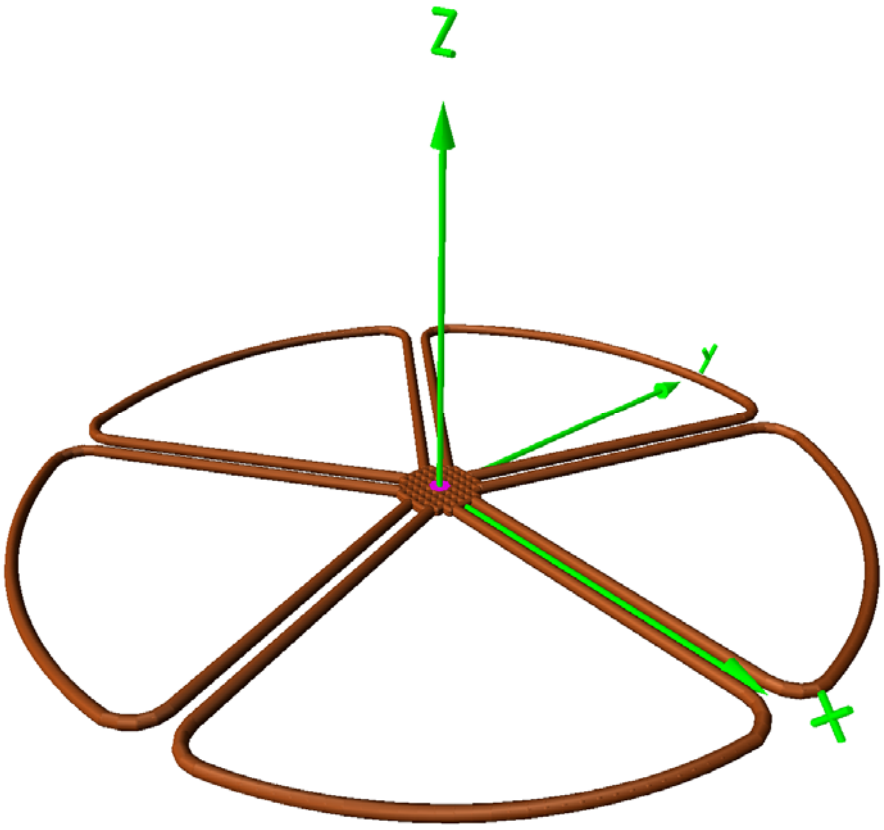

Fig. 76 Prototype Simulated with v3 3D Rendering

Appendix F: MATLAB Code for Reflector NEC File Generation

As part of this project, a MATLAB code was developed to generate NEC-2 code describing reflectors of several different geometries. This code is in the MATLAB file reflector.m distributed with this report. The code does not run on its own, and is instead made to be copied and pasted into other MATLAB codes used for creation of NEC-2 files, such as loop.m (see Appendix A, p. 110), cdc.m (see Appendix B, p. 112) or bigwheel2.m (see Appendix D, p. 117).

The file reflector.m contains all the descriptions necessary to use the reflector simulation code. Figures 77, 78 and 79 below show the types of reflectors the code can be used to simulate. In this project, mainly circular reflectors with rectangular mesh were used for curved dipole cross simulations. This is because they showed what we deemed was the most realistic pattern (although none of the reflector simulations were truly tested experimentally).

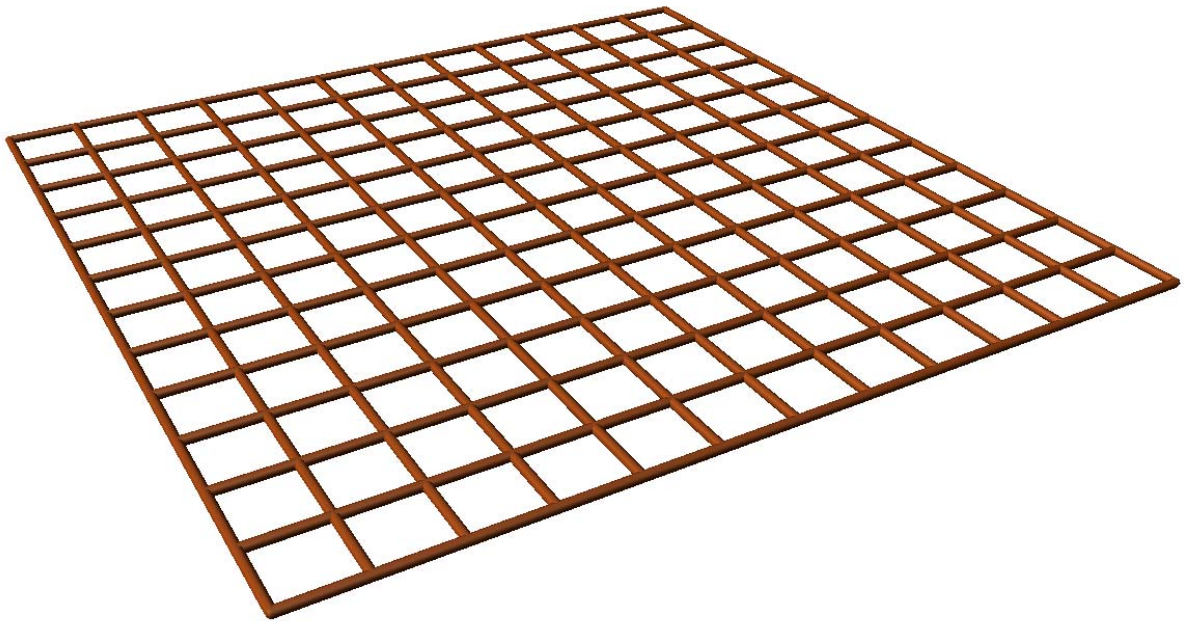

Fig. 77 Rectangular Mesh Square Reflector 3D Rendering

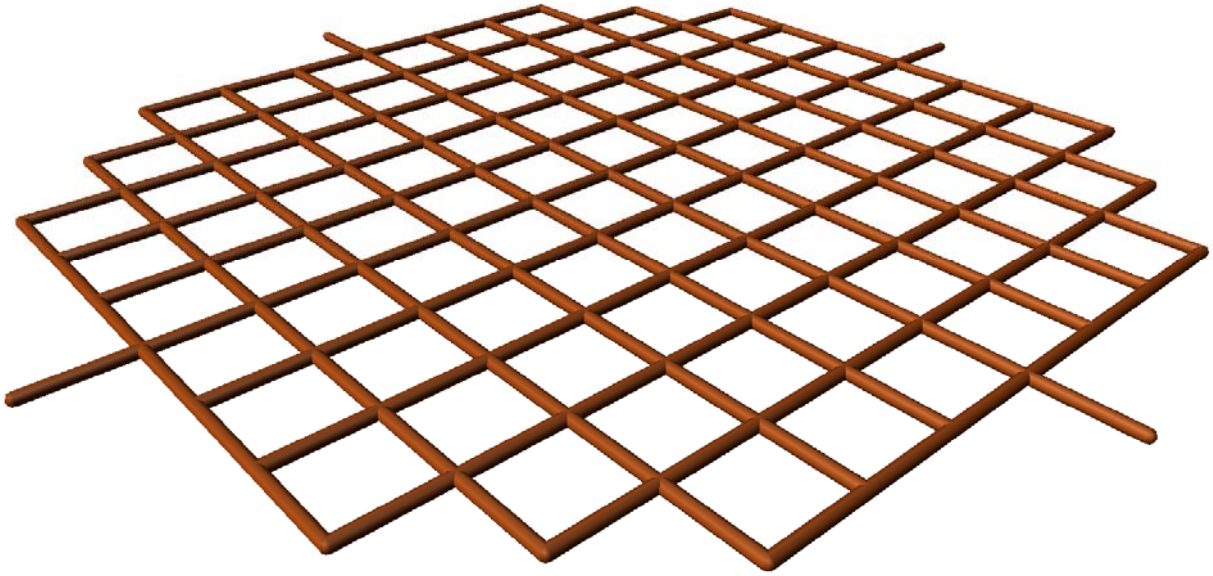

Fig. 78 Rectangular Mesh Circular Reflector 3D Rendering

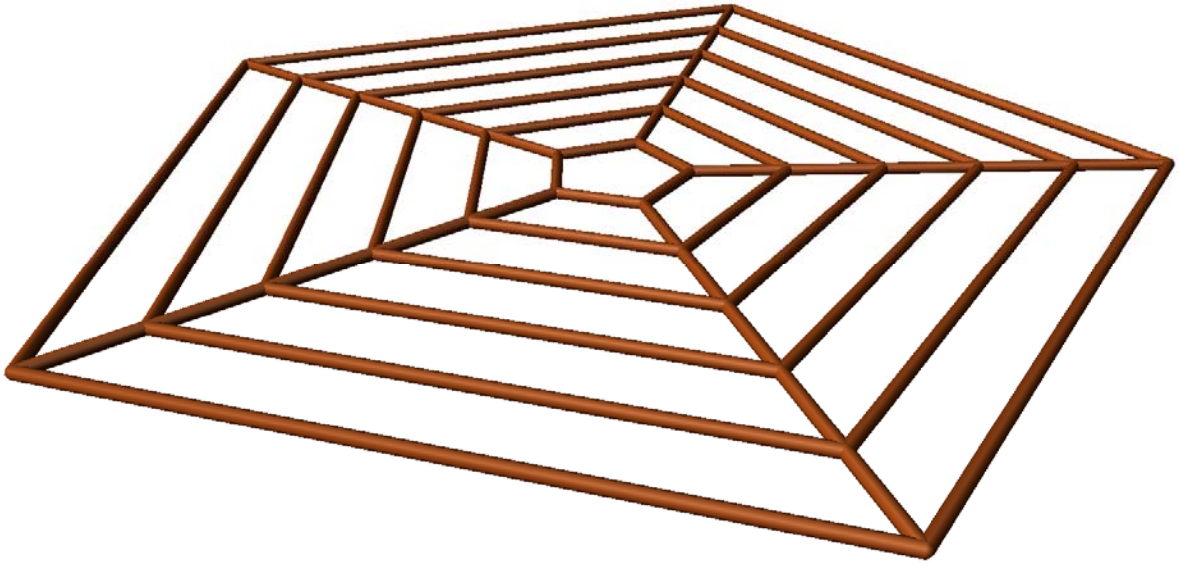

Fig. 79 Radial Mesh Circular Reflector Rendering

Appendix G: Central Plate Illustration

Figure 80 below illustrates the central plates that were used for both Group 39's 3-petal and the 5-petal prototypes.

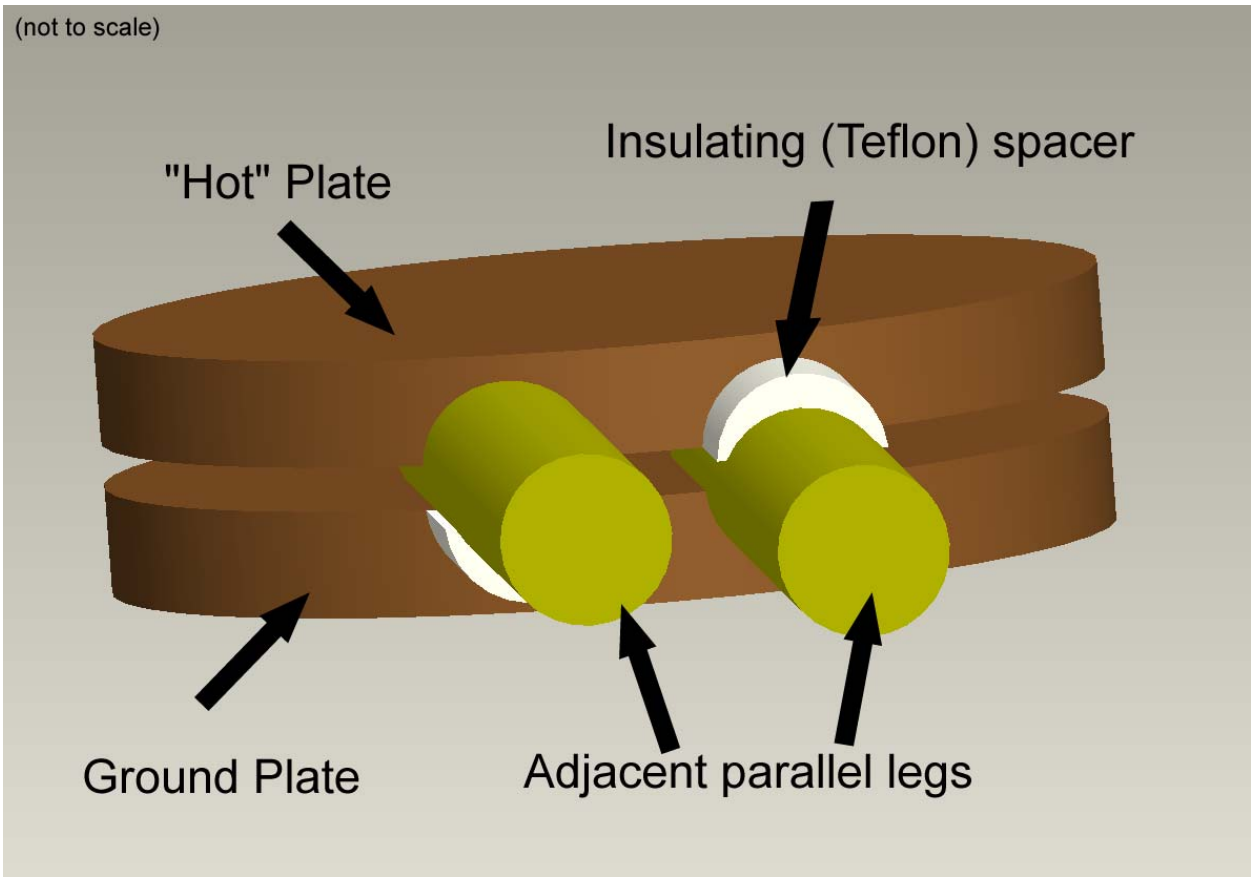

Fig. 80 Central Plate Configuration Illustration

The Type N female coaxial connector was grounded to the bottom plate with the (insulated from the ground plate) central spike going through the plate and connecting to the top plate. $\frac{1}{16}\,in$ Teflon spacers were used to insulate the legs from the plates that they were supposed to be insulated from. The plates were held together with 3 to 5 bolts that ran through the plates and were insulated from the "hot" plate using plastic bushings.

The main problem with this configuration was the interval between plates is only the thickness of the spacers, which is just $\frac{1}{16}\,in$. This made the plates very difficult to tweak and work with, and also made the configuration very sensitive to impact and reassembly.

The plates were made of copper, same as the legs.

One of the recommendations of this project is to replace the central parallel plate configuration with a more durable and less sensitive one. See chapter 7 (p. 99) for one suggested configuration.

Bibliography

[1] 1993, "IEEE Standard Definitions of Terms for Antennas," IEEE Std 145-1993.
[2] Balanis, C. A., 2005, *Antenna Theory Analysis and Design*, 3rd ed., John Wiley & Sons, Inc., Hoboken, NJ.
[3] Public Domain, 2007, "Image:Spherical Coordinates," http://en.wikipedia.org/wiki/Image:Spherical_Coordinates.svg.
[4] Hambley, A. R., 2005, *Electrical Engineering Principles and Applications*, 3rd ed., Pearson Education, Inc., Upper Saddle River, NJ.
[5] Pozar, D. M., 2004, *Microwave Engineering*, 3rd ed., John Wiley & Sons, Inc., Hoboken, NJ.
[6] 2001, "Telecommunications: Glossary of Telecommunication Terms," ANS T1523-2001.
[7] Germes LLC, 2005, "DVB - T Antenna," http://www.germes-online.com/catalog/88/91/1342/page3/153672/dvb_t_antenna_.html.
[8] Schwarzbeck Mess-Elektronik, 2007, "Image:Half-Wave Dipole," http://en.wikipedia.org/wiki/Image:Half_%E2%80%93_Wave_Dipole.jpg.
[9] Halliday, D., Resnick, R., and Walker, J., 2005, *Fundamentals of Physics*, 7th ed., John Wiley & Sons, Inc., Hoboken, NJ.
[10] Griffiths, D. J., 1999, *Introduction to Electrodynamics*, 3rd ed., Prentice-Hall, Inc., Upper Saddle River, NJ.
[11] Agilent Technologies, 2007, "Agilent Advanced Design System (ADS)," http://eesof.tm.agilent.com/products/ads_main.html.
[12] Ludwig, R., and Bretchko, P., 2000, *RF Circuit Design: Theory and Applications*, Prentice-Hall, Inc., Upper Saddle River, NJ.
[13] Makarov, S. N., 2002, *Antenna and EM Modeling with Matlab*, John Wiley and Sons, Inc., New York, NY.
[14] Nittany Scientific Inc, 2005, "Nittany Scientific, Inc.," http://www.nittany-scientific.com/.
[15] Burke, G. J., and Poggio, A. J., 1996, "NEC-2 Manual, Part III: User's Guide," ulisse.polito.it/matdid/3ing_tlc_F0532_TO_0/pcnec/nec2_092.doc.
[16] Kraus, J. D., and Marhefka, R. J., 2002, *Antennas for All Applications*, 3rd ed., McGraw-Hill College, Blacklick, OH.
[17] Li, S., and Chen, L., 2007, "Towards Rapid Redesign: Pattern-Based Redesign Planning for Large-Scale and Complex Redesign Problems," Journal of Mechanical Design, **129**, pp. 227-233.
[18] Brent, R. P., 1973, *Algorithms for Minimizations without Derivatives*, Prentice-Hall Professional Technical Reference, Englewood Cliffs, NJ.
[19] Forsythe, G. E., Malcolm, M. A., and Moler, C. B., 1976, *Computer Methods for Mathematical Computations*, Prentice-Hall Professional Technical Reference.